

Doctoral Thesis

Influence of binder composition on powder injection moulding process

**Vliv kompozice polymerního pojiva na proces vstřikování
práškových materiálů**

Author: **Ing. Eva Hnátková**

Study programme: Process Engineering P3909

Study course: Tools and Processes 3909V013

Supervisor: doc. Ing. Zdeněk Dvořák, CSc.

Consultant: prof. Ing. Berenika Hausnerová, Ph.D.

Reviewers: prof. Ing. Pavel Alexy, PhD.
doc. RNDr. Ivan Fortelný, DrSc.
prof. Ing. Petr Svoboda, Ph.D.

Zlín, June 2019

© Eva Hnátková

The publication was issued in year 2019

Key words in English: *powder injection moulding, highly filled polymers, critical powder loading, binder, molecular weight, polyethylene glycol, backbone, stearic acid, rheology, activation energy, thermal properties*

Key words in Czech: *vstřikování práškových materiálů, vysoce plněné polymery, kritické plnění, pojivo, molekulová hmotnost, polyetylen glykol, páteřní polymer, kyselina stearová, reologie, tepelné vlastnosti*

CONTENTS

ABSTRACT	4
ABSTRACT IN CZECH	5
ACKNOWLEDGEMENTS	6
GLOSSARY	7
THEORETICAL BACKGROUND	8
1 INTRODUCTION TO POWDER INJECTION MOULDING	8
1.1 The role of binder in PIM process.....	9
1.2 PIM feedstock formulation.....	11
1.3 Determination of critical powder loading	17
1.4 Rheological characterization of PIM feedstocks.....	21
2 AIM OF THE THESIS	26
EXPERIMENTAL PART	27
3 MATERIALS AND METHODS	27
3.1 Powder and binder characteristics.....	27
3.2 PIM feedstocks formulation and processing	33
3.3 Rheology of PIM feedstocks	37
3.4 Mechanical properties of sintered tensile samples.....	42
4 RESULTS AND DISCUSSION	45
4.1 Effect of major component.....	46
4.2 Effect of backbone.....	58
4.3 Effect of surfactant	65
CONCLUSION	75
CONTRIBUTION TO SCIENCE AND PRACTICE	78
REFERENCES	79
LIST OF FIGURES	86
LIST OF TABLES	88
LIST ABBREVIATIONS AND ACRONYMS	89
LIST OF PUBLICATIONS	92
CURRICULUM VITAE	96

ABSTRACT

Powder injection moulding (PIM) is a modern technological process combining powder metallurgy and plastic injection moulding. PIM is suitable for mass production of small metal or ceramic items, with complex geometry and tight tolerances. Polymer binders for PIM technology are still in the developing area due to the complexity of their requirements. One of the main challenges in PIM technology is optimization of PIM process and detection/elimination of powder binder separation resulting in inhomogeneous final products.

The research team at Tomas Bata University in Zlín under prof. Hausnerová has been involved in investigating the interactions and chemical mechanisms occurring within a binder system. The aim of this thesis is devoted to polymer binder composition based on previous results, including binder components characterization and their influence on PIM process. Particular emphasis was also placed on an eco-friendly approach and maximisation of solid loading.

Major component/s of binder systems provide low viscosity and easy removal in the first stage of debinding. Polyethylene glycol (PEG) is a suitable candidate due its non-toxicity, solubility in water and commercial availability. The first part was dedicated to the effect of PEG molecular weight on the overall PIM process. Results showed that PEG molecular weight affected processing parameters, but without any final impact on mechanical properties of sintered Inconel 718. Feedstock viscosity can be tailored via PEG molecular weight.

The second part was devoted to backbone components, especially to carnauba wax (CW) and acrawax (AW) as possible substituents of polyolefin based binder systems. Previous research showed twice stronger binding for AW/PEG than for CW/PEG, suggesting strong interactions between polymers. Feedstocks based on CW and AW showed overall lower viscosity than polyolefin-based ones and commercial feedstocks, and additionally a binder based on CW, could be used for reactive powders due to low processing temperatures.

Concentration of stearic acid (SA) as a surface active agent was investigated in third part in order to increase powder loading and improve flow properties of feedstocks. Surfactant SA positively affected processing parameters and its appropriate concentration is strongly dependent on binder composition. Optimal concentration of SA can increase maximal powder loading.

Binders are designed as multi-component polymer systems, in which each component performs a specific task. Better understanding of each component in this process can help eliminate some drawbacks, improve processing and produce less defective parts.

ABSTRACT IN CZECH

Vstřikování práškových materiálů (PIM) je moderní technologický proces kombinující práškovou metalurgii s vstřikováním plastů. PIM technologie je vhodná zejména pro hromadnou výrobu malých kovových nebo keramických dílů komplexního tvaru a s úzkou tolerancí. Polymerní pojiva pro tuto technologii jsou stále ve vývoji z důvodu komplexních požadavků. Jednou z výzev v této technologii je optimalizace procesu detekce a/nebo eliminace fázové separace, t má za následek nehomogenní finální produkty.

Vědecký tým na Univerzitě Tomáše Bati ve Zlíně pod vedením prof. Hausnerové se zabýval studiem interakcí a chemických mechanismů, ke kterým dochází v polymerním pojivu. Cíl této práce zaměřený na kompozici polymerního pojiva na základě předchozích výsledků, charakterizaci jednotlivých komponentů a jejich vliv na PIM proces. Klade důraz ekologické hledisko a zvýšení objemového plnění, které je taktéž důležitým aspektem této technologie.

Hlavní komponent polymerního pojiva zaručuje nízkou viskozitu a snadné odstranění pojiva v první fázi. Polyetylen glykol (PEG) je vhodným kandidátem, protože není toxický, je rozpustný ve vodě a je komerčně dostupný. První část této práce se zabývá vlivem molekulou hmotností PEG na celkový PIM proces. Výsledky ukázaly, že molekulová hmotnost PEG ovlivní procesní parametry, ale nebude mít vliv na finální mechanické vlastnosti sintrovaného Inconelu 718. Teplota při odstraňování polyetylen glykolu měla zásadní vliv na vznik defektů a na hustotu sintrovaných dílů. Viskozita PIM směsí může být nastavena na míru pomocí molekulové hmotnosti PEG.

Druhá část se zaměřuje na tzv. páteřní polymery, konkrétně se jedná o karnaubský vosk (CW) a acrawax (AW), jako možné substituenty pro polymerní systémy na bázi polyolefinů. Předchozí výsledky ukázaly dvojnásobně silnější vazby pro AW/PEG než pro CW/PEG, což naznačuje silnou interakci mezi polymery. Viskozita směsí na bázi CW a AW se snížila oproti viskozitě směsí na bázi polyolefinů a komerčního pojiva. Pojiva na bázi CW mohou být použitelná pro zpracování reaktivních prášků z důvodů nízké zpracovatelské teploty.

Koncentrace kyseliny stearové (SA) povrchově aktivní látky byla zkoumána v třetí části za účelem možnosti zvýšení práškového plnění a zlepšení tokových vlastností plněných směsí. SA pozitivně ovlivnila zpracovatelské parametry, ale její vhodná koncentrace bude silně záviset na složení polymerního pojiva.

Pojiva jsou navrženy jako více komponentní systémy, ve kterých má každý komponent specifickou roli. Lepší porozumění jednotlivých složek v procesu pomůže eliminovat některé nedostatky, zlepšit proces a snížit výrobu defektů.

ACKNOWLEDGEMENTS

First of all, I would like to thank my supervisor, assoc. prof. Zdeněk Dvořák and my consultant prof. Berenika Hausnerová for giving me help, consultation, directions to my work and providing me with a lot of experience and advice.

In addition, many thanks belong to the Department of Materials Science and Engineering at Sheffield University, especially to my colleagues MPhil Andrew Ben Hales and MEng. Lukaš Jiránek as part of my research was based on joint work with them.

I would also to express my thanks to assoc. prof. Věra Kašpárková for her help with thermal analysis, and assoc. prof. Petr Filip for his help with measurements and evaluation of rheological measurements.

Further, I would like to thank all persons who accompanied me through doctoral training and helped me form my scientific and personal views in various ways.

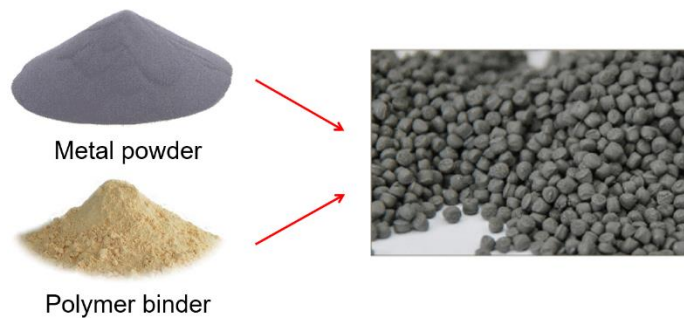
I am deeply grateful for the support of my family, my friends and my colleagues.

This dissertation work was also supported by the following projects: CPS (CZ.1.05/2.1.00/03.0111), CPS+ (LO 1504) and by the Internal Grant Agency of Tomas Bata University in Zlín: IGA/FT/2016/002, IGA/FT/2015/001, IGA/FT/2014/003, IGA/FT/2013/022, where I worked as a member of research teams.

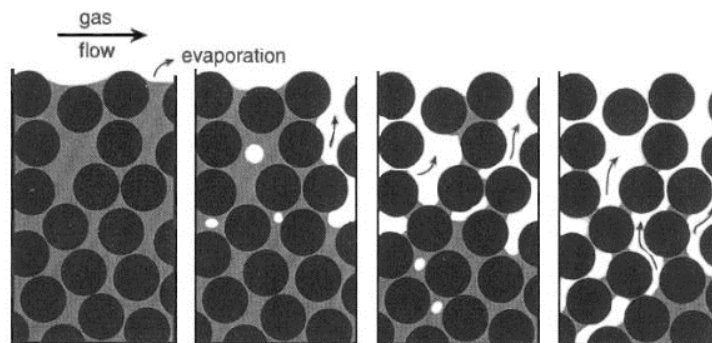
GLOSSARY

Basic terminology used in PIM technology:

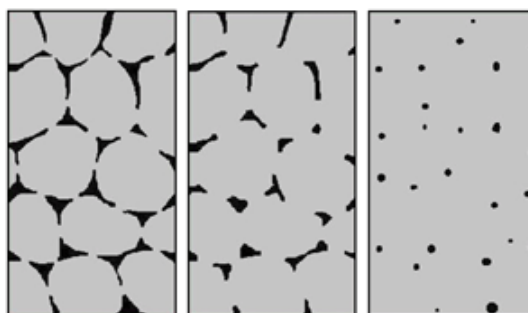
- **Powder** – fine ceramic or metal particles
- **Binder** – an individual component or a composition of polymeric materials
- **Feedstock** – a mixture of powder and binder



- **Mixing** – a process of compounding powder and binder into feedstock
- **Injection moulding** – a process in which the feedstock is injection moulded into mould cavity
- **Debinding** – a process in which the binder components are removed from moulded component



- **Sintering** – a thermal process during which powder particles are bonded and densified at a high temperature



THEORETICAL BACKGROUND

1 INTRODUCTION TO POWDER INJECTION MOULDING

Powder Injection Moulding (PIM) is an expanding technology for small ceramic or metal items of complex shapes with tight tolerances, which are expensive and/or difficult to produce by conventional methods [1-4]. Up to date, various application areas such as automotive, electronics, medical field, or communication and information technology are moving towards miniaturization, and there is still huge potential for mass production of PIM components [5]. As an example, Fig. 1 shows a connector that has been produced in tens of millions per week [6].



Fig. 1 Lightning connector produced by PIM [6].

As sketched in Fig. 2, the PIM technology consists of four basic steps. Firstly, the binder is mixed together with powder particles and processed into homogenous feedstock pellets. Then, PIM feedstock is injection moulded into an oversized mould cavity of the desired shape using the injection moulding machine. After that, the polymer binder is removed from moulded components. And at the end, the powder particles are densified at high temperature in special sintering furnaces.

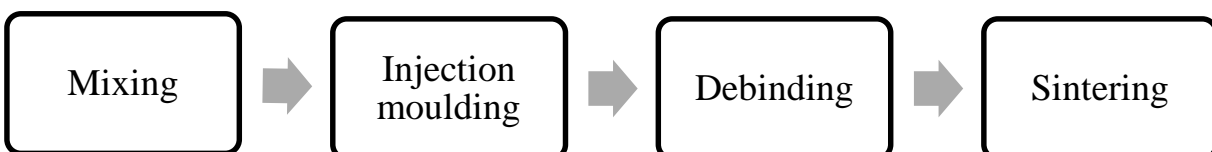


Fig. 2 Basic steps in PIM technology

1.1 The role of binder in PIM process

A binder plays a crucial role during the entire process and has to fulfil several tasks. Especially, a binder must allow:

- the flow of the powder into the mould cavity, and
- shape retention of moulded components.

Binder requirements

First of all, binder assists during the mixing stage which has to result in uniform distribution of powder particles. It is desirable that the binder has a low contact angle with powder particles to ensure appropriate surface wetting. Sufficient adhesion between powder and binder should prevent them from segregation. A binder also needs to be chemically inert with respect to powder, which means there is no reaction which could cause degradation of binder components.

During injection moulding, the binder acts as a vehicle medium which allows powder particles to move into the mould cavity. A binder needs to provide stable flow and appropriate viscosity of feedstock without phase separation or formation of any defects. Extremely low feedstock viscosity can lead to phase separation, while too high viscosity can cause problems during mixing and mould filling. Feedstock viscosity has to possess low temperature sensitivity to avoid fluctuation during injection moulding.

Once the feedstock is moulded into the mould cavity, the molten material is cooled down and binder holds the powder particles together and retains the shape of the component. A binder has to guarantee dimensional and shape stability of moulded components without large thermal contraction. A binder system also has to provide sufficient strength of injection moulded components for secure handling.

After injection moulding, the removal of the binder from moulded components should be carried out step by step without shape distortion or cracking [7], and at the same time the residual binder has to retain the shape of porous structure until the particles start bonding to each other. Each of the binder components needs to be removed without forming or introducing any defects. Thermal decomposition of polymeric components should not leave any burn out products in the sintering furnace.

From the economical point of view, a binder must be inexpensive [9].

Binder composition

In order to fulfil various requirements, the polymer binders are designed as multi-component systems, in which each component performs a specific task. A typical binder system is usually composed of:

- (i) major component/s,
- (ii) backbone, and
- (iii) additive/s.

The major components of a binder are usually composed of low molecular weight polymers to provide an adequate viscosity of feedstock.

Backbones ensure sufficient strength to a moulded component and maintain its shape, until the bonds (between contacting particles) start to grow. This occurs at higher temperature in the course of late debinding and early pre-sintering stage. Thermoplastics are commonly used for this purpose.

Additives in small amounts (*e.g.* surface active agents) are usually used to improve wettability of feedstocks. Their role is to create a thin layer on the surface of powder. This layer (composed of chemical absorption bonds) acts as a lubricant. It allows easier particle sliding to each other, which reduces feedstock viscosity and facilitates the mixing and moulding process [8]. Further, surfactants reduce abrasion of machine/cavity die walls and diminish the contact angle between powder and binder. Surfactants can also enhance packing density, which is an important aspect in binder design.

Methods for binder removal

Commonly used binder removal routes are: thermal, solvent or catalytic debinding. Thermal debinding is the oldest one, in which the moulded component is slowly heated to decompose the binder. This technique requires long processing times, which result in high economical costs [10]. In addition, the time needed for binder removal is strongly dependent on section thickness.

Today, it is more popular to combine various techniques, during which the binder is removed in several steps [11]. The binder system designed for two-stage debinding offers an option of removing a major part of the binder by solvent extraction or catalytic reaction in the first stage of debinding. This will guarantee formation of opening pores, through which gaseous products of the remaining backbone can later diffuse out [12].

For the first stage of debinding, the solvent removal is faster than thermal one. However, organic solvents are often environmentally unacceptable [13]. Thus,

adoption of water-soluble solvents appears as a valuable alternative. This also illustrates the fact that since 1976 over 130 patents concerning water-soluble binders have been submitted [14]. The catalytic reaction can accelerate even more the first step of debinding. However, this method needs special equipment [15].

The second debinding stage is usually thermal decomposition and it can take part as an early stage of sintering.

1.2 PIM feedstock formulation

PIM feedstock is the starting material for a PIM process and its formulation requires several considerations. Fig. 3 shows the main important aspects which have to be considered.

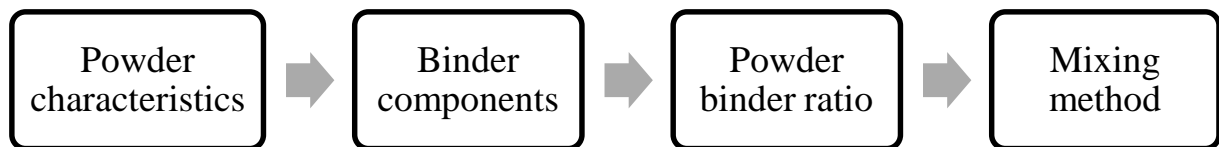


Fig. 3 The main aspects of PIM feedstocks.

Powder characteristics

The type of powder will influence final properties of sintered components. From the processing point of view, the most important powder characteristics are particle size, shape and particle size distribution, as well as particle dispersion or agglomeration.

Most of metal powder particles for PIM technology are in the range from 0.5 to 20 μm , in case of ceramics even less [3]. Particles with spherical shapes in comparison with the irregular ones increase packing density. Packing density is the ratio of particle volume and volume of the surrounding container that is needed for random close packing of particles. On the other hand, spherical particles will have tendency to diminish shape stability of components during the debinding and sintering stage. Particle shapes and sizes can be observed by scanning electron microscopy (SEM) and particle size distribution is nowadays mostly obtained by laser diffraction using a dry or wet method. Density of powder can be evaluated by gas pycnometer. Chemical composition of the powder can be analysed by energy dispersive X-ray spectroscopy (EDX).

Binder components

Waxes are widely used as major components due to their low melting temperature and viscosity [16]. Some commonly used waxes, with melting points of less than 100 °C, are Paraffin (PW), Beeswax (BW) or Carnauba Wax (CW). However, Thomas-Vielma *et al.* [17] reported that feedstocks with a high content of PW are not suitable for PIM due to poor shape retention of the component during the first stage of debinding. Then, consequences are highly defective sintered parts. Using only pure CW is not recommended either due to its narrow melting range and poor mechanical properties [18]. On the other hand, other studies have shown that waxes, such as PW and CW, have a great perspective in wax-based binder systems [19-20] due to their low processing temperatures and low viscosity. They can also find applications in processing reactive powders, such as Al₂O₃ or titanium in low pressure injection moulding and/or in micro injection moulding.

Polyethylene glycol (PEG), is another major component which has been extensively reported, especially in the design of partially water-soluble binders due to its non-toxicity, commercial availability and solubility in water [21-22]. PEG is a semicrystalline polyether available in various molecular weights. At a molecular weight smaller than 1,000, PEGs are viscous, colourless liquids, while those with higher molecular weights are waxy, white solids. Molecular weights of PEGs typically employed in PIM range from hundreds to 20,000, and they are proportional to melting temperatures. A binder system based on PEG was first reported by Cao *et al.* [23]. Then, Hens and German [24] examined the role of PEG in feedstocks aimed at simplifying processing and shape retention during debinding. Therefore, partially water-soluble binders based on PEG have been widely investigated for both metal and ceramic feedstocks [25-28]. Although PEG based feedstocks are well documented in the literature, there has only been limited scientific research concerning the effect of PEG molecular weight on the PIM process [29-32].

Most commonly used backbone polymers are polyethylene (PE), polypropylene (PP), ethylene vinyl acetate (EVA) and poly(methyl methacrylate) (PMMA). Huang and Hsu [33] demonstrated that the backbone strongly affects dimensions and mechanical properties of sintered parts. Therefore, proper material selection is required in order to increase dimensional accuracy and quality of sintered parts. They also observed that high density polyethylene (HDPE) with a higher molecular weight provides better dimensional stability. In contrast, the use of the low density polyethylene (LDPE) resulted in favourable

flow behaviour of feedstock giving advantages for the injection moulding stage. Bakan *et al.* [34], who studied the binder composition of PMMA and PEG, found that a lower content of PMMA allows higher solid loading to be moulded. On the other hand, it lowers stiffness and strength of moulded components. PMMA is often used, especially with PEG in binder systems.

Stearic acid (SA) and oleic acid (OA) are the most commonly used surfactants [35]. It was reported, that a small addition of SA improves the mixing process by obtaining more homogenous feedstock [17]. However, a high amount of it will not be beneficial any more.

Tab. 1 summarises typical binder components used in PIM technology.

Tab. 1 Most commonly used binder components used for PIM.

Major part	PW, CW, AW, BW, PEG, POM
Backbone	PP, PE, LDPE, HDPE, EVA
Additives/surfactants	SA, OA

Recently, many efforts have been made to obtain more environmentally acceptable PIM processes. For this purpose an optimised eco-binder system is required [36]. Escobar and Santos [37] proposed a new eco-friendly binder based on natural rubber as the backbone component for ceramic injection moulding (CIM) of alumina. They found that among binder components they used a better one for an injection process was obtained for 40 wt. % of natural rubber and 60 wt. % of paraffin wax.

Powder binder ratio

In PIM, the higher powder loading (the volume ratio of powder to total volume of powder and binder), prevents compact distortion, decreases volumetric shrinkage and improves tolerance control. Volumetric powder loading (Φ) can be calculated according to Eq. (1) as a volume percentage:

$$\Phi = \frac{\frac{w_p}{\rho_p}}{\frac{w_p}{\rho_p} + \frac{w_b}{\rho_b}} \quad (1)$$

- w_p is weight fraction of powder;
- w_b is weight fraction of binder;
- ρ_p is density of powder, in kg/m³;

ρ_b is density of binder, in kg/m^3 .

Experimental results showed that minimal powder loading could not be less than 45 vol. %, otherwise there can be difficulties during debinding and sintering [38]. However, loading cannot be increased unlimitedly and the maximum powder content strongly depends on powder characteristics and binder constitution [3].

Fig. 4 demonstrates three possible situations of powder binder ratio. Fig. 4b shows critical powder loading, where all particles are covered by a thin layer. There are no voids or pores because the binder completely fulfills the inter-particle space. If there is less polymeric binder (Fig. 4a), the particles will be in direct contact to each other and the space between particles will be filled with air gaps. This situation can cause difficulties in moulding due to a strong increase in feedstock viscosity and/or it may introduce defects into further steps. On the other hand, an excess of binder (Fig. 4c) is undesirable due to possible shape distortion during debinding and a possibility of powder binder separation during moulding [39].

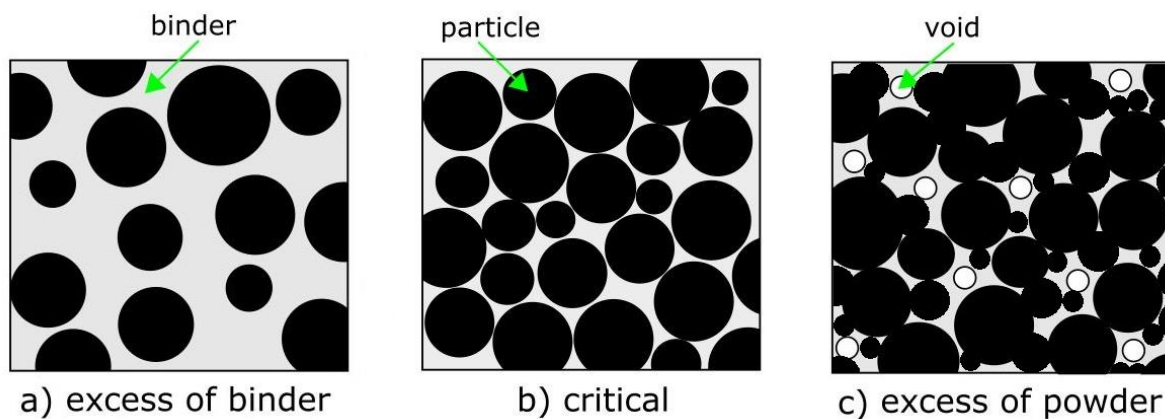


Fig. 4 Powder loading (a) excess, (b) critical, (c) insufficient.

Critical solid loading is mainly affected by the composition of binder and powder characteristics, such as the mean size (fine or coarse), particle size distribution (monomodal, bimodal, wide or narrow) and the particle shape (spherical, rounded or irregular). All of these characteristics influence the PIM process, such as mixing, flow properties and shape stabilization.

Fig. 5 shows the coating layer of a polymeric binder. Its content has a significant impact on critical powder loading, while it is desirable to mix as much powder as possible.

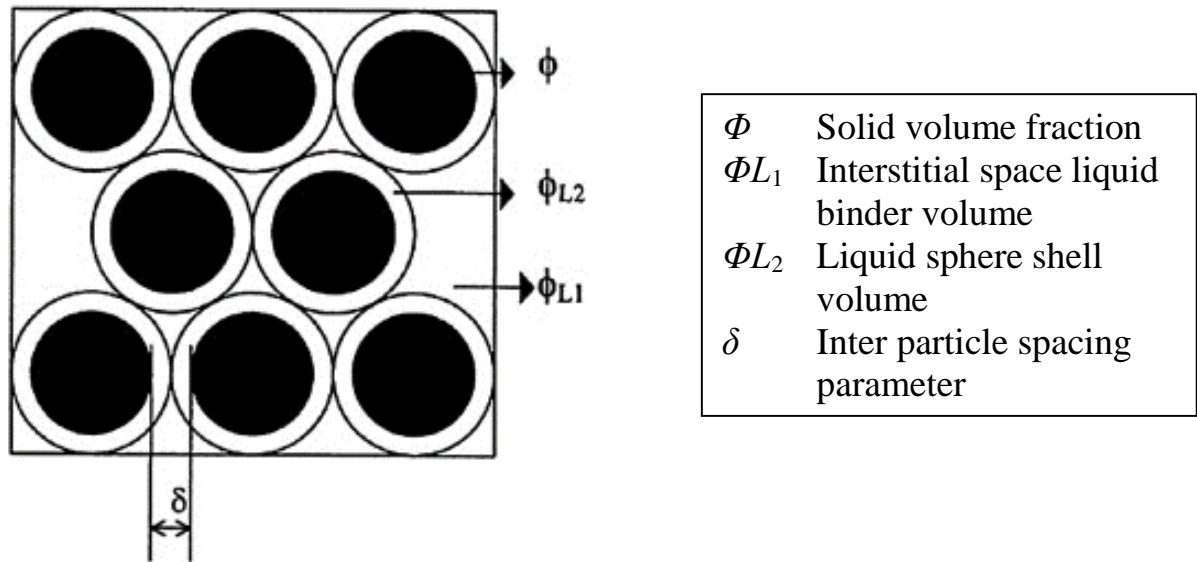


Fig. 5 Coating of spherical particles [40].

Generally, spherical particles increase packing density, while irregular or rounded particles reduce it. In case of mono-sized particles, critical solid loading occurs at 63.7 %, while broader particle size distribution reaches higher packing density up to 74 % and requires lower amounts of the binder [40]. The volume of a binder is different at room or processing temperatures, because most binders have a higher thermal expansion coefficient in comparison with powders. Moreover, variation in particles characteristics such as size distribution, shape or homogeneity dictate the feedstock to be designed with powder loading less than critical. According to German [1], optimal solid loading is approximately 2 to 5 vol. % less than critical.

One of the options of how to modify critical powder loading instead of changing the powder or its characteristics could be binder composition, because critical powder loading depends also on binder viscosity [42]. Low molecular weight polymeric components permit higher volumetric solid loading due to reduction in viscosity. A small addition of SA to the binder is beneficial as well not only because of better homogeneity and processability, but also due to a possibility to increase solid loading [43].

In previous research, there were some investigations regarding the effect of powder loading on injection moulding of ceramic or metal powders. Lin *et al.* [44] added 4 vol. % of SA to the binder for alumina feedstocks and investigated interaction between powder and binder obtaining a reduction of apparent viscosity by a factor of 20. Chan and Lin [45] studied the effect of SA concentration in alumina based feedstocks and pointed out that apart from the increase of feedstock fluidity, the use of the SA was observed to alter flow behaviour from dilatant flow

to pseudoplastic. In addition, inhomogeneous distribution of the binder in injection moulded components was minimized with increasing SA concentration. Nevertheless, as SA was enhanced, the formation of bubbles in the mixtures raised from its vaporization. Influence of SA concentration on zirconia based feedstocks for micro injection moulding was investigated by Hanemann *et al.* [46]. They observed that zirconia based feedstock with powder loading higher than 30 vol. % and without SA cannot be processed reproducibly, while addition of SA enables processing of feedstocks up to 55 vol. %.

Mixing method

The powder and binder can be mixed by two different approaches, dry or wet methods. In the dry method, all components are mixed together at room temperature and then put into a compounder. While, during the wet route, which is most common, the binder is firstly molten and then the powder is gradually added. Crucial for both procedures is to form a homogenous mixture with no agglomerates and without powder binder segregation, because not sufficient homogeneity in the feedstock can introduce defects the moulded products without further possible correction.

Particles with larger size distribution and a binder with lower viscosity are more prone for powder segregation, while smaller particle size and particles with irregular shape tend to lower segregation due to higher inter-particle friction. Ceramics with smaller particles tend to form agglomerates and they need higher shearing during mixing. Otherwise, the agglomerates can lower critical solid loading [47].

The batch mixing usually occurs at high shear rates using a double planetary or Z-blade mixers, while high volume production is performed using twin screw extruders or specially designed shear rolls. During processing, it is important to avoid damage to particles and/or binder overheating. Too low mixing temperatures might enhance feedstock viscosity, which may impair the mixing process. On the other hand, a too high mixing temperature might cause degradation of binder components resulting in lower feedstock viscosity and a higher possibility of powder binder separation. Usually, the twin screw extruder exhibits a superior homogeneity compared to sigma blade mixing [48].

Using twin rotor batch mixer, the homogenous feedstock corresponds to the steady state region of mixing torque as indicated in Fig. 6.

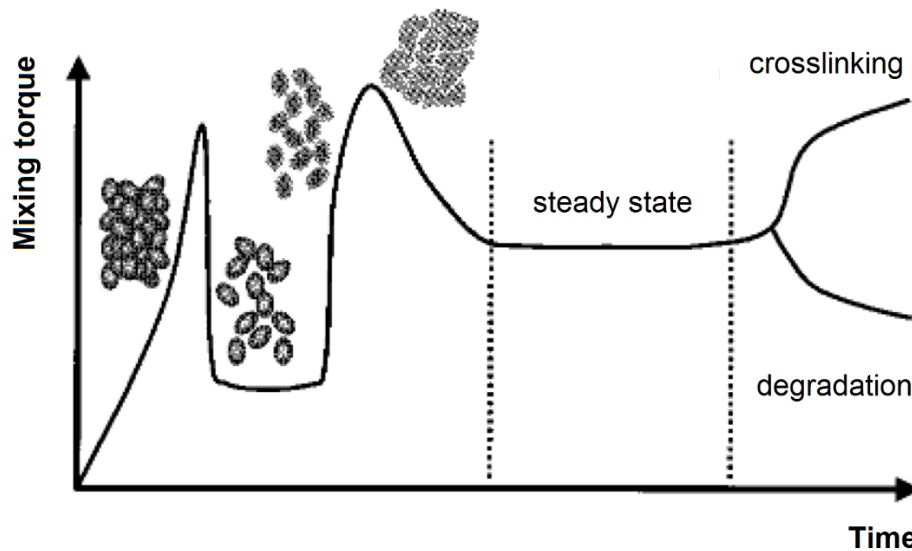


Fig. 6 Torque evolution as a function of time [49].

As the powder is added, the temperature of the feedstock decreases indicating the rapid increase in mixing torque. Consequently, the torque decreases and reaches again a steady state regime. The time required to reach the steady state depends on the material and on processing conditions, such as temperature and rotor speed. In a mixing operation, it is essential to know the time required to achieve a homogenous mixture. According to Bousmina [49] it is typically from 3 to 15 min. It is also recommended to shorten the processing time, if there is no further improvement in homogeneity, because extending the mixing time can cause a negative effect on powder contamination and/or binder degradation. Usually, an erratic torque is an indication of poor homogeneity, as well as excessive power loading.

At the end, the final homogenous feedstock has to be pelletized into PIM pellets to ensure easy feeding into the injection unit. Nowadays, there are companies producing a large variety of PIM feedstocks ready to be used (such as Catamold, PolyMIM or Embemould). In this case, powder characteristics and/or optimal binder constituents are not an issue.

1.3 Determination of critical powder loading

Critical powder loading corresponds to solid loading (see Fig. 4b), where all particles are coated with a thin polymeric layer and packed as tightly as possible without voids between them. PIM feedstocks are formulated with powder loading less than critical to ensure defectless moulding, adequate flow and process flexibility in adjusting final dimensions. Critical solid loading can be

experimentally determined by several approaches. Most commonly used are the measurement of powder-binder mixture density with specific solid loading [3], evolution of the torque during mixing process [50] and viscosity measurement [51]. Theoretical methods include both the calculation of critical solid loading [52] and rheological models that predict the critical powder concentration [53].

However, it must be noted that the interaction between the powder and the binder is not taken in account. This could explain why in some cases the calculated value of critical powder content differs significantly from the real one. Honek *et al.* [54] investigated 15 mathematical models proposed for highly filled systems. Nevertheless, they found that due to a complex structure of powders as irregular shape, particle size distribution, as well as a multi-component character of the binder, the applicability of mathematical models is still a difficult task.

Determination through activation energy

A new approach for determination of optimal solid loading was proposed by Contreras *et al.* [55] through activation energy (E_a) expressing the temperature dependence of viscosity and derived from Arrhenius equation:

$$\eta = Ae^{\left(\frac{E_a}{RT}\right)} \quad (2)$$

- η is the viscosity of PIM feedstock, in Pa.s, at given temperature;
- A is the pre-exponential factor;
- E_a is the flow activation energy, in J/mol;
- R is the gas constant (8.3145 J/K.mol);
- T is the absolute temperature, in K.

Based on their previous research, Contreras *et al.* [56] pointed out that powder particles caused the reduction of viscosity-temperature dependence as its content in the mixture is increased. Moreover, the variation of activation energy with solids loading appeared to follow a parabolic trend, with the minimum value coinciding with optimal solids loading. They thought that minimum activation energy could be a useful indicator for determination of optimal solid loading. According to Li *et al.* [39], the flow activation energy of feedstocks firstly decreases with the increase of powder loading achieving the lowest value of activation energy for feedstock with optimal solid loading, after that the activation energy starts to increase. In their case optimal solid loading was established on the basis of compacts (with different shapes) distortion. They concluded that

higher powder loading is beneficial for feedstock rheological properties in terms of temperature sensitivity. The same phenomenon was confirmed by Aggarwal *et al.* [57] and Kong *et al.* [58].

Determination via density

The feedstock density (ρ_f) deepens on volumetric powder loading (Φ), which can be theoretically calculated using Eq. (3):

$$\rho_f = \Phi\rho_p + (1 - \Phi)\rho_b \quad (3)$$

With a higher amount of powder loading, the measured feedstock density follows a theoretical calculation, as is depicted in Fig. 7.

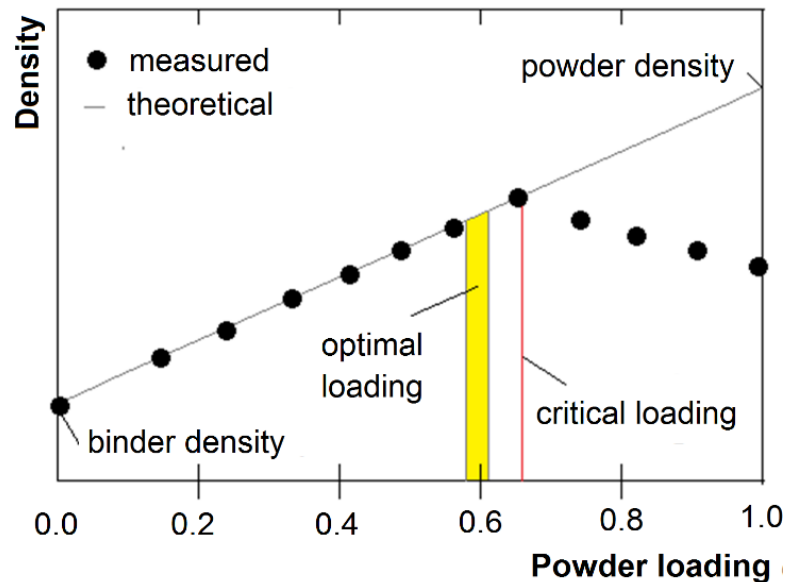


Fig. 7 Experimental mixture density vs powder loading.

However, once the powder volume reaches critical loading, the density falls down from the theoretical line due to formation of voids. Recently, Mukund *et al.* [59] used gas pycnometer for determination of feedstock density in order to obtain critical solid loading, and their analysis coincided well with the results achieved from mixing torque.

❖ Determination via viscosity

The viscosity determination concerns relative viscosity (η_r) defined as:

$$\eta_r = \frac{\eta}{\eta_0} \quad (4)$$

η is viscosity of the filled system,
 η_0 is viscosity of pure binder [57].

As solid loading increases, the capillary forces resist void formation by pulling particles together. This intensifies friction between them up to critical solid loading, where the viscosity becomes essentially infinite, as shown in Fig. 8. The viscosity can be measured on capillary or torque rheometers.

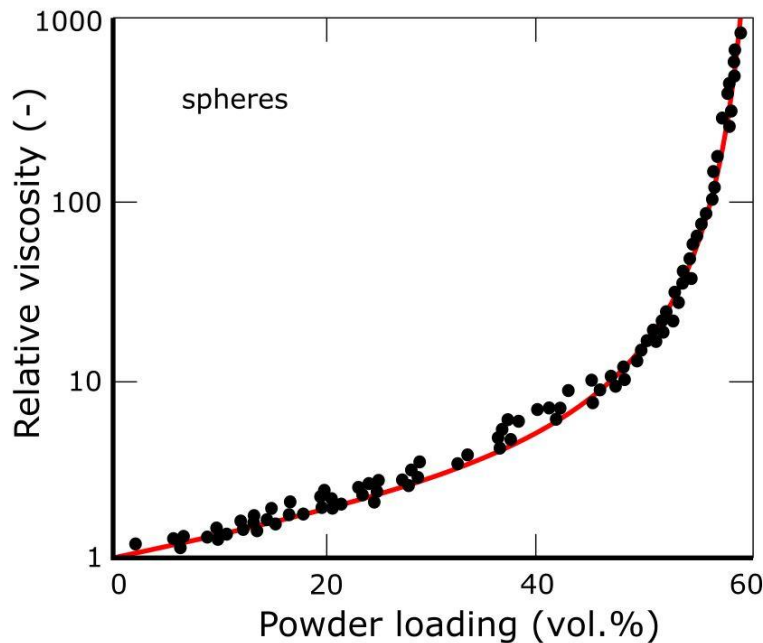


Fig. 8 Relative viscosity as function of powder loading.

Determination via mixing torque

Measurement of mixing torque, also called torque rheometry, is a common method used for the experimental determination of critical solid loading. Fig. 9 demonstrates the evolution of the torque for different solid loading. As can be noticed, when the powder content is increased, the viscosity, and consequently the torque values become higher. As can be observed, there is a dramatic increase in mixing torque at a certain point, and then the torque does not achieve stabilization. This occurs at critical solid loading, when mixing becomes erratic due to a closer contact of particles causing enhanced viscosity. Then, addition of more powder than critical will result in void formation reducing the viscosity which leads to decreasing of torque value.

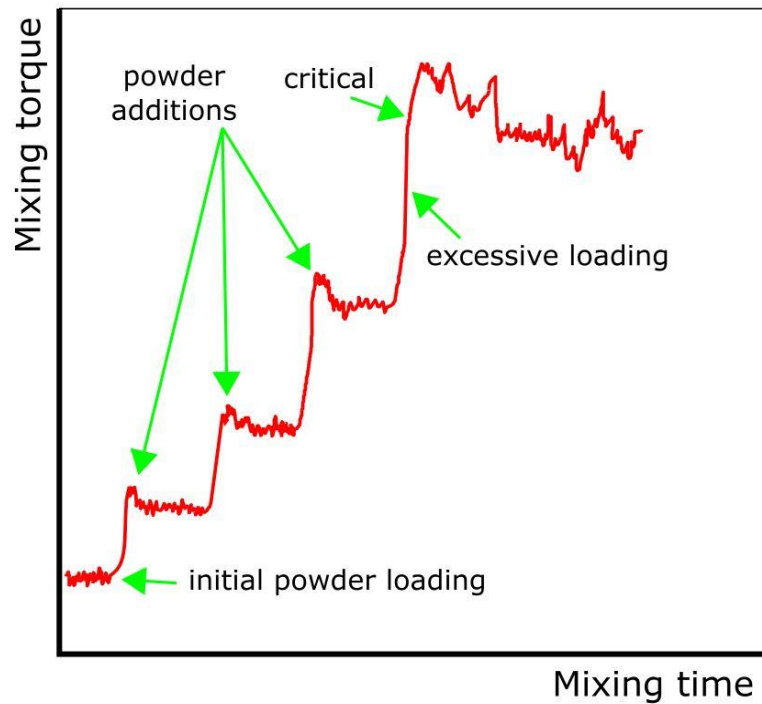


Fig. 9 Torque evolution by continuously increasing powder loading.

Critical powder loading from mixing torque can be obtained by two different ways. It can be carried out by continuously increasing powder loading in the binder system [57] or by increasing powder loading for each batch separately [58]. The advantage of the continuously adding method is fast measuring, while the drawback is that the mixing chamber is filled each time with a higher amount of material that can influence obtained mixing torque. Moreover, the complete testing cycle takes longer time, which can lead to decomposition of low molecular weight binder components.

1.4 Rheological characterization of PIM feedstocks

Successful injection moulding of PIM feedstocks is dictated by its rheological behaviour. Therefore, the knowledge of flow properties is an essential task. PIM feedstocks exhibit complex flow behaviour Fig. 10 that depends on several factors [60]. The most important is shear viscosity, which relates shear stress and shear rate. It is well known that PIM compounds are strongly shear rate dependent despite the fact that low molecular weight components in a binder behave like Newtonian fluids [61]. Adding more powder in the mixture, the Newtonian plateau becomes reduced or disappears in a measured shear rate range [63], as illustrated in Fig. 10.

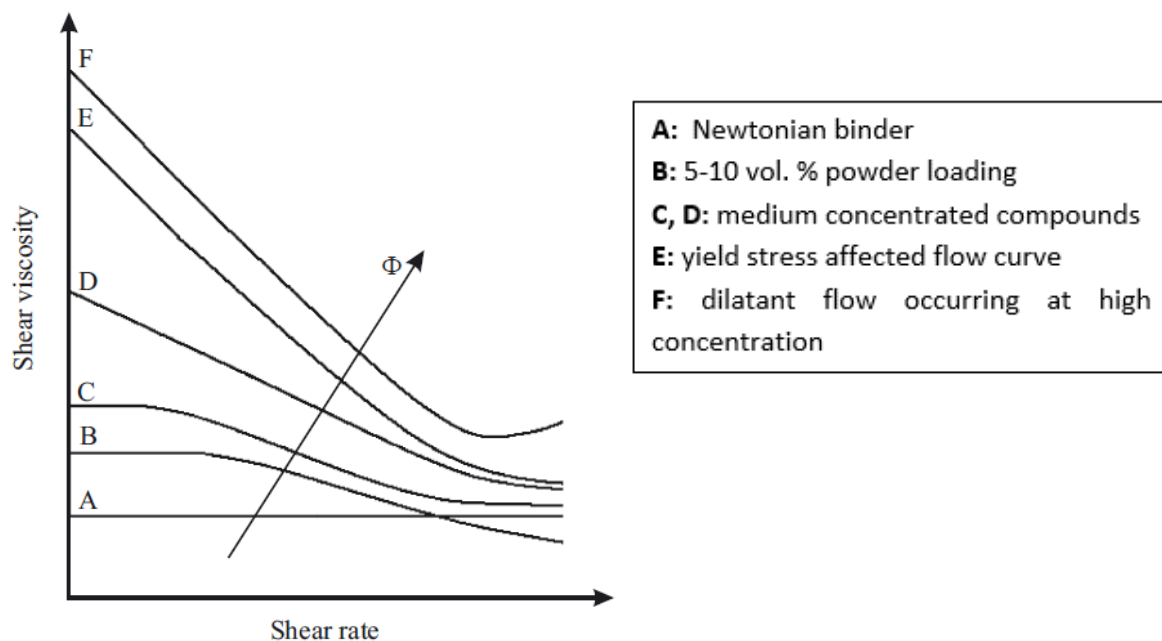


Fig. 10 Schematic view of PIM compound flow properties [63].

As it is well known, the viscosity of feedstock also decreases with a higher temperature. However, processing of PIM feedstocks at enhanced temperature can prolong cooling time and cause some defects in moulded samples due to thermal expansion of the binder.

In addition, most of highly filled systems have to overcome a yield stress to initiate viscous flow. The yield point is the lowest shear-stress value about which a molten feedstock will behave like a fluid. The presence of yield stress is indication of a particle network structure due to strong particle-particle interaction and internal cohesion force. It has a direct relation to the particle size [64]. At a low shear rate the particles are forming a three-dimensional consistent stable structure within the melt. At higher shear rates (after the yield point has been exceeded) this structure is broken and the viscosity is dominated by hydrodynamic interactions [65]. Another phenomenon, which often occurs during flow of highly filled compounds, is wall slip. Mooney proposed a method to detect wall slip during rheological measurements [66-67].

Rheological properties of PIM feedstocks can be obtained from both capillary and/or torque rheometers. Capillary rheometers offer a shear rate range usually from 100 to 10 000 1/s, which corresponds more to real conditions occurring during injection moulding. The results of flow behaviour are then plotted usually in two types of diagrams: as flow curves (shear stress dependence on shear rate) or as viscosity curves (viscosity dependence on shear rate, eventually on shear stress).

For pseudoplastic materials, obtained values from capillary rheometers have to be corrected in order to obtain real values.

Contraction flow at the capillary entrance and exit region causes an extra pressure drop due to stretching and relocation of fluid elements [68] as illustrated in Fig. 11a. The correction of wall shear stress due to entrance and exit effects can be performed by Bagley correction [69] using a series of capillary dies with the same diameter D , but different lengths L , or by using a nominally zero-length capillary, called an orifice die.

Fig. 11b demonstrates the divergence from parabolic velocity profile for non-Newtonian materials inside a capillary die. Correction of apparent shear rate within a capillary die can be calculated according to Weissenberg-Rabinowitsch correction [70] using a non-Newtonian index. The correct shear rate at the wall will depend on the shear sensitivity of the feedstock viscosity. The non-Newtonian index (n) represents the divergence from the Newtonian behaviour and can be obtained from the slope $d(\log \tau)/d(\log \dot{\gamma})$. In the measured shear rate range, the value of this index can vary from point-to-point or it can be constant to all data points. Therefore, there are more possible ways for its determination.

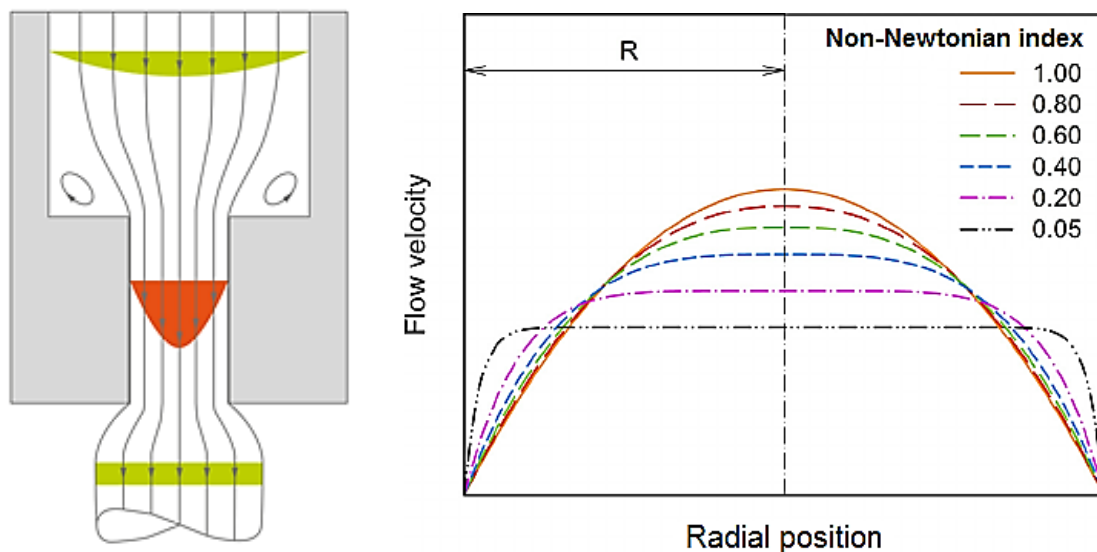


Fig. 11 Schematic view of relocation of melt flow inside a capillary die (a), velocity profiles in a capillary die based on value of non-Newtonian index (b).

Corrections must be performed in the following order: slip correction, entrance-pressure correction and non-parabolic velocity profile correction.

Viscosity-temperature dependence

One of important requirements on PIM feedstocks is their low temperature sensitivity. The relationship between viscosity (η) and temperature (T), the temperature sensitivity of feedstock viscosity can be expressed as flow activation energy according to Arrhenius, Eq. (2). Flow activation energy is the energy required to activate the viscosity flow. Therefore, the flow activation energy (E_a) as a temperature sensitivity indicator is another important aspect of PIM feedstocks [72]. Smaller activation energy is desirable in order to diminish the problems, such as process fluctuation, and further stress concentration, cracks and shape distortion.

Since polymers are non-Newtonian materials, their viscosity at fixed temperature is dependent on shear stress or shear rate. Therefore, a clear differentiation between activation energy at constant shear stress ($E_{a,\tau}$) and activation energy at constant shear rate ($E_{a,\dot{\gamma}}$) must be done. Some authors has shown that activation energy at a constant shear stress ($E_{a,\tau}$) remains constant over a broad range of shear stresses, while activation energy at a constant shear rate ($E_{a,\dot{\gamma}}$) does not [64]. Ren *et al.* [73] investigated the change of activation energy at a constant shear rate and found out that $E_{a,\dot{\gamma}}$ increased with a higher shear rate.

However, the conditions under which the activation energy (E_a) was obtained is sometimes missing in rheological papers [32]. Therefore, the values cannot be compared with other results. Nevertheless, the understanding of temperature sensitivity of shear viscosity is important in the meaning of processing conditions and consequently on the quality of moulded components.

Factors affecting flow behaviour

Fig. 12 shows the main factors affecting flow properties and consequently injection moulding process. First of all, the feedstock composition and powder binder ratio. Powder loading and powder characteristics influence flow properties. The most important characteristics are particle size, shape and particle size distribution as well as their dispersion or agglomeration. Generally, with a higher amount of powder loading the viscosity increases, and the same is valid in case of fixed powder concentration with smaller particle sizes having a larger surface area that leads to an increase in the interaction between powder particles [74]. Higher inter-particle friction then increases the viscosity and can cause difficulties during mixing or injection moulding. Wide particle size distribution tends to reduce the viscosity of filled systems at a fixed loading level [64], because smaller particles

are interposed between larger particles, causing a reduction in the inter-particle impact resulting in decrease in viscosity.

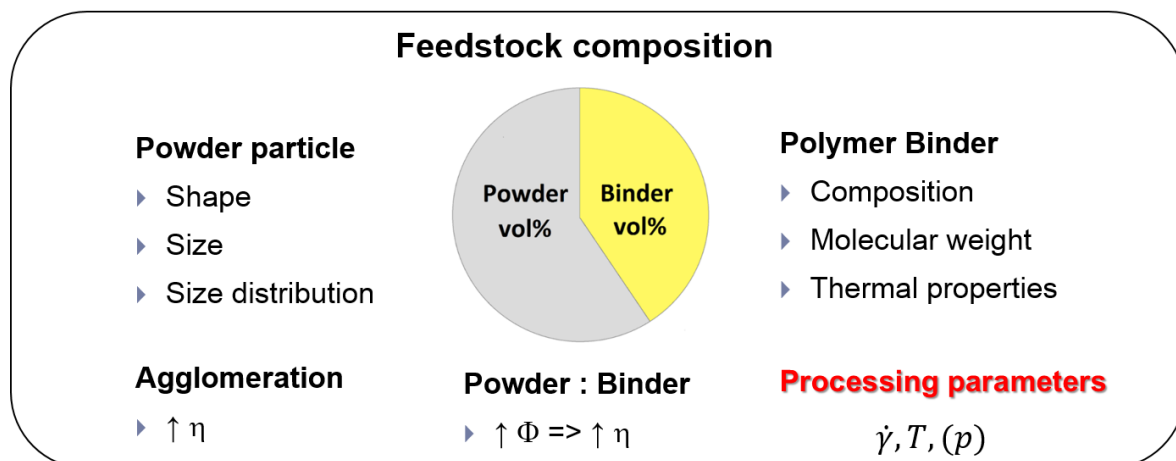


Fig. 12 Main factors affecting flow properties of PIM feedstocks.

The most appropriate method of studying the effect of a polymeric binder is by understanding the steady shear viscosity changes using different polymer systems, but with the same filler and at a fixed level of loading [64]. Feedstock viscosity can be possibly enhanced by a high molecular weight of the binder involved. The viscosity of highly filled systems is less temperature sensitive than viscosity of a pure binder, which is obviously true, because fillers provide very little free volume changes with temperature in relation to a polymer binder [64]. Hayat *et al.* [32] found out that activation energy of feedstock decreased as PEG molecular weight increased.

2 AIM OF THE THESIS

The aim of this doctoral thesis characterization and optimization of binder systems used for PIM technology with emphasis on binder composition, rheological properties and an eco-friendly approach in order to achieve high quality final products. The main framework focuses on accomplishing the following partial aims:

Effect of PEG molecular weight on the PIM process of Inconel 718 based feedstocks.

- Rheological characterization of PIM feedstocks
- Effect of PEG molecular weight on debinding rate at different removal temperatures
- Effect of PEG molecular weight on mechanical properties after sintering and post-heat treatment

Investigation of newly developed binder systems for PIM based on AW and CW as possible substitutes of polyolefin backbone polymers.

- Rheological characterization
- Thermal analysis

Impact of SA on powder loading and flow properties of PIM feedstocks

- Evaluation of powder loading
- Effect of powder loading on flow behaviour
- Influence of SA concentration on feedstock powder loading
- Influence of SA concentration on flow behaviour

EXPERIMENTAL PART

3 MATERIALS AND METHODS

3.1 Powder and binder characteristics

Powder

Throughout the experimental part, 4 types of powders (2 metals and 2 ceramics) were used to formulate and characterise PIM feedstocks: superalloy Inconel 718; 17-4PH stainless steel; aluminum oxide (Al_2O_3), known as alumina, and zirconium dioxide (ZrO_2), known as zirconia. The shapes and sizes of powder particles were obtained by Scanning Electron Microscopy (SEM) using a Vega II LMU Tescan for metals and a Nova NanoSEM 450 (FEI) for ceramics, as is shown in Fig. 13.

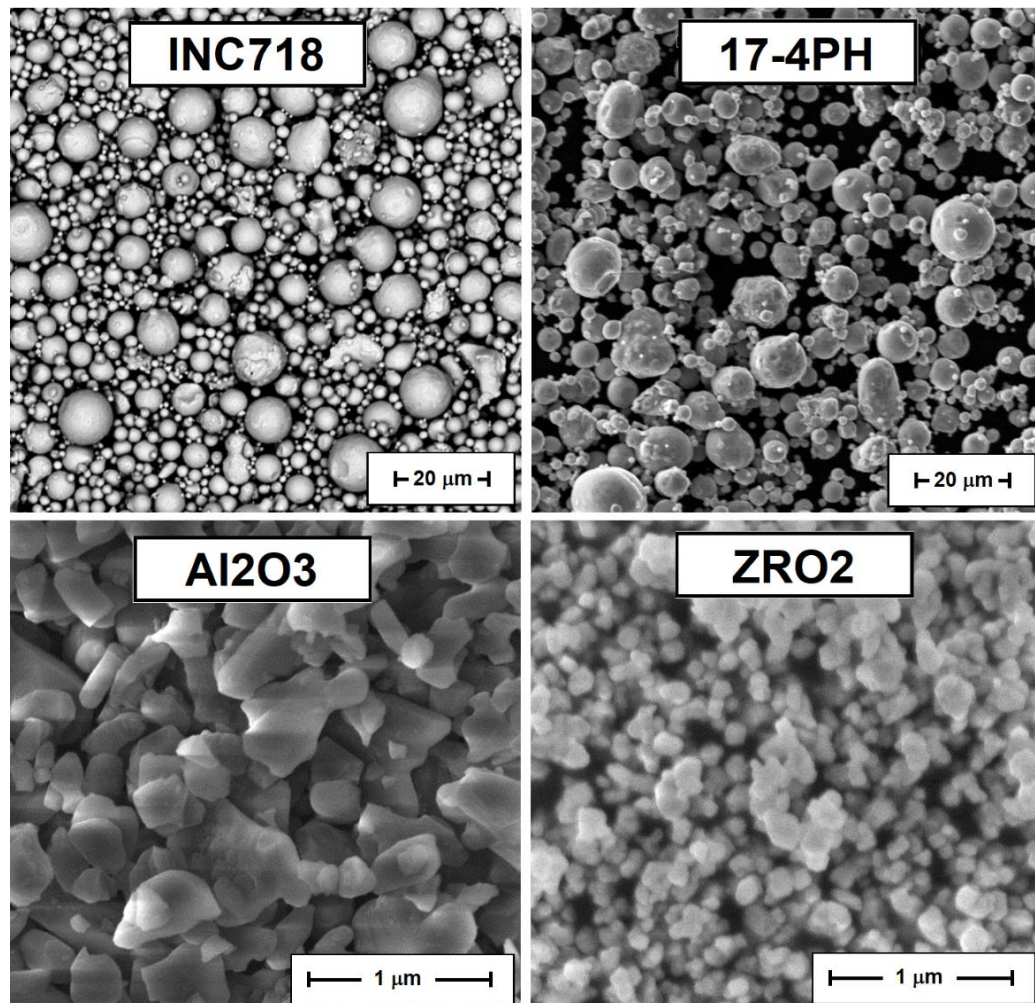


Fig. 13 SEM photographs of utilised powders.

Gas atomised nickel based superalloy Inconel 718 (IN718) and gas atomized 17-4 PH stainless steel powder were provided by Sandvik Osprey. Both metal powders have spherical shape with high purity surface. From ceramics, a highly compressive ceramic super-ground alumina (Al_2O_3) powder (Martodix MR 70) provided by Albermarle Corporation and zirconia (ZrO_2) supplied by Vibrom were used. As can be noticed, ceramic powders are one magnitude smaller than metals and have a highly irregular shape of powder particles, with a tendency to agglomerate, especially in case of zirconia.

Particle size distribution (Fig. 14) was carried out by laser diffraction using a particle size laser analyser Malvern Mastersizer 3000, and density of the powder was obtained using an UltraFoam 1200e Automatic gas pycnometer under nitrogen atmosphere. Tab. 2 summarises physical properties of powders used.

Tab. 2 Powder characteristics.

Powder	D₁₀ (μm)	D₅₀ (μm)	D₉₀ (μm)	Density (g/cm^3)
INC718	4.36	8.96	17.8	8.19
17-4PH	3.25	8.28	15.8	7.79
Al_2O_3	0.30	0.56	2.50	4.05
ZrO_2	0.12	0.43	3.80	6.24

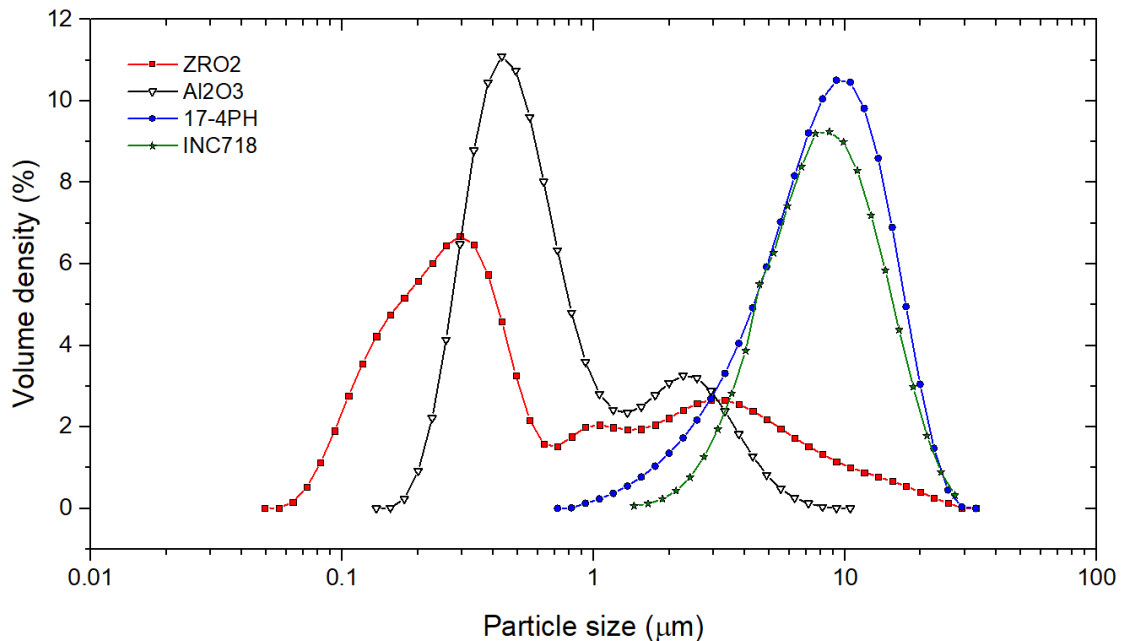


Fig. 14 Volumetric particle size distribution.

Binder components

Individual polymeric components are listed in Tab. 3 according to their role in the binder. Apart from these individual components, the commercially available binder system Licomont (unknown composition) was also utilised.

Tab. 3 List of the individual binder components.

Major component	PEG	Poly(ethylene glycol)
	PW	Paraffin wax
Backbone	EVA	Ethylene-vinyl acetate
	PMMA	Poly(methyl-methacrylate)
	LDPE	Low-density polyethylene
	CW	Carnauba wax
Surfactant	AW	Acrawax
	SA	Stearic acid
	OA	Oleic acid

❖ *Major components*

PEG is a well-known component in the design of PIM feedstocks. For the purpose of this project, its molecular weight varied in the range from 1 000 to 20 000 g/mol (using PEG 1 000, PEG 1 500, PEG 4 000, PEG 6 000, PEG 8 000, PEG 10 000, PEG 12 000 and PEG 20 000). PW is a low molecular weight component produced from petroleum. It consists of a mixture of hydrocarbon molecules containing between 20 to 40 carbon atoms. This white wax substance is insoluble in water and is beneficial for decreasing the viscosity of feedstocks. EVA an ethylene-vinyl acetate block copolymer. In solid form, it is soft and flexible.

❖ *Backbones*

PMMA as a backbone component is often used, particularly with water soluble PEG based feedstocks, while LDPE is a typical backbone component of polyolefin based feedstocks. AW is a white fine powder (in atomized form with a mean particle size of 6 μm). It is traditionally used as a lubricant and binder for cold compaction of powdered metal parts, and also as dispersants, slip additives or anti-blocking agent. CW is a natural wax formed in the leaves of the Brazilian palm, it appears as a yellow colour hard wax. In this study, both CW and AW were considered as possible substituents of polyolefin backbone polymers.

❖ *Surfactants*

SA and OA, both belonging to a category of fatty acids, are widely used in PIM technology. SA with 18 carbon atoms in a chain appears a white waxy solid and has a strong tendency to adsorb on the surface of Al₂O₃. OA is also beneficial for decreasing viscosity of mixtures and dispersion of powders. Compared to SA, OA is liquid at room temperature. Both, SA and OA are not soluble in water, but can be eliminated by thermal debinding (pyrolysis).

Binder characteristics

Material density and thermal properties are the most important characteristics for the calculation of proper amounts of each component in mixtures and for setting appropriate processing parameters. Density was measured using an automatic gas pycnometer UltraFoam 1200e (Quantachrome Instruments) under nitrogen atmosphere. Thermal properties were evaluated by different scanning calorimeter (DSC) using a DSC 1 (Mettler Toledo) from the second heating scan at the rate of 10°/min under nitrogen atmosphere. In both cases, PEGs was measured under argon atmosphere. Material characteristics including density (ρ) and melting temperature (T_m) of polymer binders used in this thesis are summarized in Tab. 4.

Tab. 4 Material characteristics of binder components.

Material	Identification	Supplier	ρ (g/cm³)	T_m (°C)
PEGs ¹	1 000 – 20 000	Sinopol, Sigma-Aldrich	1.21-1.23	Fig. 15
PW	hard, grated	Kulich Pharma	0.91	58
PMMA ²	emulsion	Scott Bader Co Ltd	1.10	-
LDPE	1200 MN 18	Total	0.92	106
EVA	Escorene™ Ultra UL 40028C	ExxonMobil Chemical	0.95	69
CW	2442	Kratoska Chemin	1.00	84
AW	Atomised C	Lonza	1.05	145
SA	95 %	Sigma-Aldrich	1.01	71
OA	Fatty acids >97%	Penta	0.85	13
Licomont ³	EK 583	eMBe	1.07	Fig. 16

¹ PEG components varied in molecular weight in a range (1000 – 20,000 g/mol).

² Specially prepared emulsion with 40 wt. % of finely dispersed 0.1 - 0.2 μ m PMMA particles (M_w – 10⁶ g/mol).

³ Commercially available multicomponent binder system of unknown composition (partially water-soluble).

Fig. 15 demonstrates thermal properties of selected PEGs (based on their molecular weights) and the commercial Licomont, respectively. As can be seen, with higher molecular weights of PEGs, there was an increase in melting temperature.

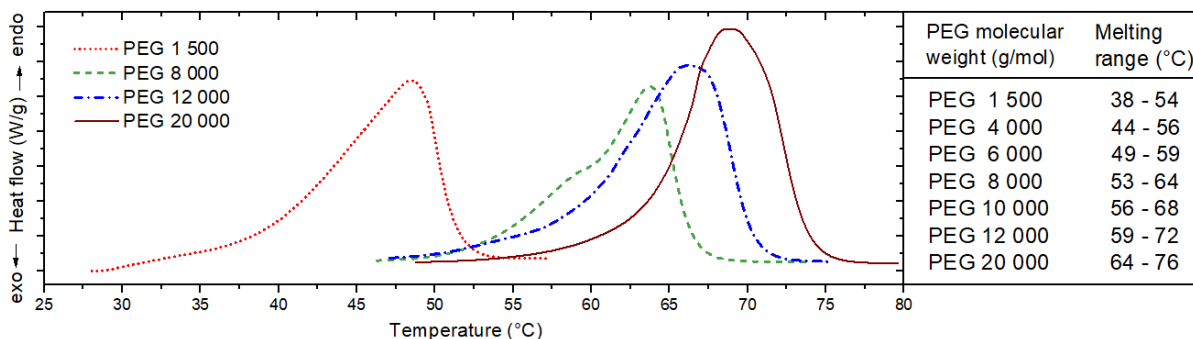


Fig. 15 Melting ranges of PEGs obtained from DSC.

Fig. 16 shows thermal properties of Licomont obtained from DSC. The three distinguished zones are observed indicating a multicomponent binder character.

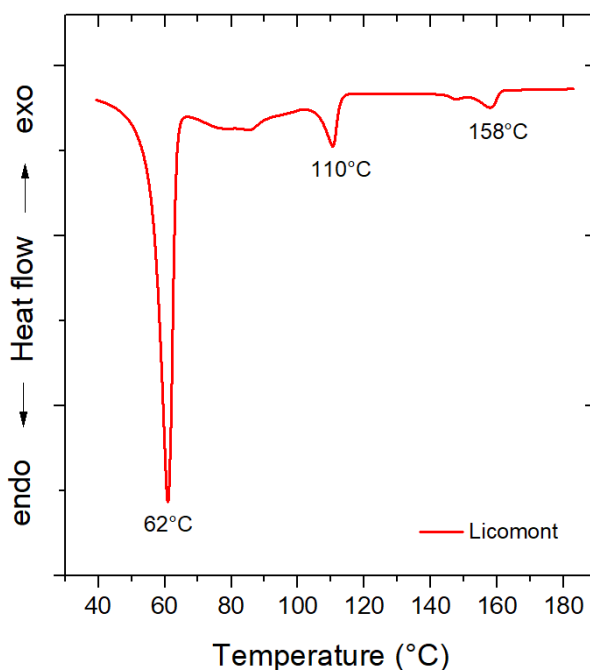


Fig. 16 Thermal analysis of Licomont.

PEG molecular weight (in the range 1.5K to 20K) was evaluated by high-performance liquid chromatography (HPLC) on a HPLC Breeze system (Waters). This equipment operated in a Gel Permeation Chromatography (GPC) mode, coupled with an Evaporative light scattering detector (ELSD) Waters 2424 set as follows: nebulizer temperature 12 °C, drift tube 40 °C, N₂ pressure 60psi.

Separation was conducted using a Shodex Ohpak SB-806M HQ bed column (300×8 mm, 13 µm particles). The mobile phase was water with flow rate equalled 1.0 mL/min and injection volume was 10 µL. The GPC system was calibrated with narrow pullulan standards ranging from 180 to 708 000 g/Varian.). All data processing was carried out using Empower software. Polymer samples of approximately 3 mg were dissolved in 1 mL of deionized water and filtered prior to analysis. Distribution of PEG molecular weights is depicted in Fig. 17.

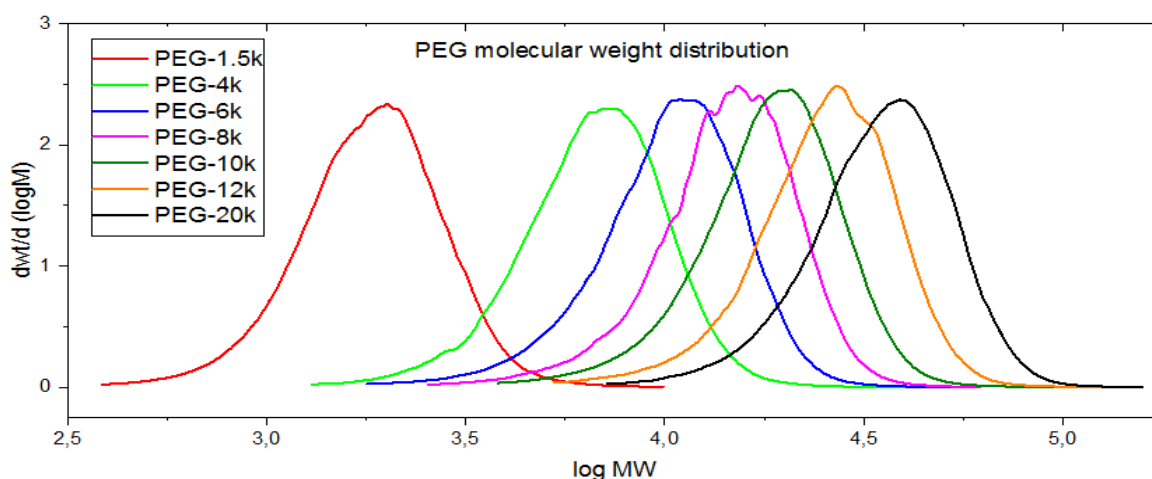


Fig. 17 Distribution of PEG molecular weight.

As can be seen, distribution of molecular weights is the same for all PEG components. Tab. 5 shows obtained values of number-average molecular weight (M_n) and weight-average molecular weight (M_w) including polydispersity index (PDI) as the ratio of M_n/M_w . The values of molecular weight varied from those indicated by producers. This can be caused by different calibration standards. However, for labelling in this work molecular weights indicated by the producer have been used.

Tab. 5 HPLC analysis of PEG molecular weight.

Sample	M_n (g/mol)	M_w (g/mol)	PDI (-)
PEG 1.5K	1600	2000	1.25
PEG 4K	5800	7100	1.22
PEG 6K	8900	11100	1.25
PEG 8K	12500	15200	1.22
PEG 10K	16000	19600	1.23
PEG 12K	21800	27100	1.24
PEG 20K	30700	37300	1.21

Multicomponent binder systems

In order to formulate PIM feedstocks, various binder systems (Tab. 5) were used throughout this work. All compositions (except of polyolefin based binder containing EVA) are partially water-soluble.

Tab. 6 Compositions of binder systems utilised though this study.

Backbone	Major binder/s	Additive/s
PMMA	PEG -	SA
LDPE	PEG PW	SA, OA
CW	PEG PW	SA, OA
AW	PEG PW	SA, OA
LDPE	EVA PW	SA
Commercial binder		Additive/s
Licomont -		SA

3.2 PIM feedstocks formulation and processing

In order to compare PIM feedstocks with others, the powder binder ratio is formulated based on volumetric powder loading (vol. %). While, the composition of binder system is indicated in weight percentage (wt. %). Detailed formulation of the feedstocks is described for each section separately (see results and discussion chapter). Volumetric powder loading (Φ) was calculated according to Eq. (1) using measured density of powder and binder components.

A summary of feedstock compositions used in this work:

- Effect of [**major part**] → various PEG molecular weight

Powder	Binder
Inc718 (59 vol. %)	PEG/PMMA/SA

- Effect of [**backbone**] binder → LDPE, CW, AW vs. commercial binder

Powder	Binder
Al ₂ O ₃ (50 vol. %)	LDPE PW PEG OA
	CW PW PEG SA
	AW PW PEG SA
	Licomont SA

- Effect of [**surfactant**] → various concentration of SA (0 - 5 wt. %)

Powder	Binders			
Torque: Al ₂ O ₃ (50 - 60 vol. %) Rheo: Al ₂ O ₃ (52 vol. %)	LDPE CW	EVA PEG	PW	SA
Rheo: ZRO ₂ (52 vol. %)	Licomont			SA

- Evaluation of [**powder loading**] → Al₂O₃, 17-4PH on critical volume and flow properties

Powder	Binder	
Al ₂ O ₃ (50 – 60 vol. %)	Licomont	SA
17-4PH (60 - 70 vol. %)		

Preparation of PIM feedstocks

Mixing of all PIM feedstocks (apart from those based on Inconel 718 powder) was performed on a Brabender Plastograph equipped with a Mixer W50 EHT (Fig. 18). The Plastograph is a universal torque rheometer for testing the quality and processability of polymeric materials. The mixer is suitable for laboratory-scale production of PIM feedstock samples usable also for further investigation.



Fig. 18 Brabender Plastograph equipped with Mixer W50.

The volume of the mixing chamber (Fig. 19a) is approximately 50 cm³ and contains roller blades with counting rotating rotors. The rotation speed of blades

was set to 50 rpm, while the mixing temperature was dependent on the binder composition and melting temperature of its polymeric components. During mixing, the Plastograph provides information on the torque, temperature values, as well as mechanical energy input in time (Fig. 19b). This makes it an optimum tool for investigation of highly filled compounds.

Feedstocks intended for rheological investigation were compounded in the mixing chamber filled to 90 % of its volume for max. 30 min, which was a sufficient time period to obtain steadily torques indicating acceptable homogeneity of the feedstocks. This device was also used to observe torque evolution with increasing powder loading during mixing. Evolution of mixing torque was carried out via two techniques: by continuously and separately increasing powder volume loading within the mixing chamber. For continuously increasing powder loading, the mixing chamber was initially filled of 75 % of its volume, while for second method, the chamber was filled at fixed 90 vol. %. These mixtures can be then utilized for rheological investigation.

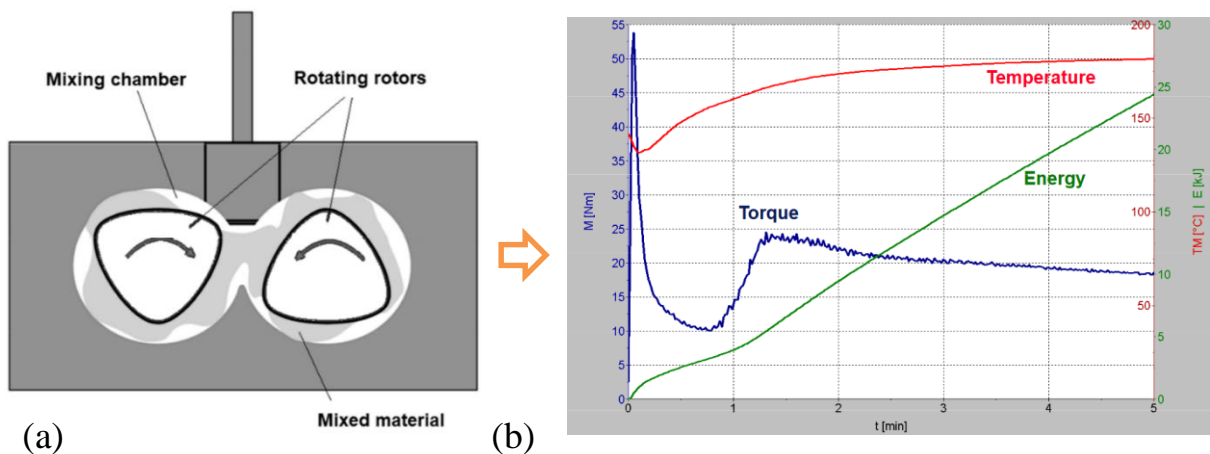


Fig. 19 Schematic view of mixing chamber (a) and measured values during mixing (b).

The mixing procedure of Inconel 718 powder and binder was performed at room temperature in a centrifugal SpeedMixer DAC 5000. This dual axial centrifuge (Fig. 20) works by spinning of its high speed mixing arm in one direction, while the basket rotates in the opposite direction. The advantage of this technique is a combination of forces in different planes enabling fast mixing. This is due to the dissipation energy generated by the shear action within mixed feedstock, causing the binder components to melt. The advantage of this method is time saving and an almost clean and comfortable preparation. On the other hand, the drawback is that the processing temperature cannot be set up or

monitored. Additionally, if excessively high temperatures are generated during mixing, it may have a negative impact on degradation of polymeric components.

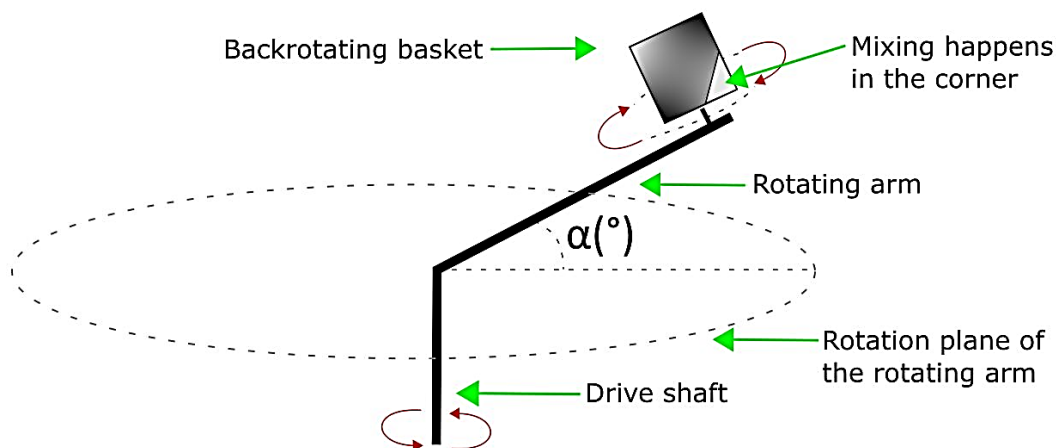


Fig. 20 Schematic principle of dual axial centrifuge.

Injection moulding

After mixing, the feedstocks based on Inconel 718 powder were dried in a laboratory oven at 30 °C for 24 h, pelletized and extruded twice by using an injection unit of Arburg 320 C Allrounder at 120 °C to ensure appropriate homogenization. Tensile bars (Fig. 21) were moulded from prepared feedstocks using the same injection moulding machine with a 30 mm diameter screw.

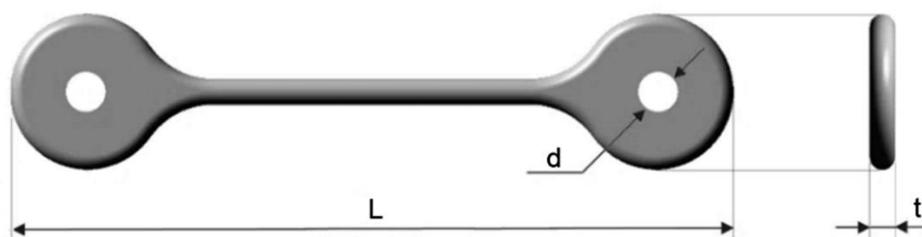


Fig. 21 Schematic view of tensile test specimen.

Debinding and sintering

Water debinding of moulded test specimens was carried out within a pre-heated distilled water bath at three temperatures: 40, 50 and 60 °C. Thermal debinding of remaining binder components (SA, PMMA) was performed as the second stage of debinding and early stage of sintering. Both, thermal debinding and sintering were carried out in one cycle using a Centorr VI MIM vacuum furnace under argon atmosphere according to the profile as illustrated in Fig. 22.

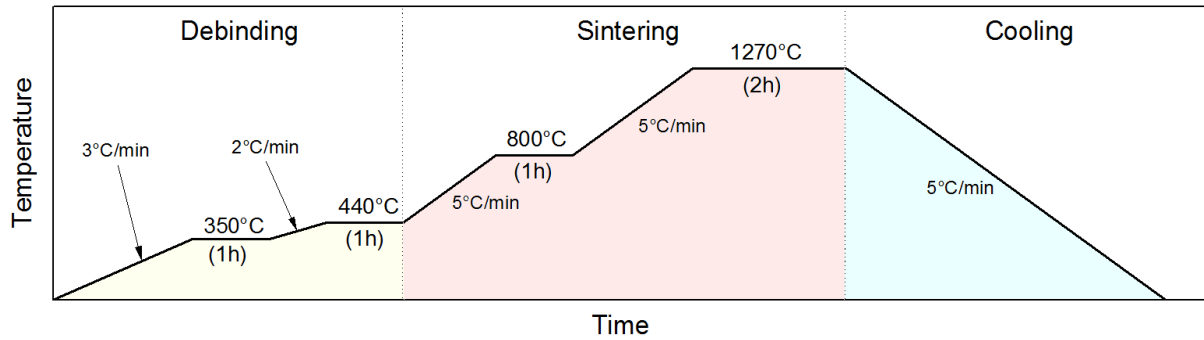


Fig. 22 Thermal debinding, sintering and cooling profile.

After the sintering process, the densities of sintered Inconel 718 tensile test specimens were measured according to ASTM B962-08 using the Archimedes' principle. Heat treatment of sintered samples was carried out according to the solution treatment and ageing profile as shown in Fig. 23. Sintered and heat treated tensile samples of Inconel 718 (only those previously debinded in water bath at 40 °C) were subjected to tensile testing.

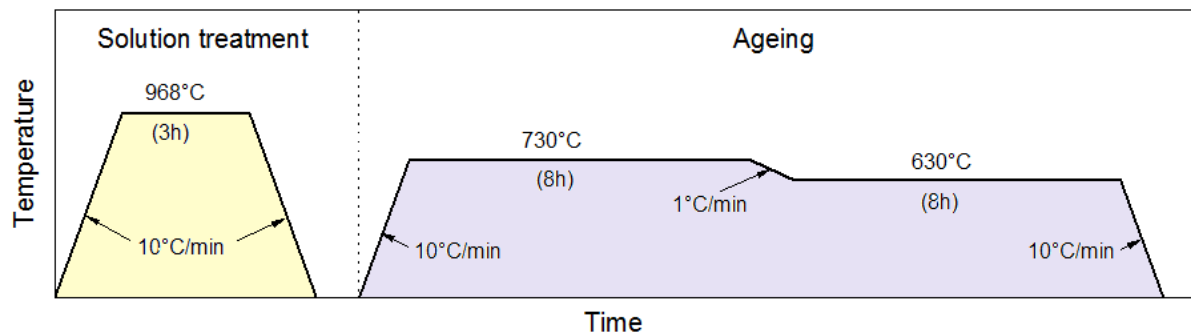


Fig. 23 Solution Treatment and Ageing Profile for Inconel 718.

3.3 Rheology of PIM feedstocks

Rheological measurements were carried out using a capillary rheometer Goettfert RG50 equipped with various length-to-diameter (L/D) capillary dies having a flat entrance angle (180°) of the L/D ratio in mm/mm: (20/1), (10/1), (5/1) and zero length capillary die (0/1) and with pressure transducers of accuracy 0.2 % within the range from 200 to 2 000 bar. All measurements were performed in a controlled-rate mode, *i.e.* at various constant piston speeds, which were subsequently converted to shear rates. The pressure generated at the bottom of the reservoir was then used to calculate shear stress. However, for non-Newtonian materials, these values are only apparent and have to be corrected.

Rheological corrections applied in this work:

- Bagley → correction to apparent wall shear stress (τ_a) due to entrance and exit pressure effects as a consequence of resistance to relocation of the fluid element from the barrel into a narrow capillary die.
- Weissenberg-Rabinowitsch → correction to apparent wall shear rate ($\dot{\gamma}_a$) due to non-parabolic velocity profile.

The contraction flow at the capillary entrance and exit region causes an extra pressure, known as end effects, due to stretching of the fluid elements. As can be seen in Fig. 24a, the pressure transducer is placed at the bottom of the barrel slightly above the capillary die. Therefore, the pressure measured (Δp) is the total pressure in the barrel and consists of three partial parts: entrance pressure (Δp_{ent}), capillary pressure (Δp_{cap}), and exit pressure drop (Δp_{exit}), as illustrated in Fig. 24b.

The entrance pressure drop (Δp_{ent}) is an excess pressure generate at the entrance of capillary die. In case of pure materials, it is a consequence of resistance to elongation due to relocation of the fluid element from the barrel into a narrow capillary die. While, the capillary pressure (Δp_{cap}) is a pressure drop generated over the length of the capillary die, where the flow is fully developed and it depends on shear viscosity of the feedstock. The exit pressure drop (Δp_{exit}) is then an excess pressure generate at the exit of capillary die due to relocation of the fluid elements.

In order to calculate with the correct pressure drop across the capillary, the excess of entrance (Δp_{ent}) and exit pressure drop (Δp_{exit}), known as end effects (Δp_{end}), must be subtracted from the total pressure drop (Δp).

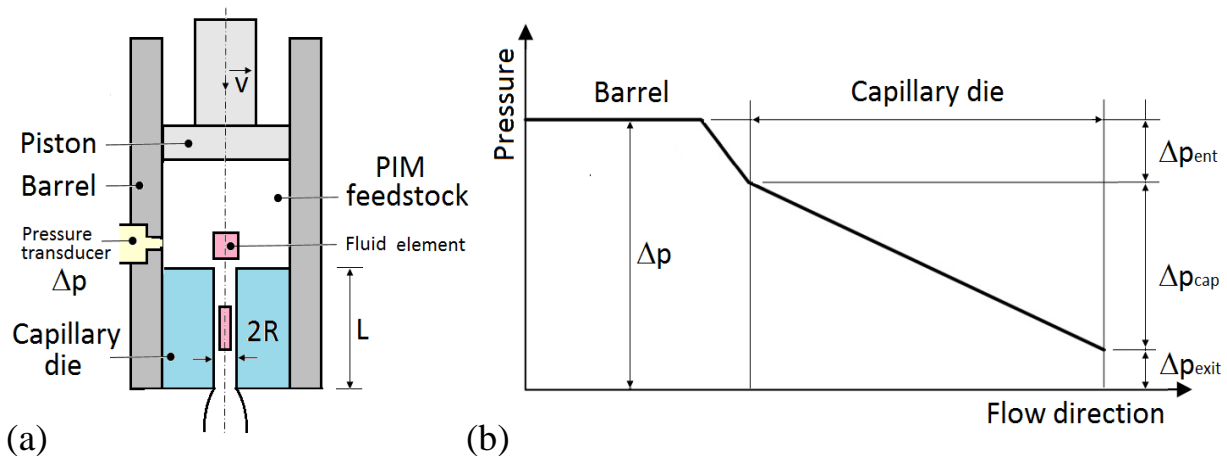


Fig. 24 Schematic view of (a) capillary rheometer, (b) pressure drops.

The values of end effects (Δp_{end}) were obtained in two ways:

- indirectly \rightarrow by using a series of capillary dies with the same diameter D but different L/D ratio (Fig. 25a) and then extrapolating the data, and
- directly \rightarrow by using an orifice (zero-length) die (Fig. 25b).

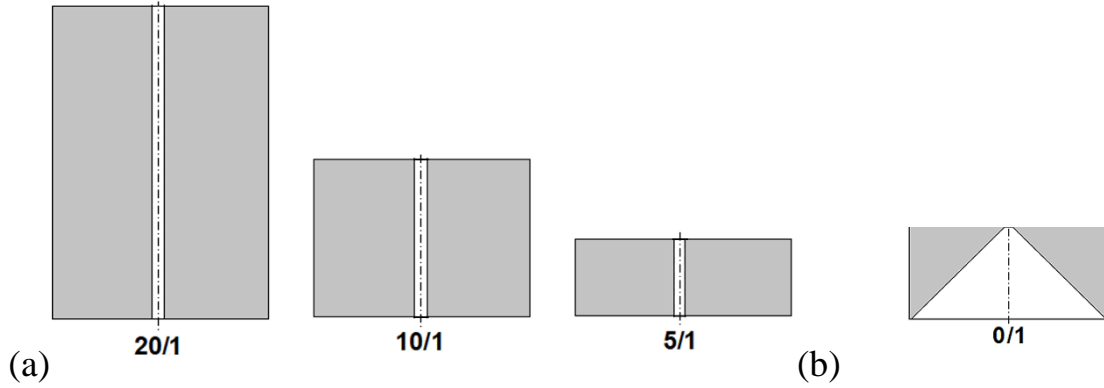


Fig. 25 Capillary dies for indirect (a), and direct (b) measurement of end effects.

Measured data processing - rheology

Rheological characteristics of PIM feedstocks were calculated by the following equations.

Apparent wall shear rate ($\dot{\gamma}_a$), in 1/s, is given by the equation:

$$\dot{\gamma}_a = \frac{4\dot{Q}}{\pi R^3} = \frac{4Sv}{\pi R^3} \quad (5)$$

- \dot{Q} is volumetric flow rate, in m^3/s ;
- R is a radius of capillary die, in m;
- S is an area of the barrel, in m^2 ;
- v is piston velocity, in m/s.

Apparent wall shear stress (τ_a), in Pa, is given by the equation:

$$\tau_a = \frac{\Delta p R}{2L} \quad (6)$$

- Δp is the measured pressure drop obtained from the barrel above the capillary die, in Pa (1bar = 100 kPa);
- L is the length of the capillary, in m.

Apparent shear viscosity (η_a), in Pa.s, is given by the equation:

$$\eta_a = \frac{\tau_a}{\dot{\gamma}_a} \quad (7)$$

Corrected wall shear stress (τ_c), in Pa, is given by the equation:

$$\tau_c = \frac{(\Delta p_{cap})R}{2L} = \frac{(\Delta p - \Delta p_{end})R}{2L} = \frac{[\Delta p - (\Delta p_{ent} - \Delta p_{exit})]R}{2L} \quad (8)$$

Δp_{cap} is the pressure drop over the length of capillary die;

Δp_{end} is the pressure drop in capillary die;

Δp_{ent} is the entrance pressure drop in capillary die;

Δp_{exit} is the excess pressure drop at the exit of the capillary die.

Corrected wall shear rate ($\dot{\gamma}_c$), in 1/s, according to Weissenberg-Rabinowitsch correction is given by the equation:

$$\dot{\gamma}_c = \dot{\gamma}_a \left(\frac{3n + 1}{4n} \right) \quad (9)$$

n is the non-Newtonian index.

Non-Newtonian index (n), without units, is given by the formula:

$$n = \frac{d \log(\tau_c)}{d \log(\dot{\gamma}_a)} \quad (10)$$

The approximation function could be given by the following formulas:

- Linear regression (1st order polynomial fit):

$$\log(\tau_c) = a \log(\dot{\gamma}_a) + b \quad (11)$$

- Non-linear regression (2nd order polynomial fit):

$$\log(\tau_c) = a \log^2(\dot{\gamma}_a) + b \log(\dot{\gamma}_a) + c \quad (12)$$

- Non-linear regression (3rd order polynomial fit):

$$\log(\tau_c) = a \log^3(\dot{\gamma}_a) + b \log^2(\dot{\gamma}_a) + c \log(\dot{\gamma}_a) + d \quad (13)$$

The non-Newtonian index (n) is derived from:

- the 1st polynomial fit, Eq. (11), as follows:

$$n = \frac{d \log (\tau_c)}{d \log (\dot{\gamma}_a)} = a \quad (14)$$

- the 2nd polynomial fit, Eq. (12), as follows:

$$n = \frac{d \log (\tau_c)}{d \log (\dot{\gamma}_a)} = 2a(\dot{\gamma}_a) + b \quad (15)$$

- the 3rd polynomial fit, Eq. (13), as follows:

$$n = \frac{d \log (\tau_c)}{d \log (\dot{\gamma}_a)} = 3a(\dot{\gamma}_a)^2 + 2b(\dot{\gamma}_a) + c \quad (16)$$

Corrected viscosity (η_c) in Pa.s, is then given by the formula:

$$\eta_c = \frac{\tau_c}{\dot{\gamma}_c} \quad (17)$$

Temperature sensitivity of feedstock viscosity, expressed as the flow activation energy (E_a), was calculated according to Arrhenius Eq. (2). The natural logarithm of it is given by the equation:

$$\ln \eta = \ln A + \left(\frac{E_a}{R} \right) \frac{1}{T} \quad (18)$$

According to Eq. (18), activation energy (E_a) can be calculated from the slope of ($\ln \eta$) vs. ($1/T$) as graphically illustrated in Fig. 26. The viscosity used is obtained at a certain shear rate or shear stress.

Activation energy at constant shear stress ($E_{a,\tau}$), in J/mol, is given as follows:

$$E_{a,\tau} = R \left[\frac{\ln A}{(1/T)} \right]_{\tau} \quad (19)$$

Activation energy at constant shear rate ($E_{a,\dot{\gamma}}$), in J/mol, is given as follows:

$$E_{a,\dot{\gamma}} = R \left[\frac{\ln A}{(1/T)} \right]_{\dot{\gamma}} \quad (20)$$

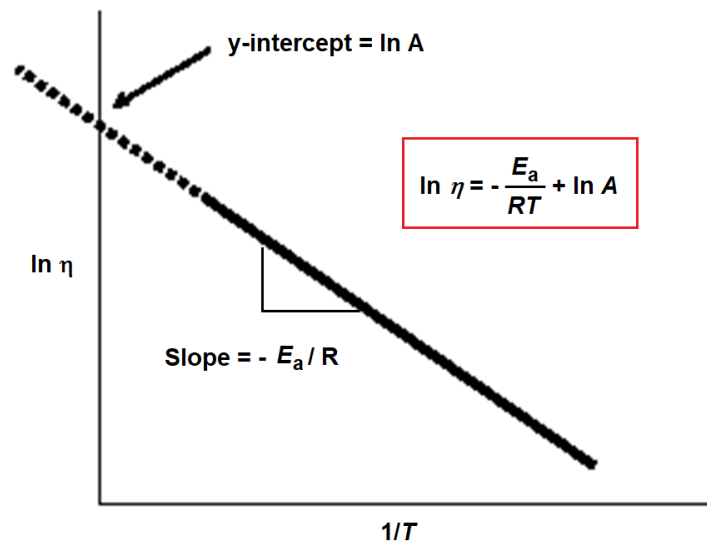


Fig. 26 Arrhenius plot.

3.4 Mechanical properties of sintered tensile samples

Sintered and heat treated tensile samples of Inconel 718 were subjected to tensile testing at room temperature using Zwick Roell Z050 machine. An initial load of 10 N had been applied before the test speed (force-controlled) increased to 0.5 N/s and persisted until the sample was fractured. Then, the following values were calculated:

- Tensile strength (R_m) - stress, corresponding to the maximum force.
- Proof strength ($R_{p0.2}$) is the stress at which extension is equal to a 0.2 % of the gauge length.
- Young's modulus (E) is a mechanical property that measures the stiffness of a solid material.

Schematic view of stress-strain plot is illustrated in Fig. 27.

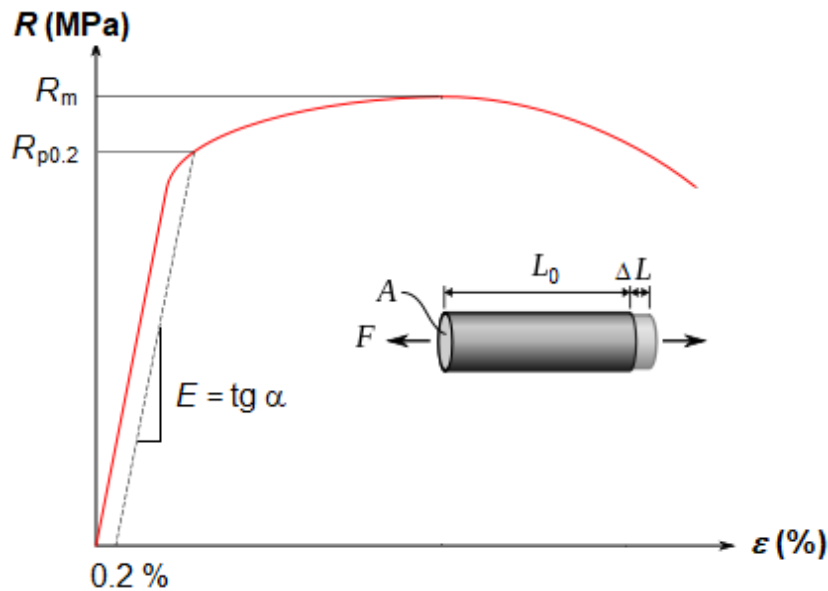


Fig. 27 Schematic view of stress-strain diagram.

❖ Measured data processing - Tensile testing

Tensile strength (R_m), in Pa, is given by the equitation:

$$R_m = \frac{F_m}{S_0} \quad (21)$$

F_m is a maximum (the greatest) force which the test piece withstands during the test, in N;

S_0 is an original cross-sectional area before testing, in m^2 .

Proof strength ($R_{p0.2}$), in Pa, is given by the equitation:

$$R_{p0.2} = \frac{F_{0.2}}{S_0} \quad (22)$$

$F_{0.2}$ is a force which the test piece reach at a plastic strain of 0.2 %, in N.

Young's modulus (E), in Pa, is given by the equitation:

$$E = \operatorname{tg} \alpha = \frac{R}{\varepsilon} = \frac{F/A}{\Delta L/L_0} = \frac{F \cdot L_0}{A \cdot \Delta L} \quad (23)$$

R is the uniaxial stress (in the elastic region) in Pa;

ε is the strain, without units;

F is the tensile force, in N;

- A is the nominal cross-section of the specimen, in m^2 ;
- ΔL is the change in gauge length, in m;
- L_0 is the initial gauge length, in m.

Statistics

For a data set, the arithmetic mean (\bar{x}), as the central value of a discrete set of numbers, is calculated according to the given equation:

$$\bar{x} = \frac{1}{n} \sum_{i=1}^n x_i \quad (24)$$

- \bar{x} the arithmetic mean of measured values;
- n the size of the set of values;
- x_i is an each of values of the data.

Error bars in this work are graphical representations of the variability of data indicating standard deviations.

Standard deviation (SD) is calculated according to equation:

$$SD = \sqrt{\frac{\sum_{i=1}^n (x_i - \bar{x})^2}{(n - 1)}} \quad (25)$$

4 RESULTS AND DISCUSSION

In order to investigate the overall area of PIM and explore the influence of binder components as well as powder loading, the presented chapter on the results and discussion within the experimental part was divided according to individual objectives of the thesis into the following sections:

- Effect of [**major component**]
- Effect of [**backbone**]
- Effect of [**surfactant**] – including evaluation of powder loading

Each section consists of a brief introduction, results and discussion.

The presented results have been also published in the following papers:

- I. Rheological Investigation of Highly Filled Polymers: Effect of Molecular Weight**
Hnatkova E., Hausnerova B., Hales A., Jiranek L., Alcon J. M.
Novel Trends in Rheology VI, 1662 (2015) 040003-1-04040003-8.
- II. Processing of MIM Feedstocks based on Inconel 718 Powder and Partially Water-Soluble Binder Varying in PEG Molecular Weight**
Hnatkova E., Hausnerova B., Hales A., Jiranek L., Derguti F., Todd, I.
Powder Technology, 322 (2017) 439-446.
- III. Effect of Backbone Binders on Rheological Performance of Ceramic Injection Molding Feedstocks**
Hausnerova B., Kasparkova V., Hnatkova E.
Polymer Engineering and Science, 57 (2017) 739-745.
- IV. Impact of Stearic Acid on Powder Loading and Flow Properties of Ceramic Injection Molding Feedstocks**
Hnatkova E., Hausnerova B.
Submitted to Ceramics International in 2019

4.1 Effect of major component

The main objective of this section was to investigate the effect of PEG molecular weight on overall the PIM process chain including its eventual impact on final mechanical properties of Inconel 718 (see paper I, II). This part of research was based on joint work with the Department of Materials Science and Engineering at Sheffield University. For this purpose, 7 feedstocks with a fixed amount of powder loading (59 vol. %) and the same binder composition differing in PEG molecular weight (in a range from 1,500 to 20,000 g/mol) were investigated. Fig. 28 shows a schematic view of feedstock composition.

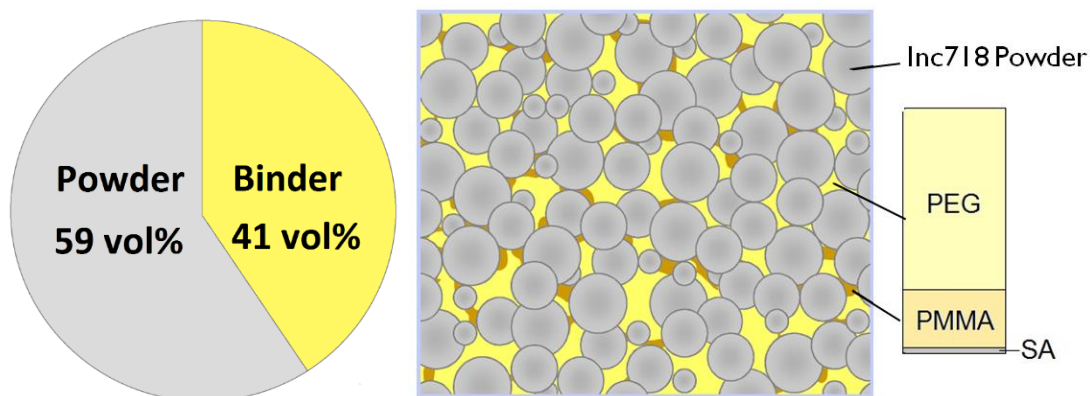


Fig. 28 Illustration of PIM feedstock composition based on Inconel 718.

The binder system was designed for a two-stage debinding process. The major component (PEG) should provide the feedstocks with low viscosity simultaneously enabling its easy removal in water, the backbone polymer (PMMA) ensures the strength of the moulded part, and the surfactant (SA) facilitates lubrication. The formulation of feedstock compositions is summarized in Tab. 7.

Tab. 7 Composition of feedstocks based on different PEG molecular weights.

Feedstock	Powder (59 vol. %)	Binder system (41 vol. %)		
		83 wt. %	15 wt. %	2 wt. %
P1.5K	Inconel 718	PEG 1 500	PMMA	SA
P4K	Inconel 718	PEG 4 000	PMMA	SA
P6K	Inconel 718	PEG 6 000	PMMA	SA
P8K	Inconel 718	PEG 8 000	PMMA	SA
P10K	Inconel 718	PEG 10 000	PMMA	SA
P12K	Inconel 718	PEG 12 000	PMMA	SA
P20K	Inconel 718	PEG 20 000	PMMA	SA

Rheological characterization

❖ *Flow and viscosity curves*

Rheological measurements were carried out using a capillary rheometer with a capillary die ($L/D = 20/1$) in a shear rate range from 35 to 2500 1/s. Obtained values are only apparent, without any corrections. Fig. 29 shows shear stress and viscosity dependence on shear rate at three temperatures. All feedstocks demonstrate pseudoplastic behaviour in the measured shear rate range suitable for injection moulding. What can also be noticed is that the shear rate sensitivity of most of the feedstocks tends to diminish at higher shear rates; especially at 120 °C, it seems that viscosity curves even approach the 2nd Newtonian plateau.

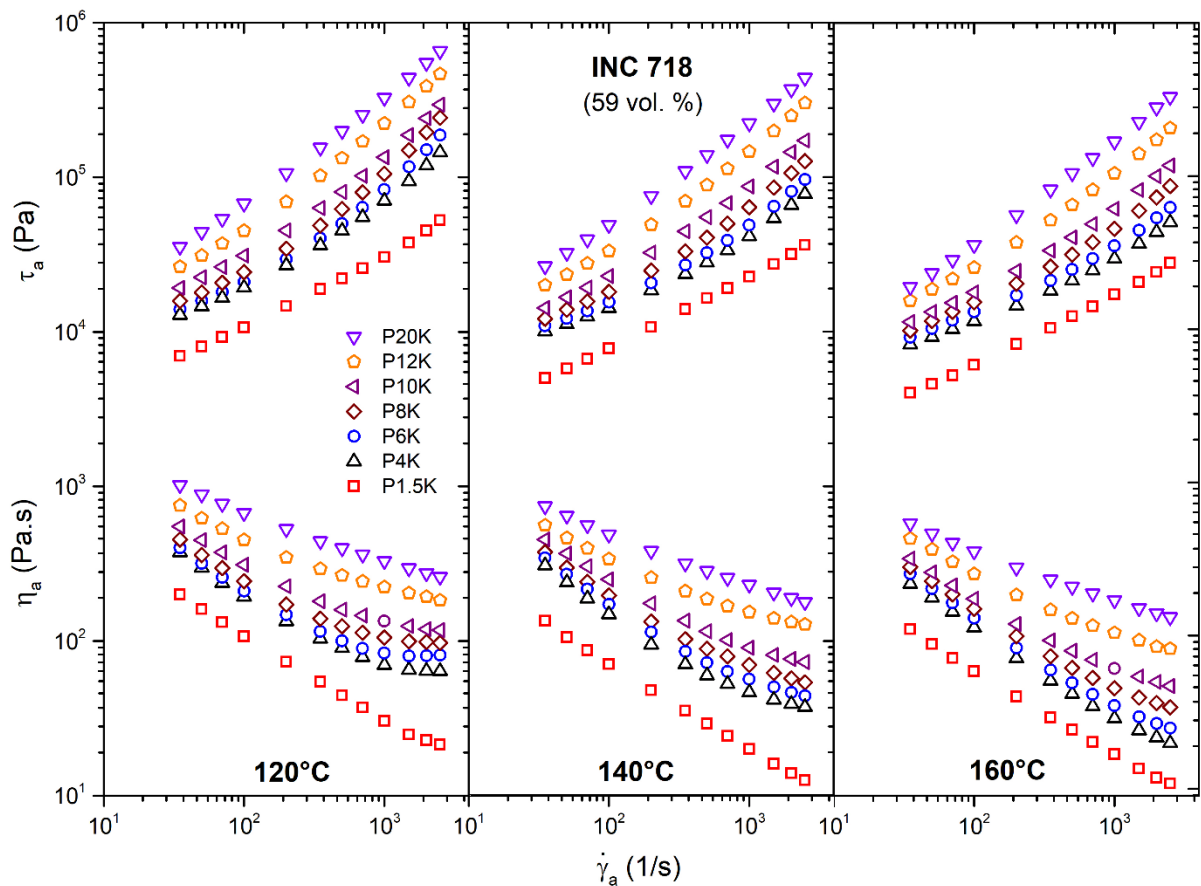


Fig. 29 Effect of PEG molecular weight on flow behaviour of Inc718 feedstocks.

At a higher temperature, the shear stress decreases and therefore also the feedstock viscosity due to a greater free volume available for molecular motion and easier disentanglement of the polymeric chain in the flow direction [75]. Moreover, it reduces friction among particles because the thermal expansion of the polymeric binder is higher than that of the powder resulting in slightly lower powder loading [76]. Nevertheless, a higher temperature is not always favourable;

e.g. Yang *et al.* [31] reported that feedstocks based on PEG 1 000 and 1 500 demonstrate dilatant flow above 80 °C as a result of possible powder binder separation.

In addition, the viscosity of feedstocks also decreases with lower molecular weight of PEG due to shorter polymeric chains allowing more mobility between particles. However, the viscosity of feedstock P1.5K (having the PEG with the lowest molecular weight) exhibited significantly lower viscosity in comparison with other feedstocks. Too low viscosity of feedstock could be more susceptible to phase separation, which is the most important issue during injection moulding, resulting in defects in the final sintered part.

These results are in accordance with the previous findings reported by Hayat *et al.* [32]. The viscosity of their feedstocks based on PEG 1500 and 4000 was also extremely low and demonstrated dilatant flow from certain shear rates at elevated temperatures, which could indicate powder binder separation.

❖ *Viscosity-temperature dependence*

Feedstock viscosity temperature dependence was calculated according to Arrhenius Eq. (2) and expressed as flow activation energy. From the processing point of view, it is desirable to have low dependence of feedstock viscosity on temperature, *i.e.* a lower value of activation energy. During injection moulding step, higher viscosity temperature dependence can cause fluctuation in the process due to rapid changes in feedstock viscosities, while during cooling it can introduce internal stresses into the moulded components.

Fig. 30 shows an example of Arrhenius plots of selected feedstocks as a function of $\ln(\eta_a)$ vs $1/T$ at a given shear rate or shear stress. The flow activation energy (E_a) is then calculated from the slopes of straight lines according to Eq. (18). Fig. 31 illustrates the obtained activation energies as a function of both, apparent shear rate ($E_{a,\dot{\gamma}}$) and apparent shear stress ($E_{a,\tau}$).

In both cases, the feedstock viscosity temperature dependence decrease with higher molecular weight of PEG, except feedstock P1.5K which behaved unusually in the whole process. However, flow activation energy at a constant shear rate (Fig. 31a) is shear dependent. Oppositely, flow activation energy at constant shear stress (Fig. 31b) demonstrated constant values from a certain shear stress. The shear dependence of activation energy at a constant shear rate diminishes with higher PEG molecular weight and in case of feedstock P20K its value is almost constant. On the other hand, feedstocks with low molecular weight of PEG, such as P4K or P6K are more shear sensitive and their flow activation

energy increases up to 30 J/mol in the measured shear rate range. Different trends for activation energy obtained at a constant shear rate or constant shear stress have been already reported by some authors [64,73].

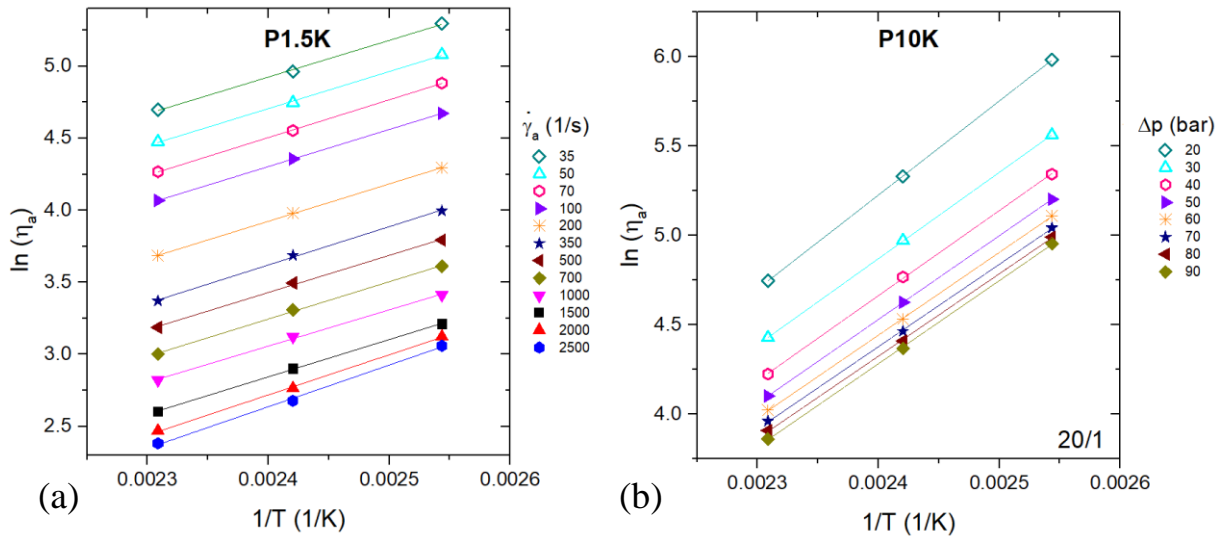


Fig. 30 Example of Arrhenius plots for viscosity obtained at constant shear rate (a) and constant pressure (b).

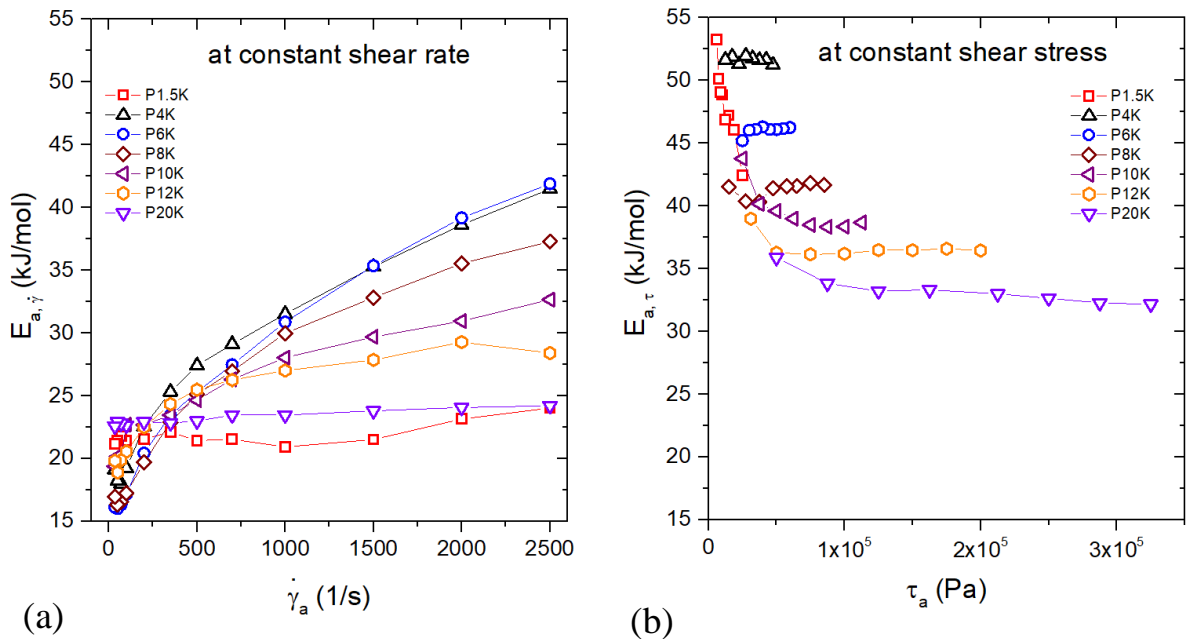


Fig. 31 Activation energy of feedstocks at constant: shear rate (a) and constant shear stress (b).

Similar results of activation energy at a constant shear rate were obtained by Yan *et al.* [31] and more recently by Hayat *et al.* [32], who tested feedstocks based on PEGs (1 500, 4 000, 10,000 and 20,000). In their case the feedstock based on PEG 1 500 did not behave unusually as in this work. Yang *et al.* reported

activation energy at a shear rate 300 1/s, where the dependence in this study is not strong, while Hayat *et al.* did not report the shear rate at which the activation energy was obtained. Based on the results in this study as well as on studies performed by other authors investigating the impact of PEG molecular weight it can be concluded that PEGs with higher molecular weight will be more suitable for injection moulding from the processing stability point of view.

❖ *Entrance and exit effects*

For corrections of capillary flow, end effects were measured and evaluated for all feedstocks at 140 °C by direct and indirect measurements in order to compare both methods. Fig. 32 shows feedstock dependence of pressure drops on apparent shear rate obtained with 3 capillaries of the same diameter (1 mm) and different lengths of 5, 10 and 20 mm.

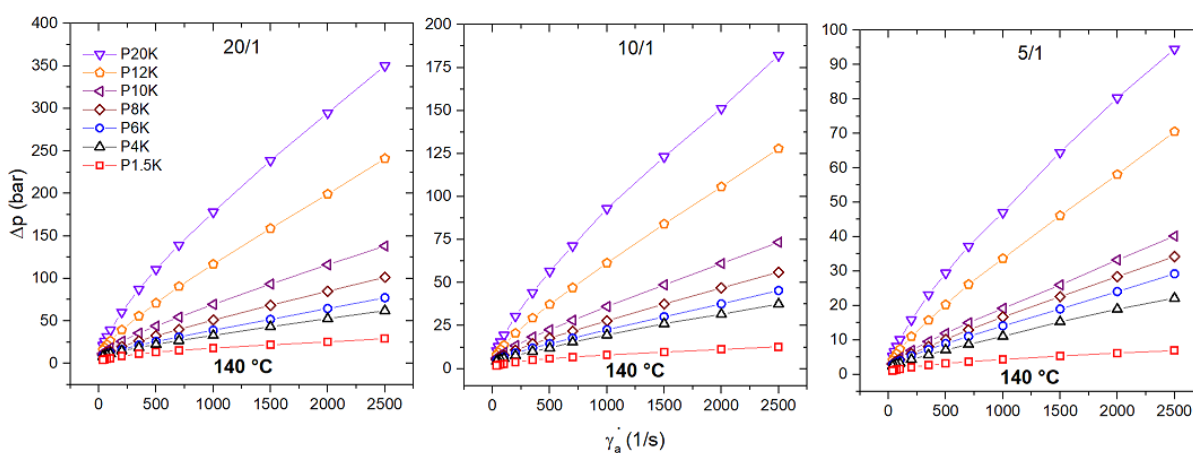


Fig. 32 Measured pressure drop of all feedstocks using three capillaries.

Further, Fig. 33 shows an example of measured pressure drops for individual feedstock plotted in the “Bagley plots” as a function of L/D ratio at a given shear rate. As can be noticed, there is a linear increase of pressure (along) with the length of the capillary die. Thus, the end effects (Δp_{end}) can be indirectly measured by the extrapolation of fitted data from the y-axis, where the ratio L/D is 0.

Direct measurements of end effects were carried out using a zero “orifice” die of the same diameter and with a nominal length of 0.2 mm. However, the nominal length was neglected for further calculation.

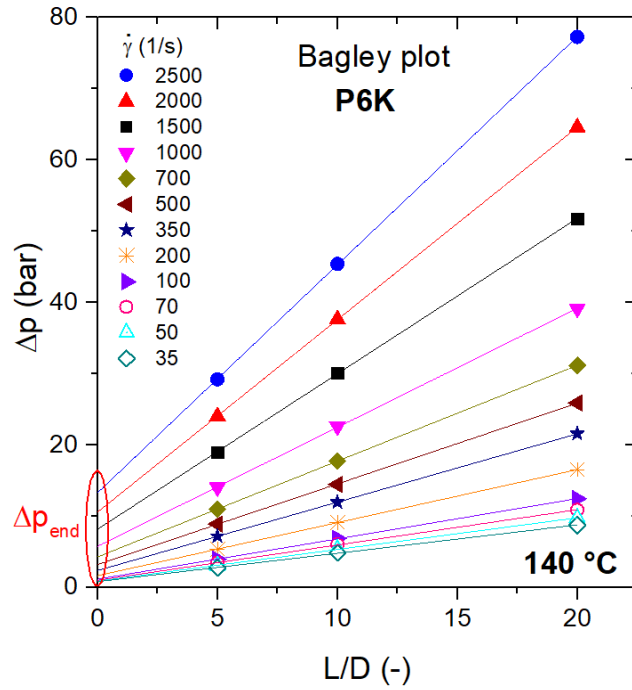


Fig. 33 Extrapolation of end effects from Linear Bagley plots.

Fig. 34 shows a comparison of results between these two methods, *i.e.* from direct measurement (zero die) and indirect extrapolation (Bagley). Feedstock P1.5K was excluded from the graphical comparison. Its pressure was too low and almost constant in the measured shear rate range used; at a shear rate of 2500 1/s, the pressure drop of feedstock P1.5 K did not reach 1 bar using the zero length die. As can be seen, both methods bring almost the same values of end effects with a slight deviation in case of feedstocks P10K and P20K. For further comparison or corrections, the end effects obtained from the zero die were considered. Further, Tab. 8 summaries measured pressure drops of feedstocks for selected capillary dies at a shear rate of 2500 1/s and highlights influence of end effects pressure drops.

Tab. 8 Measured pressure drops Δp in bar at shear rate of 2500 1/s using various capillary lengths and impact of end effects on it in %.

L/D	0/1	20/1	10/1	5/1		
Feedstock	Δp_{end} (bar)	Δp (bar)	Δp (%)	Δp (%)	Δp (bar)	Δp (%)
P4K	10.4	62.2	17	37.5	28	47
P6K	13.9	77.3	18	45.4	31	48
P8K	14.3	101.5	14	56.1	26	42
P10K	10.8	138.2	8	73.4	15	27
P12K	16.0	241.0	7	127.8	13	23
P20K	16.7	350.2	5	182.1	9	18

The values in the highlighted columns show impact of end effects (Δp_{end}) on measured pressure drop (Δp) in %. It is obvious that with a shorter capillary length the influence of end effects is higher. However, end effects of feedstocks constituted with lower molecular weight of PEG will have greater impact on Bagley correction influencing corrected shear stress. This means, that comparison of apparent values of viscosity curves can bring incorrect results.

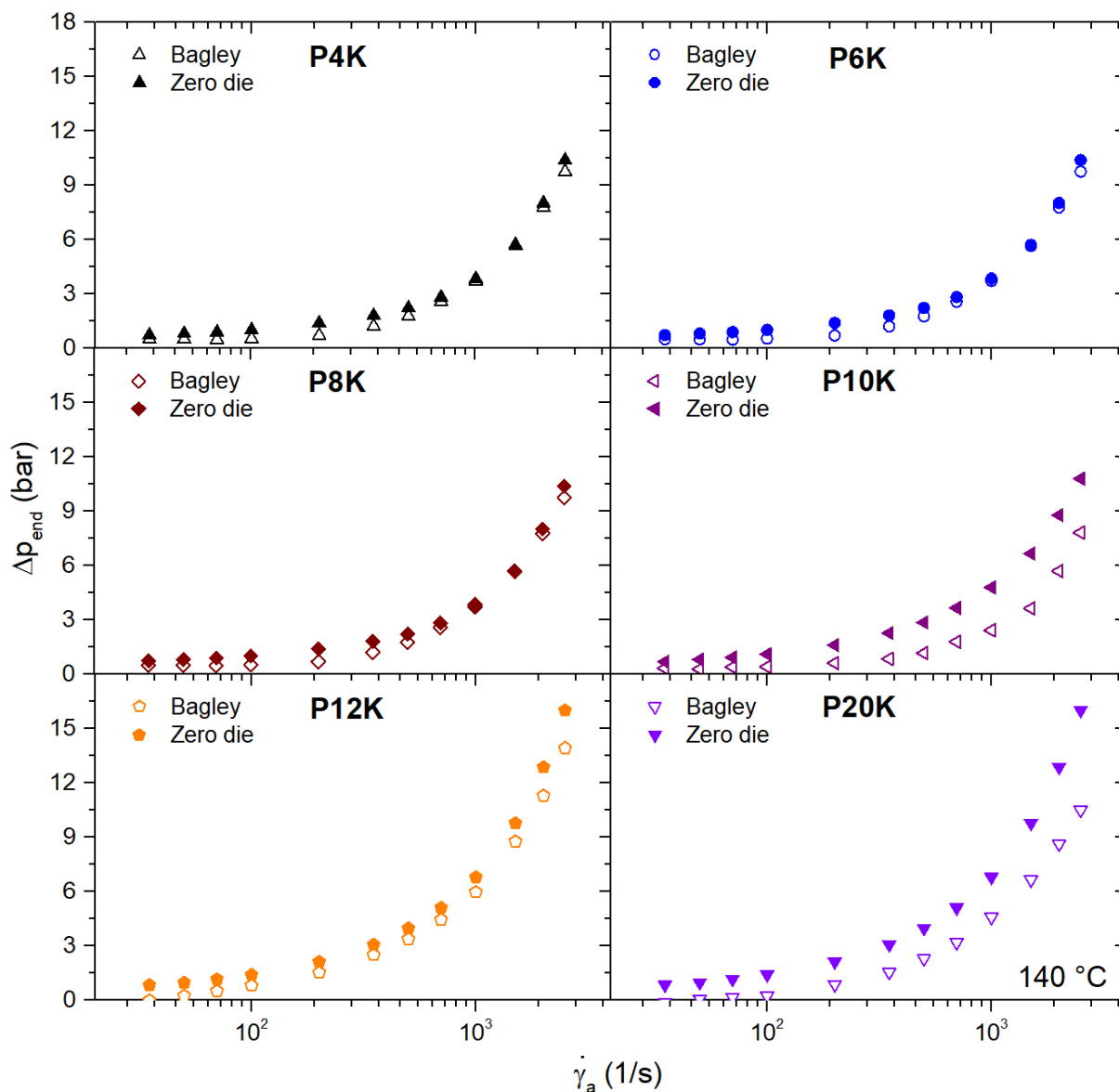


Fig. 34 Comparison of end effects obtained from direct and indirect measurements.

❖ Non-Newtonian index

The Non-Newtonian index (n) representing shear sensitivity of feedstock viscosity, can vary from point-to-point, or it can be constant at all data points in

the shear rate range measured. Therefore, the main issue is how to properly determine it according to Eq. (10) from discontinuous data set of τ_c and $\dot{\gamma}_a$ measured experimentally. Fig. 35 shows for comparison an example of fitted data based on different approximate functions (linear and non-linear approximation).

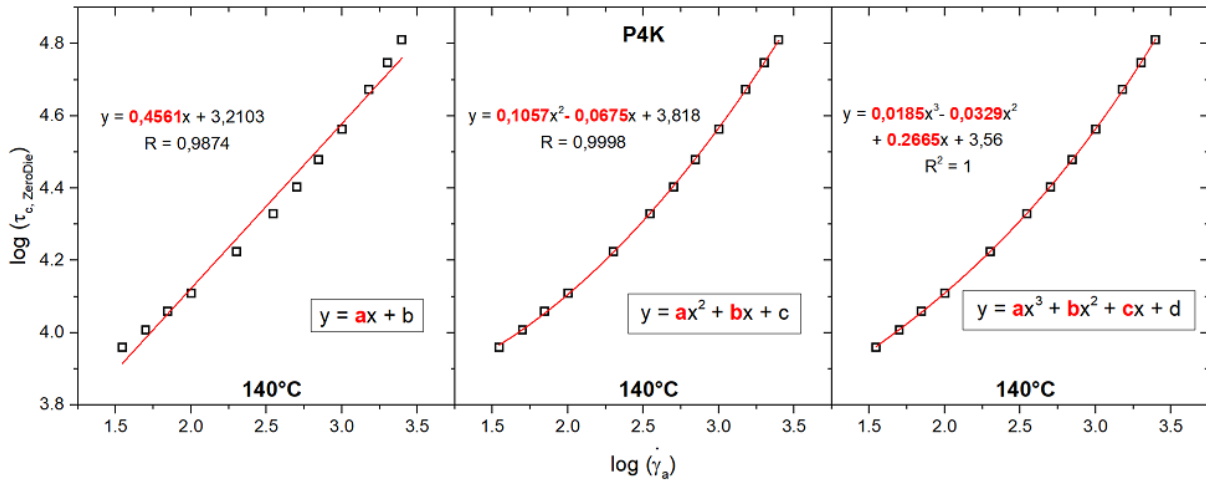


Fig. 35 Linear and non-linear slope of log-log plots of feedstock P4K for three approximate functions.

Tab. 9 demonstrates non-Newtonian indexes derived from those functions according to Eq. (26), Eq. (27) and Eq. (28) for linear regression, polynomial function of the 2nd and polynomial function of the 3rd grade, respectively.

Tab. 9 Effect of approximate function (linear or polynomial regression) on the value of Non-Newtonian index as an example for the P4K at 140 °C.

τ_c (Pa)	$\dot{\gamma}_a$ (1/s)	$\log \tau_c$ (-)	$\text{Log } \dot{\gamma}_a$ (-)	$n - (1^{\text{st}})^*$ (-)	$n - (2^{\text{nd}})^*$ (-)	$n (3^{\text{rd}})^*$ (-)
64738	2500	4.81	3.40	0.46	0.65	0.69
55915	2000	4.75	3.30	0.46	0.63	0.66
47073	1500	4.67	3.18	0.46	0.60	0.62
36548	1000	4.56	3.00	0.46	0.57	0.57
30166	700	4.48	2.85	0.46	0.53	0.53
25288	500	4.40	2.70	0.46	0.50	0.49
21331	350	4.33	2.54	0.46	0.47	0.46
16756	200	4.22	2.30	0.46	0.42	0.41
12875	100	4.11	2.00	0.46	0.63	0.36
11453	70	4.06	1.85	0.46	0.32	0.33
10191	50	4.01	1.70	0.46	0.29	0.32
9128	35	3.96	1.54	0.46	0.26	0.30

* Non-Newtonian index obtained from (1st), (2nd) and (3rd) polynomial fitting.

As can be observed, the non-Newtonian index $n - (1^{st})$ obtained from the linear regression (1st polynomial order) is a constant value of 0.46, in case of feedstock P4K at a given temperature, while, the non-Newtonian index $n - (2^{st})$ obtained from the 2nd polynomial approximation, which is more appropriate for this feedstock, is dependent on shear rate. Its value raised from 0.26 to 0.65 in the given shear rate range. Similar values were obtained for the 3rd polynomial approximation which should be even more appropriate, if the curves fit properly. Nevertheless, for further calculation the value of polynomial function from the 2nd order was adopted in this study.

Fig. 36 shows a graphical comparison of non-Newtonian indexes obtained for selected feedstocks at 140 °C from the linear regression with those obtained from 2nd polynomial fitting as the function of shear rate. As can be seen, for this type of feedstock there is a huge difference of values of non-Newtonian indexes obtained depending on the selective approximate function. Feedstock viscosity dependence on shear rate increases with a lower molecular weight of PEG, which means that these feedstocks will be more sensitive to shear rate. In case of pure macromolecular materials, it is desirable to have higher shear rate dependence, as viscosity decreases at a higher shear rate. For highly filled systems it cannot be concluded which behaviour is better for processing of PIM feedstocks. However, these results should be taken into consideration when comparing with other rheological characterization of PIM feedstocks.

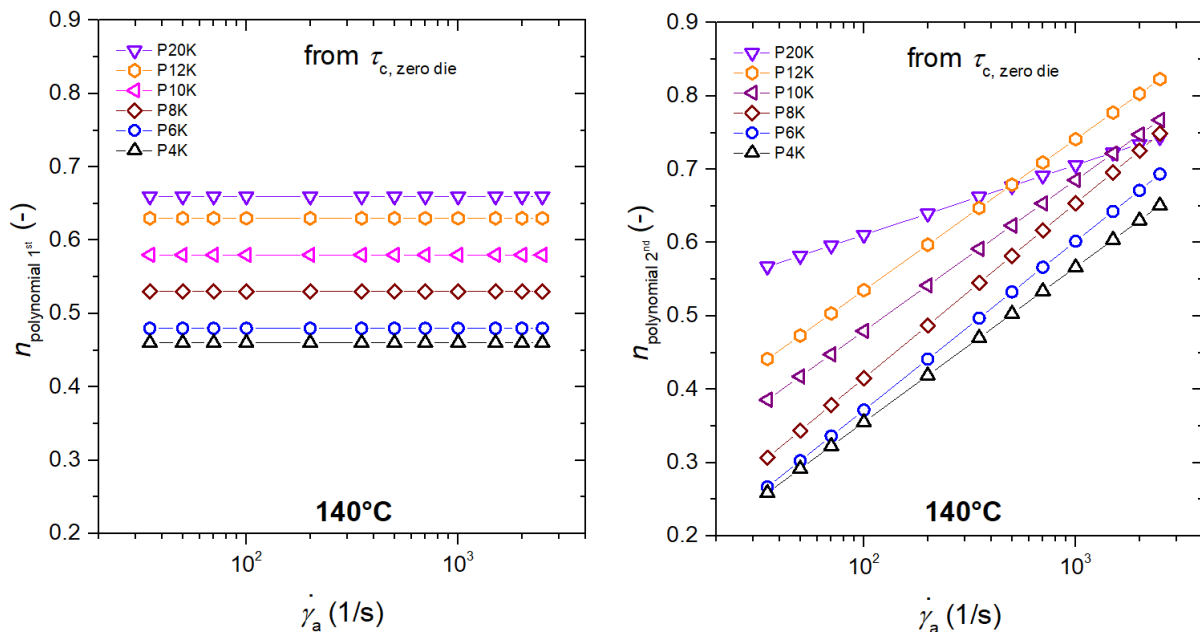


Fig. 36 Non-Newtonian indexes obtained from the (a) linear and, (b) 2nd polynomial fitting in dependence on apparent shear rate.

❖ Corrections of capillary flow

Fig. 37 demonstrates differences between apparent and corrected viscosity curves using end effects obtained from the zero dies and non-Newtonian indexes calculated from the 2nd polynomial fitting. As can be noticed, the corrected viscosity curves are more affected with a higher molecular weight of PEG. This is due to higher influence of end effects considering the results from Tab. 8. The corrected viscosity curves are desirable, especially if data is to be used for flow simulations of an injection moulding process. However, most of the equations or corrections were designed for pure macromolecular materials. That is why it is questionable, to which extend the corrected data are precise, because there are other factors affecting the results. One of them is slip wall, which was not taken into consideration in this study, but is often present in processing of compounds with high solid loading [77].

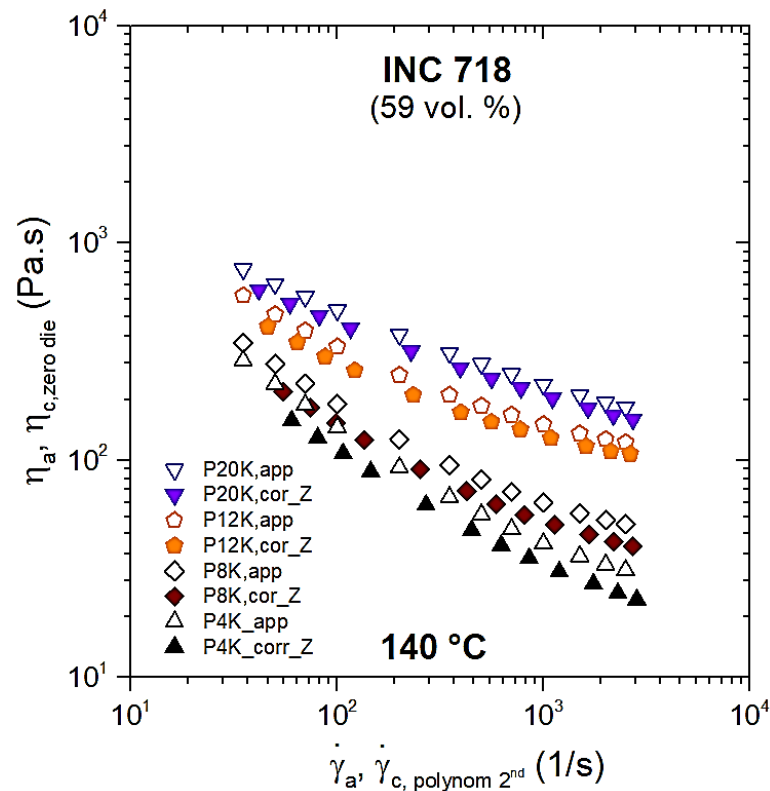


Fig. 37 Apparent and corrected viscosity curves for selected Inc718 feedstocks.

Debinding at different temperatures

PEG is soluble in water, and this offers that a major part of this binder could be removed in water baths as the first stage of debinding. The advantage of this method is formation of open-pore channels in the moulded compact, which will

further allow rapid removal of residual binders in the second thermal debinding stage. Fig. 38 displays the PEG removal (weight loss in % due to PEGs leaching from moulded tensile specimens) in a water bath at three temperatures as functions of time.

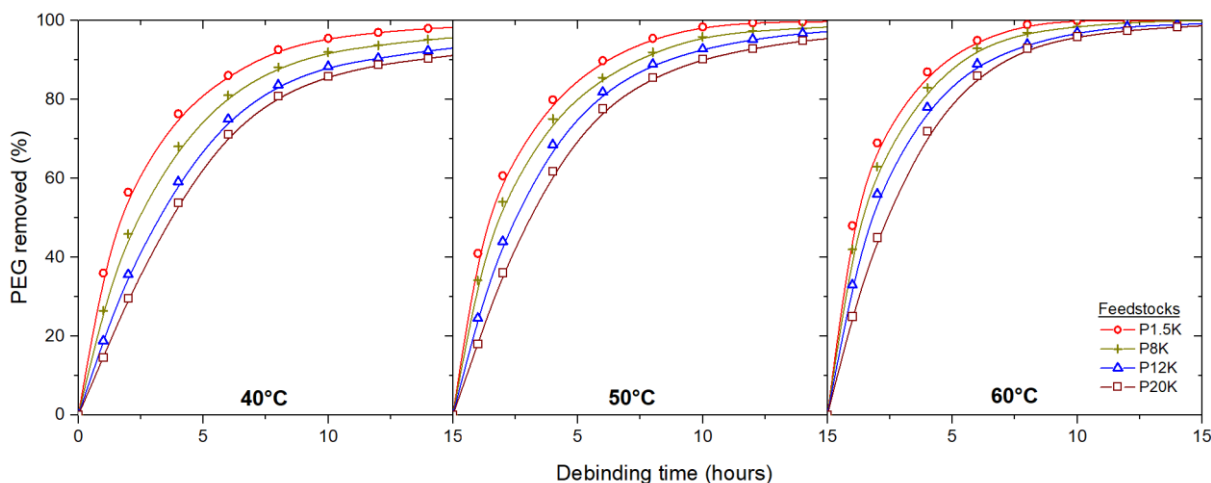


Fig. 38 PEG removal rate during water debinding at three temperatures.

As can be seen, in the first hours there was a rapid removal rate; afterwards the PEG leaching gradually slowed down. Moulded specimens from feedstocks containing PEG with higher molecular weights required a prolonged time to achieve corresponding weight loss. Higher temperatures of water (50 and 60 °C) accelerated the debinding rate, however resulting in a few part defects. In case of tensile samples prepared from feedstock P1.5K particular defects were found inside the tensile specimens indicating a probability of void formation during solidification in the previous processing step. Similar internal defects were also found by other researchers [78-79].

Introductions of other defects at higher debinding temperatures can have a correlation with a rapid enlargement creating internal stresses due to thermal expansion, and then consequently structural damage. This finding is also reported by German [3] demonstrating that a too high debinding rate results in a strength loss, formation of cracks and blisters, distortion or even collapse of the compact.

In previous research, Liu *et al.* [75] examined the effect of PEG 600 and PEG 4,000 in binder composition and found that during water debinding at 40 °C the CIM parts formulated with PEG 4,000 resulted in surface defects originated from swelling, such as blistering and cracking, while using PEG 600 brought difficulties to maintain the shape of the component.

Park *et al.* [80] investigated water-soluble binder systems consisting of cellulose and PEG; moulded components from feedstocks containing low

molecular weight PEGs exhibited excellent shape retention during extraction in water at room temperature, while the components containing PEG with molecular weights higher than 8,000 exhibited cracks at the edge of the moulded parts because of swelling during PEG removal. Similar results were obtained by Hayat *et al.* [32], their samples containing PEG 20,000 significantly swelled and cracked during water debinding at 50 °C. Based on these studies and confirmed by our results, components based on PEGs with a higher molecular weight are more prone to cracks and blisters during the debinding process.

Tensile testing of sintered and post-heated treatment samples

After water debinding, the tensile samples underwent sintering stage. Those parts which were damaged during water debinding at a higher temperature cracked after the sintering stage. Fig. 39 shows a variation of Inconel 718 sintered densities based on debinding temperatures.

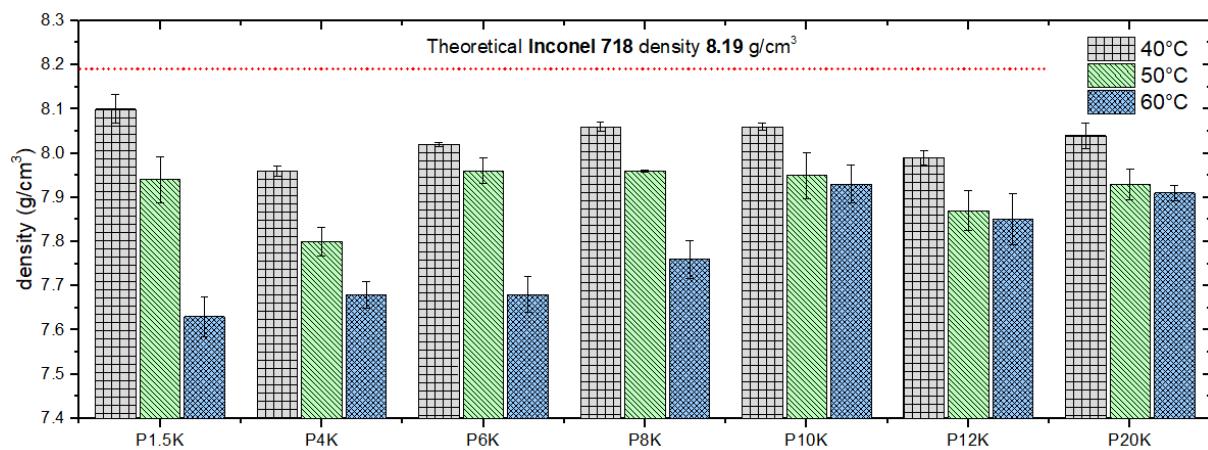


Fig. 39 Densities of sintered Inc718 based on water debinding temperatures.

As can be observed, there is a huge impact of water debinding temperatures on Inconel 718 component density after sintering. Particularly, the components from feedstocks with lower molecular weight of PEG reached lower densities at water debinding at 60 °C in comparison with those debinded at 40 °C.

This phenomenon might be explained by larger thermal expansion and swelling, which probably increased the pore size among powder particles and caused more defects. Due to the formation of defects during water debinding at higher temperatures, tensile properties were measured on sintered and heat treated tensile bars previously debinded at 40 °C. The results from tensile testing, in terms of tensile strength (R_m), proof strength ($R_{P0.2}$) and Young's modulus (E) of Inconel 718 are shown in Fig. 40. As can be seen, PEG molecular weight did not affect

the final mechanical properties, and also there is no relation between part density and corresponding mechanical properties.

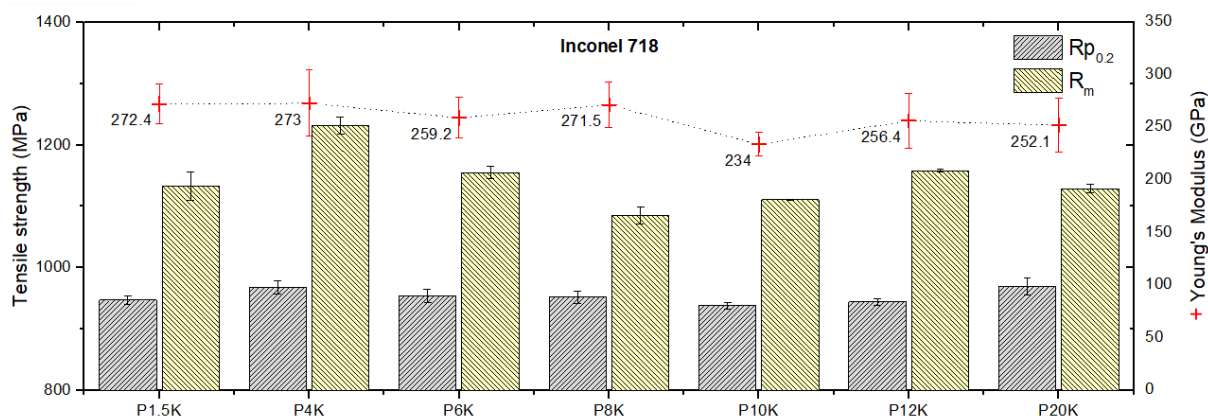


Fig. 40 Tensile properties of sintered Inc718 previously debinded at 40 °C.

4.2 Effect of backbone

In this section newly developed binder systems contacting CW or AW were investigated as possible substituents of polyolefin based binders for CIM feedstocks (see paper III). Ceramic powders are about one order of magnitude smaller than metallic ones and they are more prone to form agglomerates, as can be seen in Fig. 41. Moreover, small size and irregular particle shape enhance the resistance to flow. This leads to increased demands on the selection of binder composition which will guarantee low viscosity, and simultaneously good adhesion to powder.

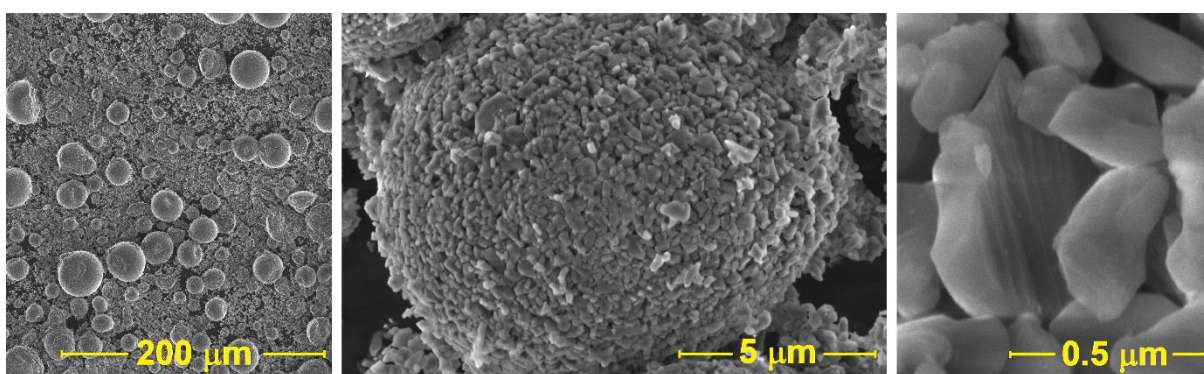


Fig. 41 SEM image of Al_2O_3 – tendency to agglomeration.

In previous research, AW and CW exhibited higher interactions of AW/PEG blend and superior debinding properties with gradual thermal extraction up to late debinding [81][83]. Based on this ground, these two candidates were selected as

backbone components for further investigation in terms of rheological and thermal behaviour. Ceramic feedstocks based on novel proposed binders were evaluated and compared with feedstocks containing LDPE or a commercial binder with respect to their suitability for injection moulding.

All analysed feedstocks were formulated with a fixed amount of Al₂O₃ (50 vol. %) and various binder compositions, as listed in Tab. 10. Initial polyolefin based feedstocks were designed with LDPE, PW and PEG of the same or different molecular weights. In the newly developed feedstocks, the LDPE was substituted with CW or AW. Additionally, all feedstocks adopted in this study contained 1 wt. % of surfactant (SA or OA). Mixing of all PIM feedstocks was carried out within the Brabender mixing chamber at adequate processing temperatures dependent on melting temperatures of the particular components.

Tab. 10 Binder composition (content of each component is given in wt. %).

In-house Binder	LDPE	CW	AW	PW	PEG			SA	OA
					6000	4000	1000		
LDPE 1	40	-	-	10	49	-	-	1	-
LDPE 2	40	-	-	10	25	14	10	1	-
LDPE 3	40	-	-	10	25	14	10	-	1
Carnauba 1	-	40	-	10	49	-	-	1	-
Carnauba 2	-	40	-	10	25	14	10	1	-
Carnauba 3	-	40	-	10	25	14	10	-	1
Acra 1	-	-	40	10	49	-	-	1	-
Acra 2	-	-	40	10	25	14	10	1	-
Acra 3	-	-	40	10	25	14	10	-	1
Commercial Binder	Licomont							SA	OA
	99							1	-

Rheological characterization

Rheological measurements of feedstocks were carried out using a capillary rheometer with capillary a die ($L/D = 20/1$) at three different temperatures suitable for processing of a given binder system in a shear rate range from 35 to 1000 1/s. Values obtained are only apparent, without any corrections. The flow behaviour of feedstocks based on in-house binders with various compositions is shown in Fig. 42. In addition, feedstock based on a commercial binder is also considered for comparison (Fig. 43).

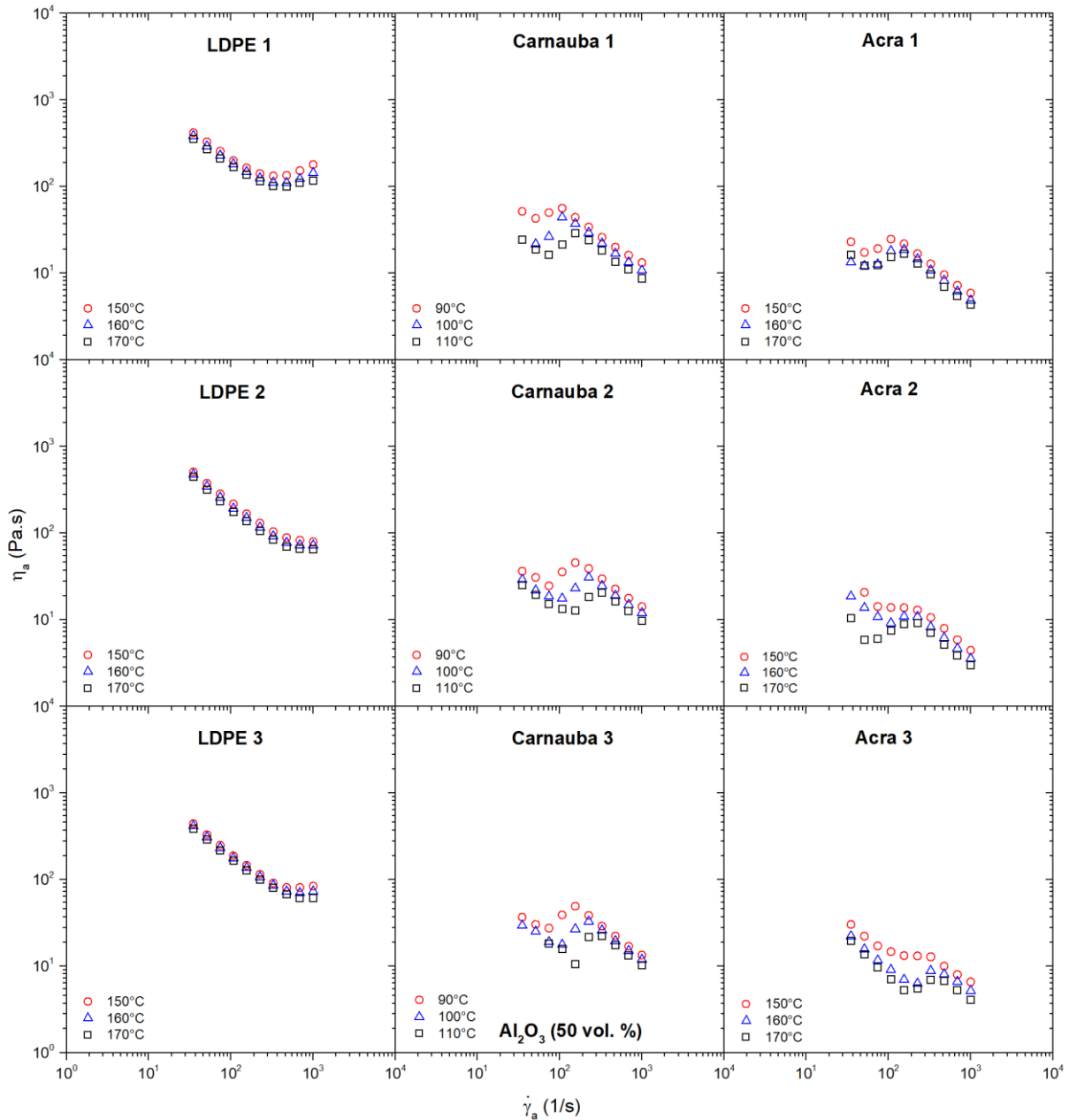


Fig. 42 Flow properties of Al_2O_3 feedstocks (50 vol. %) based on binders with LDPE, CW or AW as backbone component.

As can be seen, viscosity dependence on a shear rate of investigated ceramic feedstocks is rather complex. Pseudoplastic behaviour was observed only in a specific shear rate range. All viscosities were below 1 000 Pa.s, which is, according to German [1], suitable for injection moulding from processing point of view. Moreover, feedstocks based on CW and AW showed a significant reduction in feedstock viscosity, which is about one magnitude lower in comparison with polyolefin and Licomont based feedstocks.

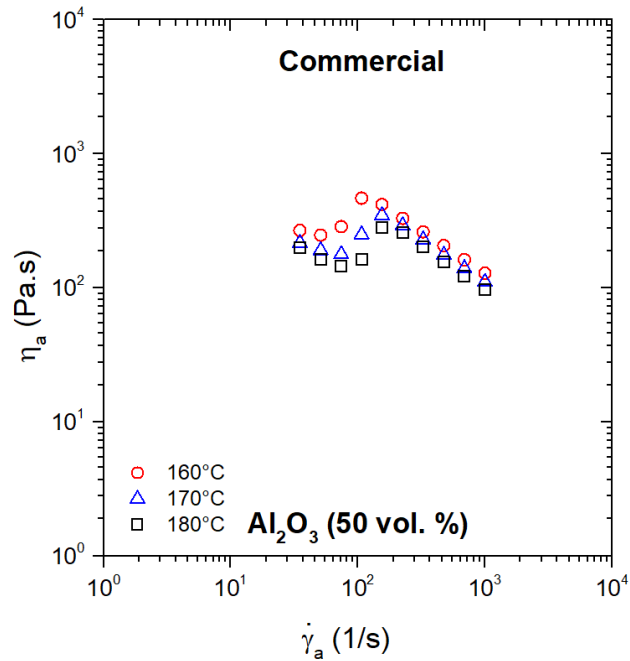


Fig. 43 Flow properties feedstock based on Al_2O_3 and commercial binder.

In case of LDPE based feedstocks, viscosity dependence on a shear rate shows pseudoplastic behaviour up to a shear rate of about 500 1/s then the flow turns into dilatant in the shear rate region approaching real processing conditions. On the other hand, both novel feedstocks based on CW, AW including a commercial Licomont exhibit pseudoplastic behaviour in this range. The pseudoplastic regions indicate that polymeric chains and powder particles are orienting in the same direction with flow. The abrupt change of the flow course of LDPE based feedstock was satisfactorily explained by Hoffman as early as 1972 [84] as the consequence of inability of particles to form layers and slide over each other at a certain shear rate. However, the flow of wax (CW and AW) and Lincomont based feedstocks is even more complex. Their viscosity curves show overshoots at certain shear rates. The onset of overshoots was postponed to higher shear rates at higher processing temperatures.

The overshoot is caused by particle structure reorganization, and a mathematical model has been proposed recently, which was employed successfully for fitting of rheological data of Al_2O_3 with a commercial binder Licomont [28]. Additionally, CW as a backbone component allows processing of feedstock around 100 °C, which is beneficial in comparison to polyolefin or AW based binder systems.

Considering the effect of various PEG molecular weights, the flow of traditional polyolefin (LDPE2) based feedstock is only affected in the dilatant region, which is in case of various molecular weights of PEG postponed towards

higher shear rates. In case of CW (Carnauba²) based feedstocks, combination of various PEGs shifted the transition from pseudoplastic to dilatant and back to pseudoplastic flow towards higher shear rates (about 100 1/s). From processing point of view, a high molecular weight PEG (PEG 6,000 in our case) in combination with CW shows better performance. However, in case of AW (Acra²), various PEG combinations bring viscosity decrease in the overall measured shear rate range.

Finally, role of surfactant (OA and SA) was considered. These two surfactants are often used with a presumption that their effect on the flow properties will be the same. In case of binder components studied within this work, it can be confirmed. The overall performance of the investigated novel feedstocks is in accordance with previous research [81],[82] as well as with findings obtained from contact angle measurement of wettability of the respective binders [83].

Thermal properties

Characterization of thermal properties was conducted using DSC analysis, which is a suitable technique for assessing polymer miscibility. This means that any change of the peaks, such as a shift of melt temperatures may disclose occurrence of interactions between individual polymers, their mixtures and the powder. Thermal characterization, in terms of melting temperatures (T_m), was conducted including: (1) each single binder component, (2) binder component with Al₂O₃, and finally (3) binder component/Al₂O₃ /PEG. The list of analysed samples can be seen in Tab. 11.

Tab. 11 Composition of model samples used for DSC measurements.

Binder	Binder/powder	Binder/powder/PEG
LDPE	LDPE/ Al ₂ O ₃	LDPE/ Al ₂ O ₃ /PEG
CW	CW/Al ₂ O ₃	CW/Al ₂ O ₃ /PEG
AW	AW/Al ₂ O ₃	AW/Al ₂ O ₃ /PEG
PW	PW/Al ₂ O ₃	PW/Al ₂ O ₃ /PEG
PEG	PEG/Al ₂ O ₃	-

Within all studied samples, the only strongly hydrophilic component was PEG. Thus, it can be assumed that its miscibility with respective non polar binder (AW, CW, LDPE, and PW) can influence behaviour of PIM feedstocks. Therefore, mutual miscibility of PEG with each of the nonpolar binders in presence of Al₂O₃ was determined.

Fig. 44 shows results from thermal analysis. DSC curves were obtained from the 2nd heating scan to avoid thermal history of the samples.

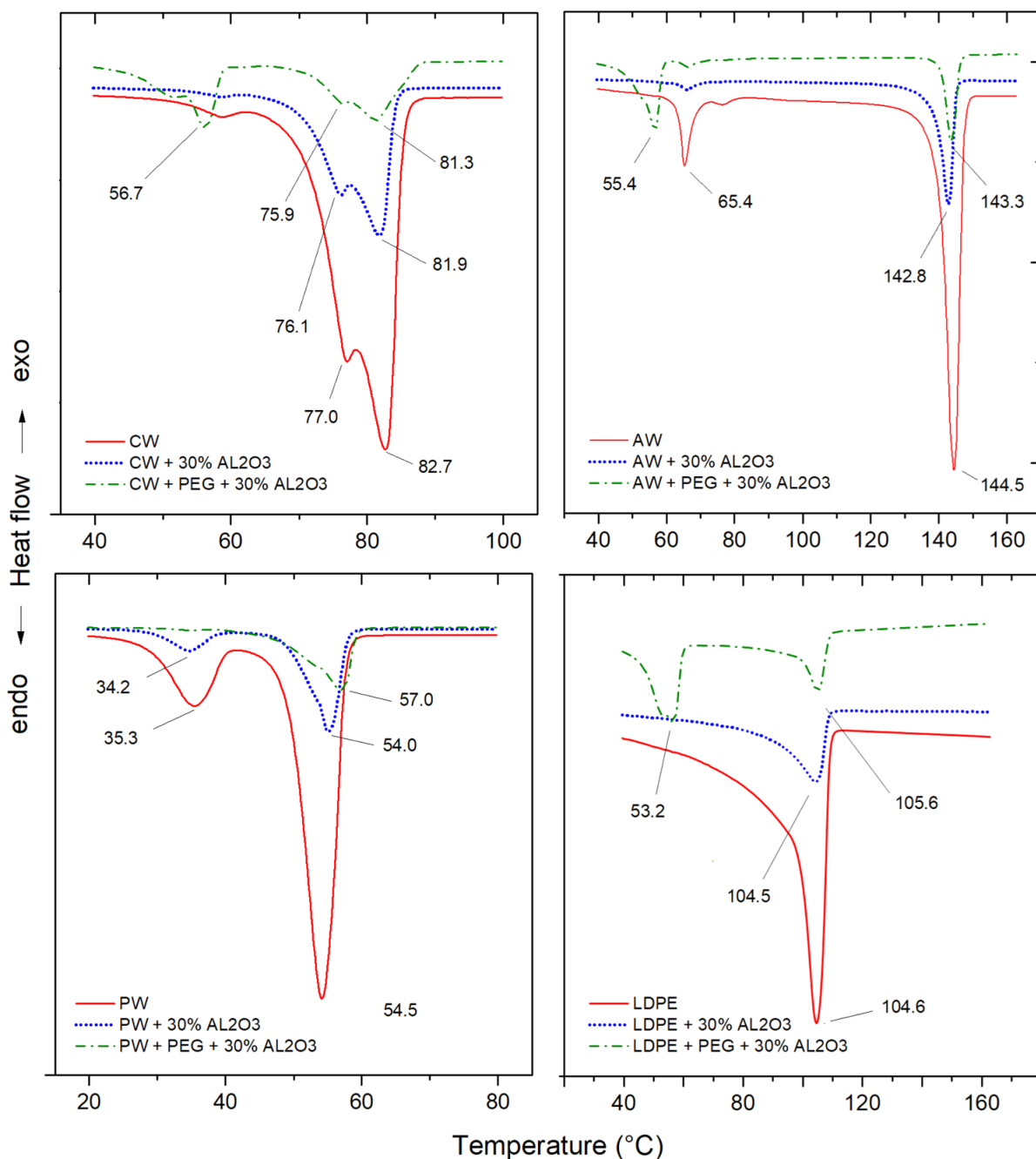


Fig. 44 DSC curves of each analysed samples from the 2nd heating scan.

Then, Tab. 12 lists melting temperatures (T_m) corresponding to the peaks obtained from thermal analysis. DSC curves show different thermal behavior of studied components. They differ both in melting temperatures (T_m) and the course of melting. LDPE, PEG and CW exhibited a single melting peak, in case of CW a sign of a peak split was recorded. On the other hand, AW and PW melted in two

steps, and in addition to the main melting peak, a second, well separated melting peak with lower melting temperature (T_m) was present.

Tab. 12 Melting temperatures of individual samples obtained from DSC.

	Melting temperature T_m (° C)				
	CW	AW	LDPE	PW	PEG
Individual binder	82.7	144.5	104.6	54.5	60.8
	77.0*	65.4**			
Binder/Al ₂ O ₃	81.9 (76.1)*	142.8	104.5	54.0	58.0
Binder/Al ₂ O ₃ /PEG	81.3 (75.9)*	56.7 143.3	55.4 105.6	53.2 57.0	n.a.

*Partially split single peak; **Two melting peaks. In both cases minor peaks given in parentheses; n.a. not applicable. Melting temperature of PEG peak in three-component mixture is in grey.

Firstly, melting properties of two-component mixtures (binder/Al₂O₃) were compared with those of individual binders. Taking T_m of individual binder as a reference, in all cases, adding of Al₂O₃ lowered T_m of the mixture. The shift was most pronounced for PEG/Al₂O₃ with a decrease of about 3 °C. Surprisingly, no change was observed for LDPE/Al₂O₃. The presence of ceramic particles within a binder can hinder mobility of polymeric chains, whether it is polymer or wax. This could initiate a reduction of their crystalline domains, thus causing a melting point depression.

Secondly, changes of melting behaviour of three-component mixtures (binder/Al₂O₃/PEG) were evaluated. These mixtures behaved in different ways. All samples (apart from that containing PW) showed two clearly separated endothermic peaks, one originating from PEG and the other from the respective binder (AW, CW or LDPE).

Mixtures with PW (PW/Al₂O₃/ PEG) behaved differently, as only a single melting peak (with T_m of 57 °C) was observed and notable shift in T_m relatively to both individual PW (54.5 °C) and PEG (60.8 °C) was recorded. This behaviour might point to miscibility of latter mentioned components in the ratio used. The uniform thermal behaviour might be favourable when using these two components in more complex samples. Regarding T_m of AW and CW in their respective mixtures they decreased by about 1.2 (AW) and 1.4 °C (CW); oppositely, no melting point depression was observed in case of LDPE and PW showing T_m increase relatively to the individual binder. The melting peaks

originating from PEG in mixtures were displaced to lower temperatures (Tab. 12), a T_m depression of PEG was the greatest observed in LDPE/Al₂O₃/PEG,.

In general, a decrease in T_m in a mixture can be caused both by morphological effects, such as for example a decrease in lamellar thickness, and by thermodynamic factors (inter-chain interactions, interactions with particular material, change in crystal size).

Fig. 45 clearly shows differences in behaviour of both wax-based feedstocks (CW, AW) compared to those containing hydrocarbons, *i.e.* PW and LDPE. Taking into account that Al₂O₃ powder is of a polar character, as reported by Bleyan *et al.* [82], it seems credible that both CW and AW containing polar groups enable better miscibility with PEG and powder compared to PW and LDPE.

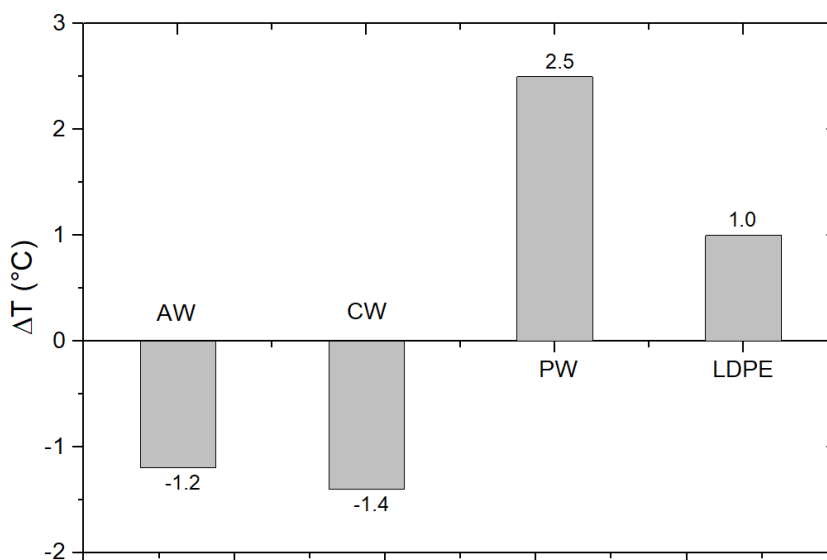


Fig. 45 Change in peak melting temperature ΔT of three-component mixture (binder/Al₂O₃/PEG) relatively to corresponding individual binder.

4.3 Effect of surfactant

In this section, an impact of SA concentration on powder loading and flow properties of PIM feedstocks was investigated for 3 different binder compositions in which concentration of SA varied from 0 to 5 wt. % (see paper IV), as listed in Tab. 13. Additionally, this part also includes an evaluation of powder loading and effect of powder loading on flow behaviour. Ceramic powders with submicrometric size and irregular shape represent a very high specific surface area [5]. This behaviour tends to reduce powder loading, while it is desirable to mix as much powder as possible in order to avoid distortion, as well as to lower

volumetric shrinkage. Surface active agents incorporated in the binder composition improve particle sliding to some extent and optimal concentration may considerably influence the processability of ceramic compounds and enhance their efficiency in sense of critical (respectively optimal) solid loading.

Tab. 13 Composition of binder components used (wt. %).

A	PEG	CW	PW	SA
	45-50	40	10	0-5
B	Licomont			SA
	95-100			0-5
C	LDPE	EVA	PW	SA
	48-53	26	21	0-5

Binder A is designed with all components having a melting temperature below 100 °C, which facilitates the processing of Al₂O₃ powder and prevents from polymer degradation [85]. Polar CW was selected due to its enhanced interaction with PEG and Al₂O₃ powder [19]. This should prevent phase separation during injection moulding, which is one of the most important issue in PIM technology.

Binder B is based on the commercially available binder Licomont. This binder was selected to test a possible improvement with addition of processing aids and to compare it with other in-house binder compositions.

Binder C is a polyolefin based binder system previously investigated by Bleyan *et al.* [19] and providing stearic stabilization with copolymer EVA.

The preparation of feedstocks was performed within a Brabender mixing chamber at a given processing temperature for each binder type: 100 °C, 160 °C and 140 °C for feedstock A, B and C, respectively.

Evaluation of powder loading

Prior to study impact of SA on powder loading, the evaluation of powder loading was carried out via mixing torque measurement using two different techniques: by continuously and separately increasing powder volume loading within the mixing chamber. According to theory, both methods are used for a determination of powder loading. In order to compare both methods, two different types of powder particles were used: a highly irregular ceramic Al₂O₃ powder and a spherical 17-4 PH stainless steel powder. The composition of binder in this case consists of the commercial Licomont (98 wt. %) and SA (2 wt. %), labelled as binder type B.

The initial the solid content started at 50 vol. % and 60 vol. % in case of Al_2O_3 and 17-4 PH powder, respectively. In both cases, the increment for each level was increased by 1 vol. % of powder, then the steadily mixing torque was recorded.

❖ *Mixing torque - continuously increasing powder loading*

Both Fig. 46 and Fig. 47 demonstrate a mixing torque obtained by continuously increasing solid volume loadings. When the powder is added to the melted binder, there is a certain resistance to the rotation of the blades resulting in an increase of torque. Then, once the homogeneity of the mixture becomes uniform, the mixing torque achieves a steady state value [51].

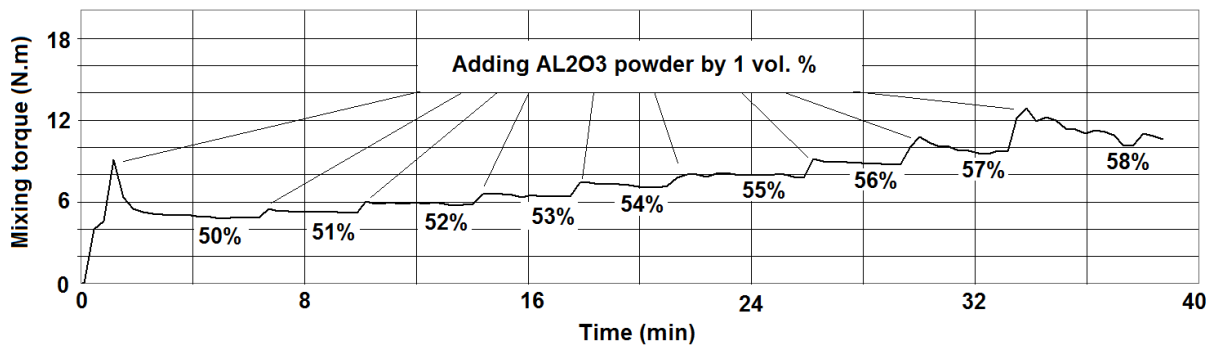


Fig. 46 Mixing torque obtained by continuous increasing volume of Al_2O_3 .

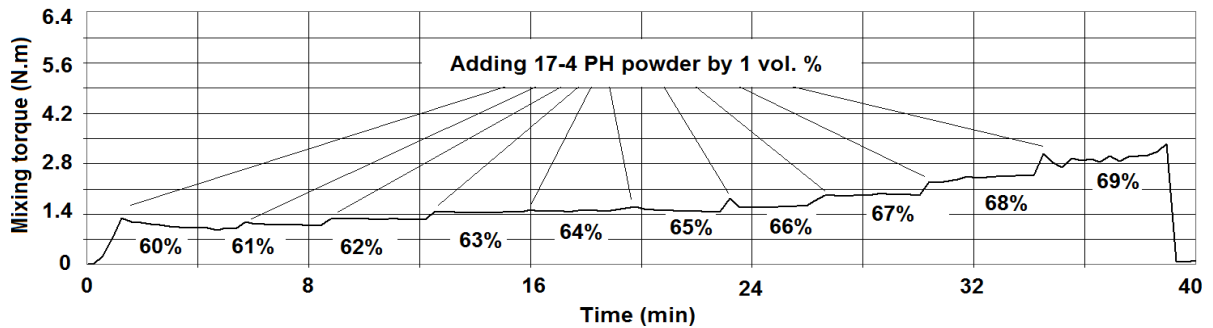


Fig. 47 Mixing torque obtained by continuous increasing volume of 17-4 PH.

As can be observed, the torque of mixture based on ceramic Al_2O_3 reached stable values of up to 56 vol. %. Exceeding this loading, the torque starts to be unstable, and at 58 vol. % becomes completely erratic. A similar situation could be observed for stainless steel powder 17-4 PH. However, the unstable torque was shifted to a higher value of solid loading and became unstable with a tendency to increase after 66 vol. %. Then, reaching powder loading of 69 vol. %, the mixing torque became completely erratic.

❖ *Mixing torque - separately increasing powder loading*

Fig. 48 illustrates an example of mixing torque as a function of time for batch mixing, where powder loading was increased in the whole volume for each time separately.

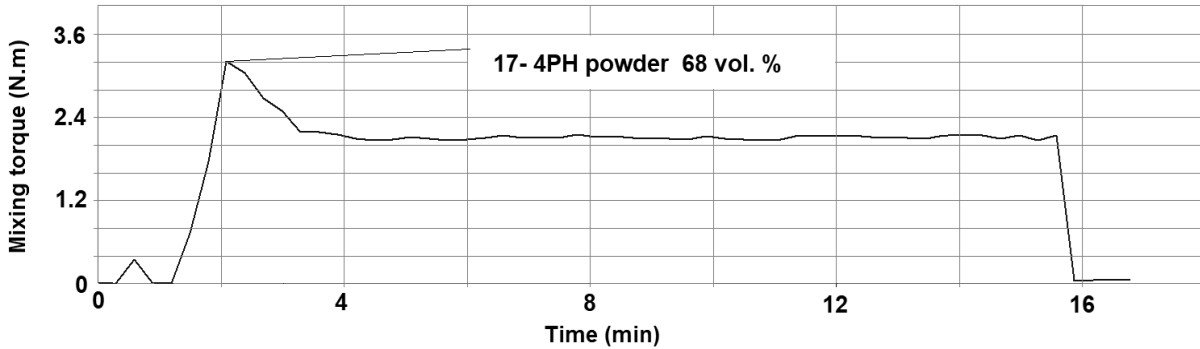


Fig. 48 Mixing torque obtained by separately increasing 17-4 PH volume.

❖ *Comparison of both methods*

Fig. 49 shows a comparison between mixing torque evolution obtained by both methods, separately and continuously adding powder. As can be noticed, both methods for obtaining mixing torque demonstrated same starting points from which, the rapid increase mixing torque occurred. This can indicate closer particles being in contact during processing, therefore increasing resistance and thus the mixing torque more rapidly.

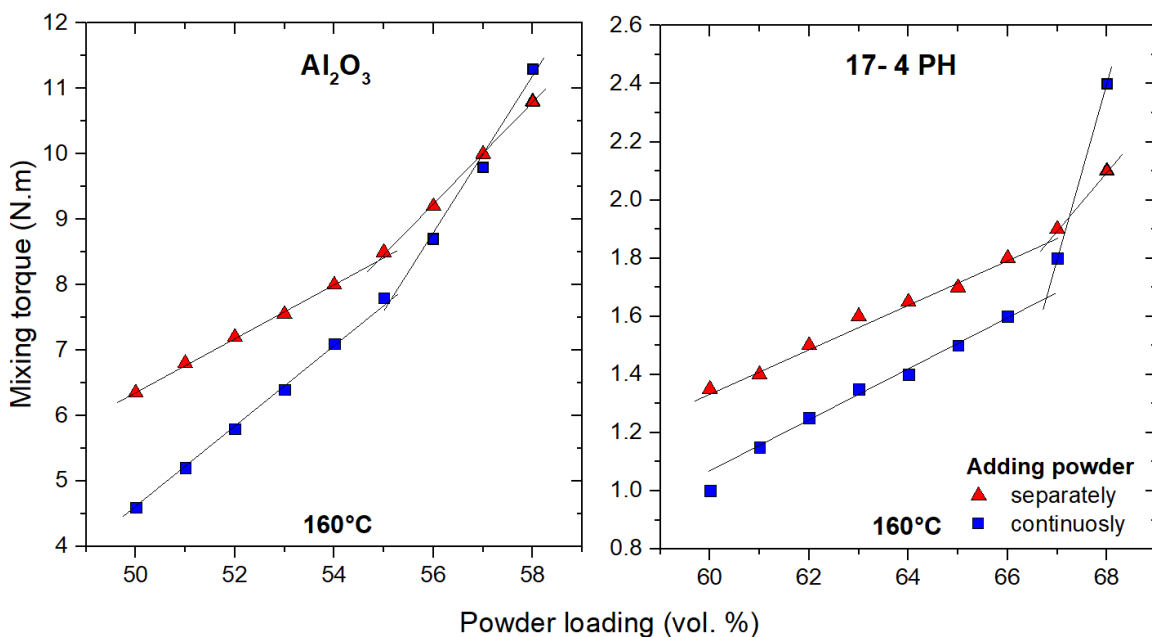


Fig. 49 Comparison of mixing torques obtained by two methods.

In both cases there is almost a linear increase in torque with higher solid loading. However, for all feedstocks, there is an abrupt (a switch point *SP*) in the slope at certain powder loading. Then, the torque progression raises up to a certain limit, where it starts to decay or becomes erratic. The decay can be explained by introducing voids among powder particles as the solid loading reaches the critical solid loading value (*CSL*).

Fig. 50 demonstrates a SEM picture of a highly filled mixture based on both Al_2O_3 (58 vol. %) and 17-4PH (68 vol. %) loading. As can be seen, all powder particles are covered with the binder. Nevertheless, it cannot be observed if there are already voids in the binder or not.

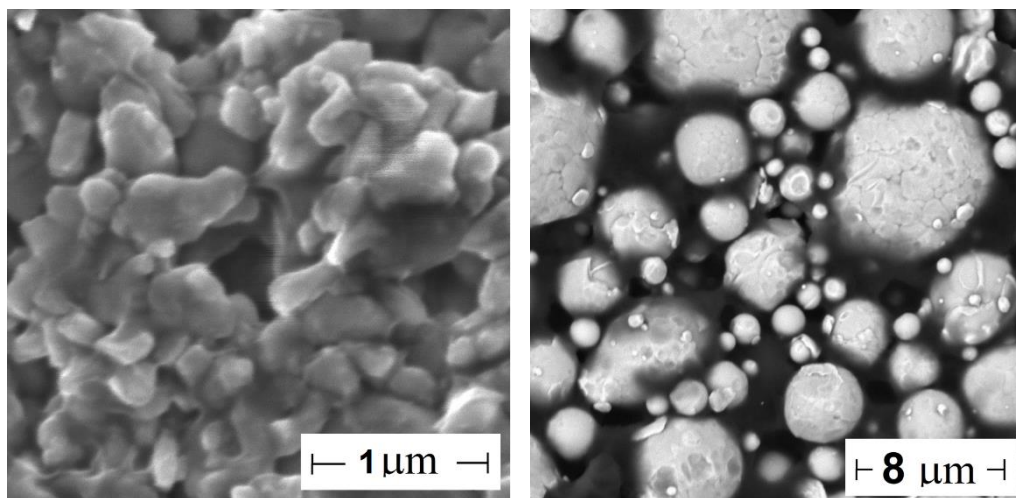


Fig. 50 SEM of feedstocks: Al_2O_3 , 58 vol. % (a) and 17-4PH, 68 vol. % (b).

Volumetric solid loading of the powder in feedstock formulations strongly varies for ceramic and metals. These results are in accordance with previous findings. Usually, powder loading of ceramic particles varies between 50 and 55 vol. %, but it is strongly dependent on powder characteristics and binder composition [3].

Effect of powder loading on flow behaviour

Rheological measurements were carried out on a capillary rheometer with a capillary die ($L/D = 20/1$) at processing temperature appropriate for their binder composition in shear rate range from 35 to 1 000 1/s. Values obtained are only apparent, without any corrections. Flow properties of feedstocks with different powder loading are shown in Fig. 51 for both powders at 160 °C. As can be seen, in case of Al_2O_3 powder, the viscosity of feedstock increases with an enhanced amount of powder, and overshoot was postponed to a lower shear rate range.

However, from certain solid loading (57 vol. %) it was not possible to measure the pressure generated, as can be seen in Fig. 52. These instabilities can be caused probably due to slip on the wall and/or as a consequence to exceeding optimal solid loading. In the case of 17-4PH, the viscosity was stable for all powder loadings measured.

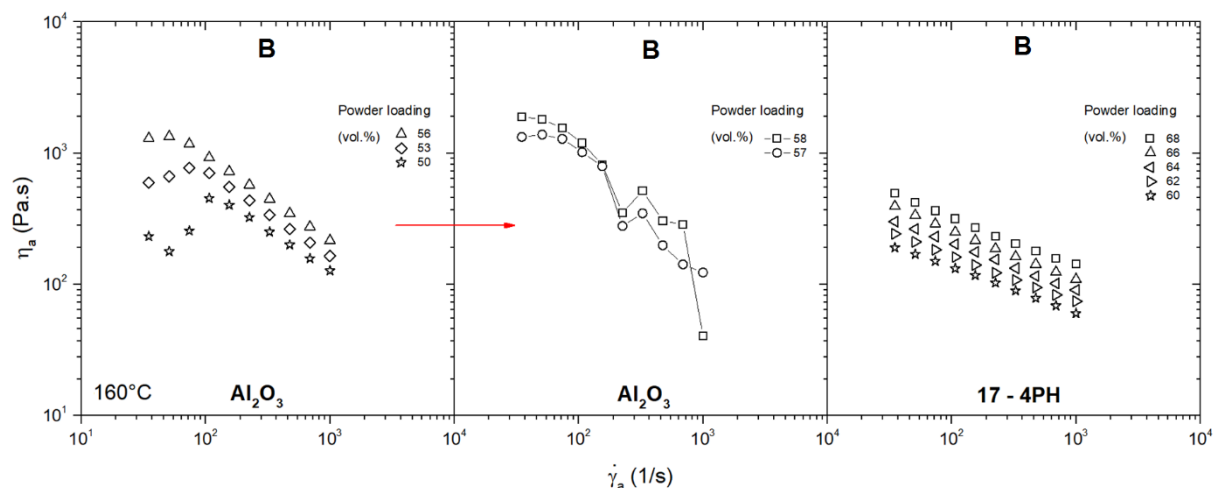


Fig. 51 Flow behaviour of feedstocks based on Al_2O_3 and 17-4PH with different powder loading.

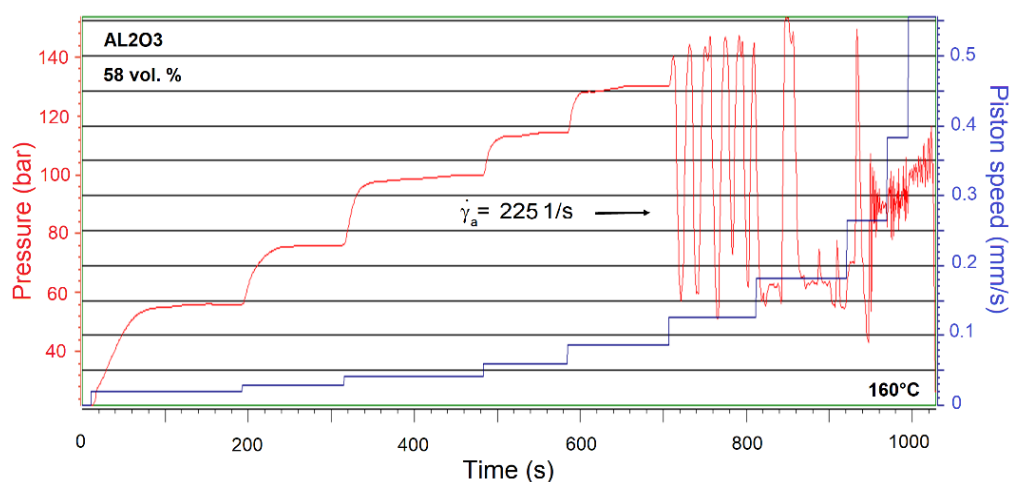


Fig. 52 Raw (online) data on rheometer of mixture with 58 vol. % of Al_2O_3 .

Influence of SA concentration on feedstock powder loading

In order to analyse the effect of surfactant concentration on powder loading, feedstocks were formulated with various amount of Al_2O_3 (50 - 60 vol. %) and three types of binder compositions A, B and C, in which concentrations of SA varied from 0 to 5 wt. %. Influence of SA concentration on mixing torque was investigated using a mixing test based on continuously increasing powder loading.

The increment was set up to 1 vol. % of Al_2O_3 in order to increase the solid content from 50 to 60 vol. %.

Fig. 53 demonstrates the evolution of mixing torques for all three binder systems as a function of both powder loading and concentration of SA. As can be seen, there is almost a linear increase in torque with higher solid loading. However, for all feedstocks, there is an abrupt (a switch point *SP*) in the slope at certain powder loading. Then, the torque progression raises up to a certain limit, where it starts to decay or becomes erratic. The decay can be explained by introducing voids among powder particles as the solid loading reaches the critical solid loading value (*CSL*). This is clearly visible for all three binder systems without SA; the critical solid loading is corresponding to 56 vol. %, 57 vol. % and 58 vol. % for feedstock A, B and C, respectively.

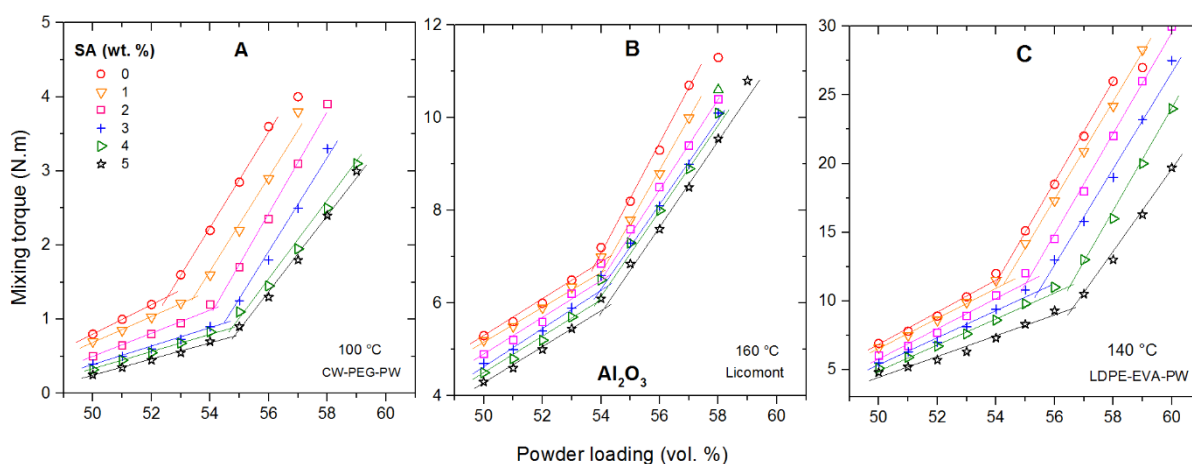


Fig. 53 Obtained torques based on powder loading and different concentration of SA for binder A, B and C.

Moreover, it can be seen that in case of binders A and C, a rapid increase in mixing torque depends on SA concentration. It was observed that the effect of SA is dependent on binder composition. For the feedstocks based on binder A, the addition of 1 to 3 wt. % of SA causes an increase of powder loading by about 3 vol. %. However, above 3 wt. % of SA, there is no increase in the shift of the *SP*. For the commercial binder B, no change in the switch point of increased mixing torque was found. In case of feedstock C the onset of the rapid change is shifted for 4 and 5 wt. % of SA as well. This can be satisfactorily explained by interactions among particular binder components. As shown recently [58], the role of SA surfactant might be, to some extent, substituted with CW, because it contains esters of stearic acid with high fatty alcohols, and exhibits very similar surface properties.

Kong *et al.* [58] observed mixing torques based on a continuously increasing powder loading testing, and indicated three zones. In the first zone, the values of the mixing torque remain almost unaffected, while in the second zone the mixing torque starts to slowly increase to reach the third zone corresponding to the abrupt torque rise. The values in the first zone might be attributed to a low filling content of the mixing chamber, because their measuring range was too large (from 50 to 78 vol. %). For this purpose, they modified the mixing test, measured the feedstocks differing in the 1 vol. % loading steps prepared separately, and obtained the torque evolution with two zones.

This is in accordance with results in this work (Fig. 53). On the other hand, Kong *et al.*, do not consider rapid increase in torque between two zones as critical solid loading. In this work, critical powder loading was considered the point, where the mixing torque drops down off the linear increasing function due to formation of voids or become erratic. To ensure an appropriate mould filling during injection moulding, the optimal solid loading was considered lower to this critical solid loading. According to German and Bose [3], optimal solid loading is proposed to be approximately 2 - 5 vol. % less than critical loading, while Dihoru *et al.* [86] recommends 7 - 8 vol. % less than critical. In both cases, they also refer to a critical solid loading as a point prior to void formation.

Incorporation of SA into the binder decreases surface tension between the powder and the binder and improves particles sliding to each other resulting into a better interparticle arrangement and an increase in critical (as well as optimal) solid loading (Tab. 14). For the binder composition A, obtained results showed that addition of 3 wt. % SA increased optimal solid loading in the tested feedstocks from 52 to 55 vol. %, in case of binder C 3 and 5 wt. % of SA raised this value from 54 to 55 and 56 vol. %, respectively.

Tab. 14 Impact of SA concentration on loading characteristics of feedstocks.

Binder	A		B		C	
	SA (wt. %)	SP (vol. %)	SP (vol. %)	CSL (vol. %)	SP (vol. %)	CSL (vol. %)
0		52.5	54	58	54.0	59
1		53.5	54	58	54.5	60
2		54.0	54	59	55.0	61
3		54.5	54	59	55.5	61
4		55.0	54	59	56.5	61
5		55.0	54	60	57.0	61

Influence of SA concentration on flow behaviour

Impact of SA concentration on feedstock flow performance was investigated on the feedstocks with the fixed amount of Al_2O_3 (52 vol. %) and all three binder compositions A, B and C. The fixed amount of powder (52 vol. %) was selected based on the previous results of torque measurements (see Fig. 53) in order to assure solid loading below the critical and also below the point where the torque rapidly increase. Fig. 54 shows the viscosity curves of feedstocks with a fixed amount of powder based on three different binder systems varying in concentration of SA.

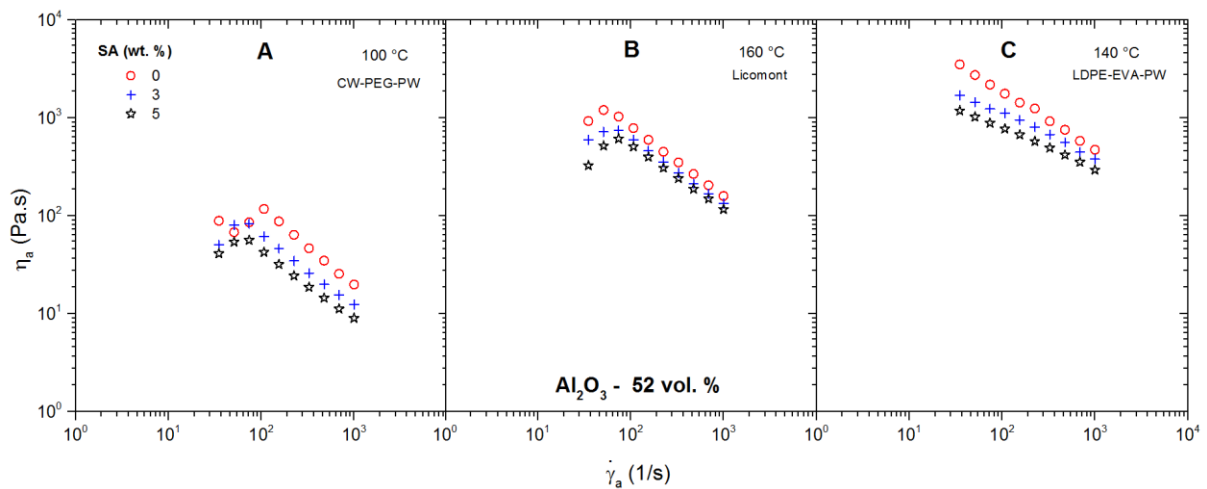


Fig. 54 Effect of SA on viscosity curves of feedstocks with 52 vol. % of Al_2O_3 .

All measured feedstocks exhibited pseudoplastic behaviour at higher shear rates which is relevant for PIM process. Nevertheless, the first two feedstocks based on binder A and B demonstrated an overshoots in the viscosity at a certain shear rate region. Further, the overshoots in the viscosity appear at certain shear rates, corresponding to structure reorganization during flow, and are shifted to higher shear rates for SA treated compounds. In this respect, SA has a similar effect on flow behavior of alumina feedstocks as the temperature [87].

Feedstocks based on binder A (CW/PW/PEG) can be processed at lower temperatures (*i.e.* around 100 °C) and provides suitable viscosity, especially for micro-injection molding; it is more than one order magnitude lower than that of the feedstock based on commercial binder. Similar values of viscosities in the corresponding shear rate range were obtained by Kong *et al.* [58] for fine 316 L stainless steel powder in CW/PW/PEG binder.

The viscosity of feedstocks based on commercial binder B can also be, to some extent, modified by SA. For fitting rheological data of this commercial binder, the recently proposed mathematical model [28] may also reflect the effect of SA.

In addition, flow properties of the feedstock based on ZrO₂ (52 vol. %) with binder B was investigated as well. As can be seen in Fig. 55, viscosity of zirconia feedstocks was even higher and flow properties demonstrated more instabilities in the flow course. Difficulties in measuring can be caused by high tendency for agglomeration, which could be also observed from SEM photograph in Fig. 13. Behaviour of these feedstocks made almost impossible their measurement.

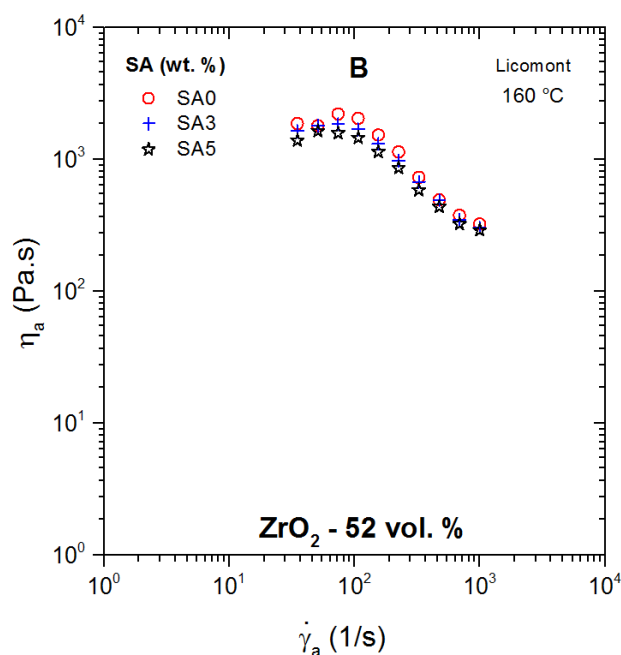


Fig. 55 Effect of SA on viscosity curves of feedstocks with 52 vol. % of ZrO₂.

Feedstock based on binder C (LDPE/EVA/PW) is characterized by a viscosity exceeding the value suggested by German and Bose [3] as suitable for PIM. On the other hand, the ethylene-based copolymer is responsible for pseudoplastic behavior of the feedstock (which is further strengthened by addition of SA), because it is formed of polymer blocks soluble in a binder and blocks that absorb on a powder surface acting as an anchor [62].

CONCLUSION

The aim of this thesis is devoted to polymer binder composition, including individual binder components characterization and their influence on powder injection moulding (PIM) process. Particular emphasis was also placed on an eco-friendly approach and maximisation of solid loading as one of the most important aspects in PIM technology. The overall framework was divided into three sections according to typical composition of a polymeric binder in which each component performs a specific task: effect of major component (i), backbone (ii) and additive (iii). Binders used in this work were designed as multi-component polymer systems with respect to previous results of a research team at Tomas Bata University in Zlín, Czech Republic and in collaboration with the Department of Materials Science and Engineering at Sheffield University, United Kingdom.

A comprehensive investigation of Inconel 718 based feedstocks demonstrated the important role of polyethylene glycol (PEG) molecular weight during PIM process. Feedstocks with various molecular weights of PEG demonstrated suitable viscosity for injection moulding due to pseudoplastic behaviour in the shear rate range measured. Higher molecular weights of PEG increased viscosity of feedstocks. On the other hand, these feedstocks were less viscosity temperature sensitive. The flow activation energy at a constant shear rate was shear dependent and increased with a higher shear rate and lower PEG molecular weight. Oppositely, the values of flow activation energy at a constant shear stress tended to be constant approaching a higher shear stress. No significant differences were found between indirect and direct measurements of end effects. Flow and viscosity curves are often based on apparent values, *i.e.* without corrections to capillary flow due to comparative character. However, it was found that the impact on a corrected shear stress is strongly dependent on PEG molecular weight used. Attention should also be paid to adequate approximate function for derivation of non-Newtonian indexes.

PEG as a major component soluble in water can be removed in the first stage of debinding by water leaching. This will create a network of interconnected pores, through which residual binders would be later thermally removed. Higher temperatures of water bath accelerated water debinding of PEG from moulded components. On the other hand, a negative aspect of acceleration was introduction of defects into debinded components. Internal voids were found, especially in case of feedstock composed from PEG 1 500, while other types of defects, such as cracking and blistering during water debinding appeared in samples composed with higher molecular weights of PEG. Sintered density of Inconel 718 tensile

samples was also affected by water debinding temperatures resulting in lower sintered density for samples debinded in water at higher temperatures. No significant differences were found in mechanical properties of sintered and heat treated Inconel 718 tensile samples, previously debinded in a water bath at 40 °C.

After the first stage of debinding, when the major part of the binder is removed, an important role is played by the backbone component/s, which has to assure shape stabilization of the component prior to sintering. In a novel binder system, carnauba wax (CW) and acrawax (AW) were considered to replace synthetic polyolefin backbone polymers, such as low density polyethylene (LDPE), enhancing the environmental sustainability of PIM technology.

Flow behaviour of investigated ceramic feedstocks was rather complex. Polyolefin based feedstocks demonstrated pseudoplastic flow up to a certain limit, then at higher shear region (approaching the real processing conditions) the flow turned into dilatant. On the other hand, both novel feedstocks based on CW, AW as well as feedstock based on the commercial binder exhibited pseudoplastic behaviour in this range. Their viscosity curves showed a sudden change in rheological behaviour (overshoots) at lower shear rates. With higher temperature, the onset of these overshoots was postponed to higher shear rates. An overshoot is probably caused by internal particle structure reorganization. Both novel multi-component binder systems, based on CW and AW, showed lower viscosity in comparison with feedstocks based on LDPE (as backbone component) or based on the commercial binder. Additionally, CW based feedstocks allow processing temperatures around 100 °C, which can be essential for injection moulding of reactive powders.

Thermal analysis was carried out via different scanning calorimetry (DSC) (from the 2nd second heating scans to eliminate thermal history of samples) in order to observe interaction between individual components (individual binder components, their mixtures and their combination with ceramic powders) within feedstocks. The presence of Al₂O₃ powder lowered melting temperatures of all tested binders except from LDPE. This may be related to changes in size of the crystalline domains of binders, caused by the presence of other components in the blends. The results obtained clearly showed differences in thermal behaviour of both wax-based feedstocks containing CW and AW in comparison to those containing hydrocarbons paraffin wax (PW) a LDPE, which are strictly non polar. Taking into account that Al₂O₃ powder has a polar character, it may indicate that both CW and AW containing polar groups provide better miscibility with PEG and the powder compared to paraffin PW and LDPE. Stronger cohesion can be beneficial for avoiding phase separation between the powder and the binder.

The powder binder separation can also be minimized by addition of small amounts of surface active agents, which lower the contact angle between the powder and binder resulting in better wettability of the powder. Surfactants create a thin layer composed of chemical absorption bonds on the surface of the powder allowing easier particle sliding that reduces viscosity of feedstocks and facilitate the processing during mixing and injection moulding. Moreover, surfactants can also enhance packing density resulting in higher powder loading. It is one of the options of how to modify critical powder loading instead of changing powder characteristics, because critical powder loading also depends on binder composition. Obtained results showed that incorporation of surfactant SA in binder composition positively affected processing parameters by lowering feedstock viscosity and consequently mixing torque as well. In order to receive higher critical solid loading, the amount of sufficient concentration of SA was strongly dependent on the type of the binder. In case of the commercially available binder Licomont, the influence of concentration of SA on the onset of a rapid increase in the mixing torque was negligible, but it reduced the viscosity of feedstock. In feedstock A, based on CW/PEG/PW, there was a notable shift of a rapid increase of mixing torque between concentrations of 0 and 3 wt. % of SA, while in using binder C based on LDPE/ethylene vinyl acetate (EVA)/PW there was a huge difference in all concentrations of SA resulting in a better interparticle arrangement with a higher amount of surfactant.

The powder loading of a feedstock plays a key role in the PIM process. Stability of feedstocks is highly sensitive to solid loading and a minimum amount of binder concentration leads to better shape retention, reduced shrinkage after solidification and a tight dimensional tolerance control. On the other hand, if the solid content is higher than critical powder loading, this may result in increased wear and process instability during the injection or debinding stage. For an evaluation of critical powder loading it is suitable to use a combination of both methods, mixing torque and rheology measurements. The onset of a rapid increase in powder loading could also be a good indicator for optimal solid loading.

In summary, this work contributed to deeper understanding of each component in PIM process. PEG molecular weight affected all processing parameters, but without final impact on mechanical properties of sintered Inconel 718. Water debinding temperature influenced sintered density and creation of defects. Feedstocks based on CW and AW showed overall lower viscosity than the polyolefin-based LDPE and the commercial feedstocks. Surfactant SA affected positively processing parameters, but its effect on critical loading strongly depends on binder composition.

CONTRIBUTION TO SCIENCE AND PRACTICE

Binder systems for PIM technology are still in a developing phase due to their requirement complexity. There are still challenges to eliminate drawbacks, improve the PIM process and produce less defective parts. The results of this study can serve for setting up suitable compositions of polymeric binders, debinding parameters and/or designing binder formulations with relevant PEG molecular weights. However, proper selection has to be always related to powder loading, powder properties, component size as well as to overall part shape complexity. PIM is an interdisciplinary approach combining polymer processing with powder technology, and not always all specifications for a given field are taken into account. For numerical simulations the values obtained from rheological measurements have to be corrected, and the present thesis offers guidelines on how to proceed with rheological evaluation (apart from phase separation).

The following findings of the presented thesis can be considered as important contributions for PIM process and science:

- Feedstock viscosity can be tailored via PEG molecular weight. The water debinding temperature for PEG removal influenced creation of defects and sintered density.
- Backbone components AW and CW are suitable, especially for micro injection moulding due to low feedstock viscosity. Feedstocks based on CW can find utilization in processing reactive powders due to low processing temperatures.
- Higher concentrations of SA can increase maximal powder loading.
- Eco-friendly approach in designed binders.

The results presented in the present thesis were also published in international scientific journals and at conferences.

Ongoing research and future perspectives

Ongoing research is carried out with mathematical modelling of PEG based feedstocks of different molecular weights. This means that viscosity of feedstocks could be tailored via PEG molecular weight. In all instances of newly developed binders it would be worth to test their tendency to phase separation. In case of CW and AW as backbone binders it is necessary to test their shape stability during late stages of debinding at higher temperatures.

REFERENCES

- [1] GERMAN, R. M. *Powder injection molding*. Metal Powder Industries Federation: Princeton, N.J., 1990.
- [2] MUTSUDDY, B. C., FORD, R. G. *Ceramic injection molding*. Springer Science & Business Media, 1994. ISBN 0-8493-3466-7.
- [3] GERMAN, R. M., BOSE, G. *Injection Molding of Metals and Ceramics*. Metal Powder Industries Federation: Princeton, N.J., 1997.
- [4] HEANEY, D. F. *Handbook of metal injection molding*. Elsevier, 2012.
- [5] CHECOT-MOINARD, D., RIGOLLET, C., LOURDIN, P. Powder injection moulding PIM of feedstock based on hydrosoluble binder and submicronic powder to manufacture parts having micro-details. *Powder Technology*, 208 (2011) 472-479.
- [6] PIM-International: Apple gives Metal Injection Moulding (MIM) a boost with its new Lightning connector. *Powder Injection Moulding International magazine*, vol.6. no. 4 December, 2012.
- [7] HAUSNEROVA, B.; KURITKA, I.; BLEYAN, D. Polyolefin backbone substitution in binders for low temperature powder injection moulding feedstocks. *Molecules*, 19 (2014) 2748-2760.
- [8] HAUSNEROVA, B., SAHA, P. KUBAT, J. KITANO, T. BECKER, J. Rheological behaviour of hard-metal carbide powder suspensions at high shear rates. *Journal of Polymer Engineering*, 20 (2000) 237-266.
- [9] CHUNG, C. I., RHEO, B. O. CAO, M. Y., LIU, C.X. Requirements of binder for powder injection molding. *1989 Advances in Powder Metallurgy*, 3 (1989) 67-78.
- [10] LOH, N. H., TOR, S. B., KHOR, K. A. Production of metal matrix composite part by powder injection molding. *Journal of Materials Processing Technology*, 108 (2001) 398-407.
- [11] ANI, S. M., MUCHTAR, A., MUHAMAND, N., GHANI, J. A. Binder removal via a two-stage debinding process for ceramic injection molding parts. *Ceramics International*, 40 (2014) 2819-2824.
- [12] OMAR, M. A., IBRAHIM, R., SIDIK, M. I., MUSTAPHA, M., MOHAMAD, M. Rapid debinding of 316L stainless steel injection moulded component. *Journal of Materials Processing Technology*, 140 (2003) 397-400.
- [13] RAK, Z. S. New trends in powder injection moulding. *Powder Metallurgy and Metal Ceramics*, 38 (1999) 126-132.
- [14] WEN, G., CAO, P., GABBITAS, B., ZHANG, D., EDMONDS, N. Development and design of binder systems for titanium metal injection molding: an overview. *Metallurgical and Materials Transactions A*, 44 (2013) 1530-1547.
- [15] GONZALEZ-GUTIERREZ, J., STRINGARI, G. B., ZUPANCIC, B., KUBYSHKINA, G., VON BERNSTORFF, B., EMRI, I. Time-dependent

- properties of multimodal polyoxymethylene based binder for powder injection molding. *Journal of Solid Mechanics and Materials Engineering*, 6 (2012) 419-430.
- [16] HSU, K. C. LIN, C. C., LO, G. M. Effect of wax composition on injection moulding of 304L stainless steel powder. *Powder Metallurgy*, 37 (1994) 272-276.
- [17] THOMAS-VIELMA, P., CERVERA, A., LEVENFELD, B., VAREZ, A. Production of alumina parts by powder injection molding with a binder system based on high density polyethylene. *Journal of the European Ceramic Society*, 28 (2008), 763-771.
- [18] QNOGUEIRA, R. E. F. Q, BEZERRA, A. C., DOS SANTOS, F. C., SOUSA, M. R., ACCHAR, W. Low-Pressure Injection Molding of Alumina Ceramics Using a Carnauba Wax Binder: Preliminary Results. In: *Key Engineering Materials*. Trans Tech Publications, 189 (1999) 67-72.
- [19] BLEYAN, D., SVOBODA, P., HAUSNEROVA, B. Specific interactions of low molecular weight analogues of carnauba wax and polyethylene glycol binders of ceramic injection moulding feedstocks. *Ceramics International*, 41 (2015) 3975-3982.
- [20] SUPRIADI, S., BAEK, E. R., CHOI, C. J., LEE, B. T. Binder system for STS 316 nanopowder feedstocks in micro-metal injection molding. *Journal of Materials Processing Technology*, 187 (2007) 270-273.
- [21] YANG, W. W. HON, M. H. In situ evaluation of dimensional variations during water extraction from alumina injection-moulded parts. *Journal of the European Ceramic Society*, 20 (2000) 851-858.
- [22] YANG, W. W., WANG, M. C., HON, M. H. Solvent debinding mechanism for alumina injection molded compacts with water-soluble binders. *Ceramics international*, 29 (2003) 745-756.
- [23] CAO, M. Y., O'CONNOR, J. W., CHUNG, C. I. A new water soluble solid polymer solution binder for powder injection molding. In: *Powder Injection Molding Symposium*, (1992) 85-98.
- [24] HENS, K. F., GERMAN, R. M. Advanced processing of advanced materials via powder injection molding. *Advances in Powder Metallurgy and Particulate Materials*, 5 (1993) 153-164.
- [25] CHEN, G., CAO, P., WEN, G., EDMONDS, N. Debinding behaviour of a water soluble PEG/PMMA binder for Ti metal injection moulding. *Materials Chemistry and Physics*, 139 (2013) 557-565.
- [26] SIDAMBE, A. T., *et al.* Metal injection moulding of CP-Ti components for biomedical applications. *Journal of Materials Processing Technology*, 212 (2012) 1591-1597.
- [27] HIDALGO, J., ABAJO, C., JIMENEZ-MORALES, A., TORRALBA, J. M. Effect of a binder system on the low-pressure powder injection moulding of water-soluble zircon feedstocks. *Journal of the European Ceramic Society*, 33 (2013) 3185-3194.

- [28] HAUSNEROVA, B., MARCANIKOVA, L. FILIP, P., SAHA, P. Optimization of powder injection molding of feedstock based on aluminum oxide and multicomponent water-soluble polymer binder. *Polymer Engineering and Science*, 51 (2011) 1376-1382.
- [29] LIANG, S., HUANG, B., AHMAD, Z. A., NOOR, A. F. M., HUSSIN, K. Preparation and evaluation of Al₂O₃ plastic forming feedstock with partially water soluble polymer as a binder, *Journal of Materials Processing Technology*, 137 (2003) 128-131.
- [30] LIU, W., YANG, X., XIE, Z., JIA, C., WANG, L. Novel fabrication of injection-moulded ceramic parts with large section via partially water-debinding method. *Journal of the European Ceramic Society*, 32 (2012) 2187-2191.
- [31] YANG, W. W., YANG, K. Y., HON, M. H. Effects of PEG molecular weights on rheological behavior of alumina injection molding feedstocks. *Materials Chemistry and Physics*, 78 (2003) 416-424.
- [32] HAYAT, M. D., WEN, G., ZULKIFLI, M. F., CAO, P. Effect of PEG molecular weight on rheological properties of Ti-MIM feedstocks and water debinding behaviour. *Powder Technology*, 270 (2015) 296-301.
- [33] HUANG, M.-S., HSU, Hung-Chuan. Effect of backbone polymer on properties of 316L stainless steel MIM compact. *Journal of Materials Processing Technology*, 209 (2009) 5527-5535.
- [34] BAKAN, H. I., JUMADI, Y., MESSER, P. F., DAVIES, H. A., ELLIES, B. Study of processing parameters for MIM feedstock based on composite PEG-PMMA binder. *Powder Metallurgy*, 41 (1998) 289-291.
- [35] TSENG, W. J. Influence of surfactant on rheological behaviors of injection-molded alumina suspensions. *Materials Science and Engineering*, 289 (2000) 116-122.
- [36] ABAJO, C., HIDALGO, J., JIMENEZ-MORALES, A., TORRALBA, J. M. Optimisation of eco-friendly binary binder system for powder injection moulding. *Powder Metallurgy*, 57 (2014) 196-203.
- [37] ESCOBAR, C. F. DOS SANTOS, L. A. New eco-friendly binder based on natural rubber for ceramic injection molding process. *Journal of the European Ceramic Society*, 35 (2015) 3567-3575.
- [38] HUANG, Y., YANG, J. *Novel colloidal forming of ceramics*. Springer Science & Business Media, (2011).
- [39] LI, Yimin; LI, Liujun; KHALIL, K. A. Effect of powder loading on metal injection molding stainless steels. *Journal of Materials Processing Technology*, 183 (2007) 432-439.
- [40] SHIVASHANKAR, T. S., ENNETI, R. T. GERMAN, R. M., ATRE, S. V. The effects of material attributes on powder-binder separation phenomena in powder injection molding. *Powder technology*, 243 (2013) 79-84.

- [41] SIGMUND, W. M., BELL, N. S., BERGSTROM, L. Novel Powder-Processing Methods for Advanced Ceramics. *Journal of the American Ceramic Society*, 83 (2000) 1557-1574.
- [42] KARATAS, C., KOCER, A., UNAL, H. I., SARITAS, S. Rheological properties of feedstocks prepared with steatite powder and polyethylene-based thermoplastic binders. *Journal of Materials Processing Technology*, 152 (2004) 77-83.
- [43] LI, Y. M. LIU, X. Q., LUO, F. H., YUE, J. L. Effects of surfactant on properties of MIM feedstock. *Transactions of Nonferrous Metals Society of China*, 17 (2007) 1-8.
- [44] LIN, S. T., GERMAN, R. M. Interaction between binder and powder in injection moulding of alumina. *Journal of materials science*, 29 (1994) 5207-5212.
- [45] CHAN, T. Y. LIN, S.T. Effects of stearic acid on the injection molding of alumina. *Journal of the American Ceramic Society*, 78 (1995) 2746-2752.
- [46] HANEMANN, T., HELDELE, R., MUELLER, T., HAUSSELT, J. Influence of Stearic Acid Concentration on the Processing of ZrO₂-Containing Feedstocks Suitable for Micropowder Injection Molding. *International Journal of Applied Ceramic Technology*, 8 (2011) 865-872.
- [47] BRICOUT, J., GELIN, J. C., ABLITZER, C., MATHERON, P., BROTHIER, M. Influence of powder characteristics on the behaviour of PIM feedstock. *Chemical Engineering Research and Design*, 91 (2013) 2484-2490.
- [48] MUTSUDDY, B. C. Rheology and mixing of ceramic mixtures used in plastic molding. *Chemical Processing of Ceramics*, 8 (1994).
- [49] BOUSMINA, M., AIT-KADI, A., FAISANT, J. B. Determination of shear rate and viscosity from batch mixer data. *Journal of Rheology (1978)*, 43 (1999) 415-433.
- [50] REDDY, J. J., VIJAYAKUMAR, M., MOHAN, T. R., RAMAKRISHNAN, P. Loading of solids in a liquid medium: Determination of CBVC by torque rheometry. *Journal of the European Ceramic Society*, 16 (1996) 567-574.
- [51] SUPATI, R., LOH, N. H., KHOR, K. A., TOR, S. B. Mixing and characterization of feedstock for powder injection molding. *Materials Letters*, 46 (2000) 109-114.
- [52] WARREN, J., GERMAN, R. M. The effect of powder characteristics on binder incorporation for injection molding feedstock. *Modern Developments in Powder Metallurgy*, 18 (1988) 391-402.
- [53] KITANO, T., KATAOKA, T., SHIROTA, T. An empirical equation of the relative viscosity of polymer melts filled with various inorganic fillers. *Rheologica Acta*, 20 (1981) 207-209.
- [54] HONEK, T., HAUSNEROVA, B., SAHA, P. Relative viscosity models and their application to capillary flow data of highly filled hard-metal carbide powder compounds. *Polymer Composites*, 26 (2005) 29-36.

- [55] CONTRERAS, J. M., JIMENEZ-MORALES, A., TORRALBA, J. M. Experimental and theoretical methods for optimal solids loading calculation in MIM feedstocks fabricated from powders with different particle characteristics. *Powder Metallurgy*, 53 (2010) 34-40.
- [56] CONTRERAS, J. M., JIMENEZ-MORALES, A., TORRALBA, J. M. Improvement of rheological properties of Inconel 718 MIM feedstock using tailored particle size distributions. *Powder Metallurgy*, 51 (2008) 103-106.
- [57] AGGARWAL, G. PARK, S. J., SMID, I. Development of niobium powder injection molding: Part I. Feedstock and injection molding. *International Journal of Refractory Metals and Hard Materials*, 24 (2006) 253-262.
- [58] KONG, X., BARRIERE, T., GELIN, J. C. Determination of critical and optimal powder loadings for 316L fine stainless steel feedstocks for micro-powder injection molding. *Journal of Materials Processing Technology*, 212 (2012) 2173-2182.
- [59] MUKUND, B. N., HAUSNEROVA, B., SHIVASHANKAR, T. S. Development of 17-4PH stainless steel bimodal powder injection molding feedstock with the help of interparticle spacing/lubricating liquid concept. *Powder Technology*, 283 (2015) 24-31.
- [60] HONEK, T., HAUSNEROVA, B., SAHA, P. Temperature dependent flow properties of powder injection moulding compounds. *Applied Rheology*, 12 (2002) 72-80.
- [61] HUANG, B., LIANG, S., QU, X. The rheology of metal injection molding. *Journal of Materials Processing Technology*, 137 (2003) 132-137.
- [62] HAUSNEROVA, B., SAHA, P., KUBAT, J. Capillary flow of hard-metal carbide powder compounds. *International Polymer Processing*, 14 (1999) 254-260.
- [63] HAUSNEROVA, B. Rheological characterization of powder injection molding compounds. *Polimery*, 55(2010) 3-11.
- [64] SHENOY, A. V. *Rheology of filled polymer systems*. Springer Science & Business Media, 2013.
- [65] ZHOU, James Z.Q. UHLHERR, Peter HT; LUO, Fang Tunan. Yield stress and maximum packing fraction of concentrated suspensions. *Rheologica Acta*, 34 (1995) 544-561.
- [66] ROSENBAUM, E. E., HATZIKIRIAKOS, S. G. Wall slip in the capillary flow of molten polymers subject to viscous heating. *American Institute of Chemical Engineers*, 43 (1997) 598-608.
- [67] LAUN, H. M. Pressure dependent viscosity and dissipative heating in capillary rheometry of polymer melts. *Rheologica Acta*, 42 (2003) 295-308.
- [68] MITSOULIS, E., HATZIKIRIAKOS, S. G. Bagley correction: the effect of contraction angle and its prediction. *Rheologica Acta*, 42 (2003) 309-320.
- [69] AHO, J., SYRJALA, S. Determination of the entrance pressure drop in capillary rheometry using Bagley correction and zero-length capillary. *Annual Transactions-Nordic Rheology Society*, 14 (2006) 143.

- [70] CARREAU, P. J., DE KEE, D., CHHABRA, R. P. *Rheology of Polymeric Systems: Principles and Applications*. Munich: Hanser Publishers, 1997.
- [71] DRABEK, J., ZATLOUKAL, M. Rheological evaluation of melt blown polymer melt. *Novel Trends in Rheology V*, (2013).
- [72] HONEK, T., HAUSNEROVA, B. SAHA, P. Temperature dependent flow instabilities of highly filled polymer compounds. *Applied Rheology*, 12 (2002) 72-80.
- [73] REN, S. B., *et al.* Effects of binder compositions on characteristics of feedstocks of microsized SiC ceramic injection moulding. *Powder Metallurgy*, 50 (2007) 255-259.
- [74] SOTOMAYOR, M. E., VAREZ, A., LEVENFELD, B. Influence of powder particle size distribution on rheological properties of 316L powder injection moulding feedstocks. *Powder Technology*, 200 (2010) 30-36.
- [75] LIU, Z. Y.; LOH N. H.; TOR S. B.; KHOR, K. A. Characterization of powder injection molding feedstock. *Materials Characterization*, 49 (2002) 313-320.
- [76] KATE, K. H., ENNETI, R. K., PARK, S. J., GERMAN, R. M., ATRE, S. V. Predicting powder-polymer mixture properties for PIM design. *Critical Reviews in Solid State and Materials Sciences*, 39 (2014)197-214.
- [77] SANETRNIK, D., HAUSNEROVA, B., FILIP, P., HNATKOVA, E. Influence of Capillary Die Geometry on Wall Slip of Highly Filled Powder Injection Molding Compounds, *Powder Technology*, 325 (2018) 615-619.
- [78] CHUANKRERKKUL, N., MESSER, P. F., DAVIES, H. A. Flow and void formation in powder injection moulding feedstocks made with PEG/PMMA binders Part 1–Experimental observations. *Powder Metallurgy*, 51 (2008) 66-71.
- [79] CHUANKRERKKUL, N., MESSER, P. F., DAVIES, H. A. Flow and void formation in powder injection moulding feedstocks made with PEG/PMMA binders Part 2–Slip band model. *Powder Metallurgy*, 51 (2008) 72-77.
- [80] PARK, M. S., KIM, J. K., AHN, S. SUNG, H. J. Water-soluble binder of cellulose acetate butyrate/poly (ethylene glycol) blend for powder injection molding, *Journal of Materials Science*, 36 (2001) 5531-5536.
- [81] BLEYAN, D., HAUSNEROVA, B., KASPARKOVA, V., PATA, V. Surface Adhesion between Ceramic Injection Molding Feedstocks and Processing Tools. *Ceramics International*, 42 (2016) 460-465.
- [82] BLEYAN, D., HAUSNEROVA, B., SVOBODA, P. The Development of Powder Injectionmoulding Binders: A Quantification of Individual Components' Interactions. *Powder Technology*, 286 (2015) 84-89.
- [83] BLEYAN, D., SVOBODA, P.; HAUSNEROVA, B. Specific Interactions of Low Molecular Weight Analogues of Carnauba Wax and Polyethylene Glycol Binders of Ceramic Injection Moulding Feedstocks. *Ceramics International*, 41 (2015) 3975-3982.

- [84] HOFFMAN, R. L. Discontinuous and Dilatant Viscosity Behavior in Concentrated Suspensions. I. Observation of a Flow Instability. *Transactions of the Society of Rheology*, 16 (1972) 155-173.
- [85] ROYER, A. BARRIERE, T., GELIN, J. C. The degradation of poly (ethylene glycol) in an Inconel 718 feedstock in the metal injection moulding process. *Powder Technology*, 284 (2015) 467-474.
- [86] DIHORU, L. V., SMITH, L. N. ORBAN, R. GERMAN, R. M. Experimental study and neural network modeling of the stability of powder injection molding feedstocks. *Materials and Manufacturing Processes*, 15 (2000) 419-438.
- [87] HAUSNEROVA, B., KASPARKOVA, V. HNATKOVA, E. Effect of backbone binders on rheological performance of ceramic injection molding feedstocks. *Polymer Engineering and Science*, 57 (2017) 739-745.

LIST OF FIGURES

Fig. 1 Lightning connector produced by PIM [6].	8
Fig. 2 Basic steps in PIM technology	8
Fig. 3 The main aspects of PIM feedstocks.	11
Fig. 4 Powder loading (a) excess, (b) critical, (c) insufficient.	14
Fig. 5 Coating of spherical particles [40].	15
Fig. 6 Torque evolution as a function of time [49].	17
Fig. 7 Experimental mixture density vs powder loading.	19
Fig. 8 Relative viscosity as function of powder loading.	20
Fig. 9 Torque evolution by continuously increasing powder loading.	21
Fig. 10 Schematic view of PIM compound flow properties [63].	22
Fig. 11 Schematic view of relocation of melt flow inside a capillary die (a), velocity profiles in a capillary die based on value of non-Newtonian index (b).	23
Fig. 12 Main factors affecting flow properties of PIM feedstocks.	25
Fig. 13 SEM photographs of utilised powders.	27
Fig. 14 Volumetric particle size distribution.	28
Fig. 15 Melting ranges of PEGs obtained from DSC.	31
Fig. 16 Thermal analysis of Licomont.	31
Fig. 17 Distribution of PEG molecular weight.	32
Fig. 18 Brabender Plastograph equipped with Mixer W50.	34
Fig. 19 Schematic view of mixing chamber (a) and measured values during mixing (b).	35
Fig. 20 Schematic principle of dual axial centrifuge.	36
Fig. 21 Schematic view of tensile test specimen.	36
Fig. 22 Thermal debinding, sintering and cooling profile.	37
Fig. 23 Solution Treatment and Ageing Profile for Inconel 718.	37
Fig. 24 Schematic view of (a) capillary rheometer, (b) pressure drops.	38
Fig. 25 Capillary dies for indirect (a), and direct (b) measurement of end effects.	39
Fig. 26 Arrhenius plot.	42
Fig. 27 Schematic view of stress-strain diagram.	43
Fig. 28 Illustration of PIM feedstock composition based on Inconel 718.	46
Fig. 29 Effect of PEG molecular weight on flow behaviour of Inc718 feedstocks.	47
Fig. 30 Example of Arrhenius plots for viscosity obtained at constant shear rate (a) and constant pressure (b).	49

Fig. 31 Activation energy of feedstocks at constant: shear rate (a) and constant shear stress (b).....	49
Fig. 32 Measured pressure drop of all feedstocks using three capillaries.	50
Fig. 33 Extrapolation of end effects from Linear Bagley plots.	51
Fig. 34 Comparison of end effects obtained from direct and indirect measurements.....	52
Fig. 35 Linear and non-linear slope of log-log plots of feedstock P4K for three approximate functions.....	53
Fig. 36 Non-Newtonian indexes obtained from the (a) linear and, (b) 2 nd polynomial fitting in dependence on apparent shear rate.	54
Fig. 37 Apparent and corrected viscosity curves for selected Inc718 feedstocks.	55
Fig. 38 PEG removal rate during water debinding at three temperatures.	56
Fig. 39 Densities of sintered Inc718 based on water debinding temperatures. ..	57
Fig. 40 Tensile properties of sintered Inc718 previously debinded at 40 °C.	58
Fig. 41 SEM image of Al ₂ O ₃ – tendency to agglomeration.....	58
Fig. 42 Flow properties of Al ₂ O ₃ feedstocks (50 vol. %) based on binders with LDPE, CW or AW as backbone component.....	60
Fig. 43 Flow properties feedstock based on Al ₂ O ₃ and commercial binder.	61
Fig. 44 DSC curves of each analysed samples from the 2 nd heating scan.	63
Fig. 45 Change in peak melting temperature ΔT of three-component mixture (binder/Al ₂ O ₃ /PEG) relatively to corresponding individual binder.....	65
Fig. 46 Mixing torque obtained by continuous increasing volume of Al ₂ O ₃	67
Fig. 47 Mixing torque obtained by continuous increasing volume of 17-4 PH.	67
Fig. 48 Mixing torque obtained by separately increasing 17-4 PH volume.	68
Fig. 49 Comparison of mixing torques obtained by two methods.....	68
Fig. 50 SEM of feedstocks: Al ₂ O ₃ , 58 vol. % (a) and 17-4PH, 68 vol. % (b)....	69
Fig. 51 Flow behaviour of feedstocks based on Al ₂ O ₃ and 17-4PH with different powder loading.....	70
Fig. 52 Raw (online) data on rheometer of mixture with 58 vol. % of Al ₂ O ₃	70
Fig. 53 Obtained torques based on powder loading and different concentration of SA for binder A, B and C.....	71
Fig. 54 Effect of SA on viscosity curves of feedstocks with 52 vol. % of Al ₂ O ₃	73
Fig. 55 Effect of SA on viscosity curves of feedstocks with 52 vol. % of ZRO ₂	74

LIST OF TABLES

Tab. 1 Most commonly used binder components used for PIM.	13
Tab. 2 Powder characteristics.....	28
Tab. 3 List of the individual binder components.....	29
Tab. 4 Material characteristics of binder components.	30
Tab. 5 HPLC analysis of PEG molecular weight.....	32
Tab. 6 Compositions of binder systems utilised though this study.....	33
Tab. 7 Composition of feedstocks based on different PEG molecular weights..	46
Tab. 8 Measured pressure drops Δp in bar at shear rate of 2500 1/s using various capillary lengths and impact of end effects on it in %	51
Tab. 9 Effect of approximate function (linear or polynomial regression) on the value of Non-Newtonian index as an example for the P4K at 140 °C.....	53
Tab. 10 Binder composition (content of each component is given in wt. %).	59
Tab. 11 Composition of model samples used for DSC measurements.	62
Tab. 12 Melting temperatures of individual samples obtained from DSC.	64
Tab. 13 Composition of binder components used (wt. %).	66
Tab. 14 Impact of SA concentration on loading characteristics of feedstocks. ..	72

LIST ABBREVIATIONS AND ACRONYMS

Abbreviations

Al ₂ O ₃	Aluminum oxide (alumina)
AW	Acrawax
BW	Beeswax
CIM	Ceramic injection moulding
CW	Carnauba wax
DSC	Different scanning calorimeter/y
EDX	Energy dispersive X-ray spectroscopy
ELSD	Evaporative light scattering detector
EVA	Ethylene vinyl acetate
GPC	Gel permeation chromatography
HDPE	High density polyethylene
HPLC	High-performance liquid chromatography
Inc718	Inconel 718
LDPE	Low density polyethylene
MIM	Metal injection moulding
OA	Oleic acid
PE	Polyethylene
PEG	Poly(ethylene glycol)
PIM	Powder injection moulding
PMMA	Poly(methyl methacrylate)
POM	Polyoxymethylene
PP	Polypropylene
PW	Paraffin wax
SA	Stearic acid (SA)
SEM	Scanning electron microscopy
ZrO ₂	Zirconium dioxide (zirconia)

Symbols

A	Pre-exponential factor
a, b, c, d	Parameters
CSL	Critical solid loading
D	Diameter
E	Young's modulus
$E_{a,\dot{\gamma}}$	Flow activation energy at constant shear rate

$E_{a,\tau}$	Flow activation energy at constant shear stress
E_a	Flow activation energy
F	Force
F_m	Maximum force
\dot{Q}	Volumetric flow rate
L	Capillary length
L_0	Initial gauge length
M_n	Number-average molecular weight
M_w	Weight-average molecular weight
n	Non-Newtonian index
PDI	Polydispersity index
R	Gas constant, capillary radius
R_m	Tensile strength
$R_{p0.2}$	Proof strength
S	Area
S_0	Original cross-sectional area
SD	Standard deviation
SP	Switch point
T	Temperature
T_m	Melting temperature
v	Piston speed
w_b	Weight fractions of binder
w_p	Weight fractions of powder

Greek letters

x_i	Each of values of the data
ρ_b	Density of the binder
ρ_f	Feedstock density
ΔL	Change in gauge length
δ	Inter particle spacing parameter
Φ	Solid volume fraction
Φ_{L1}	Interstitial space liquid binder volume
Φ_{L2}	Liquid sphere shell volume
Δp	Total pressure drop
Δp_{cap}	Capillary pressure
Δp_{end}	End effects
Δp_{ent}	Entrance pressure
Δp_{exit}	Exit pressure drop

ΔT	Change in peak melting temperature
δ	Inter particle spacing parameter
η	Viscosity of filled system
η_0	Viscosity of pure binder
η_r	Relative viscosity
ρ	Density
ρ_p	Density of the powder
n	Size of the set of values
\bar{x}	Arithmetic mean
$\dot{\gamma}$	Apparent shear rate
$\dot{\gamma}_c$	Corrected shear rate
ε	Strain
τ	Shear stress
τ_a	Apparent shear stress
τ_c	Corrected shear stress

LIST OF PUBLICATIONS

Web of Science

1. **HNATKOVA, E.**, HAUSNEROVA, B. Impact of Stearic Acid on Powder Loading and Flow Properties of Ceramic Injection Molding Feedstocks, submitted to *Ceramic International*, 2019.
2. SANETRNIK, D., HAUSNEROVA, B., FILIP, P., **HNATKOVA, E.** Influence of Capillary Die Geometry on Wall Slip of Highly Filled Powder Injection Molding Compounds, *Powder technology*, 325 (2018) 615-619.
3. **HNATKOVA, E.**, HAUSNEROVA, B. HALES, A., JIRANEK, L., DERGUTI, F., TODD, I. Processing of MIM feedstocks based on Inconel 718 powder and partially water-soluble binder varying in PEG molecular weight, *Powder Technology*, 322 (2017) 439-446.
4. HAUSNEROVA, B., KASPARKOVA, V., **HNATKOVA, E.** Effect of Backbone Binders on Rheological Performance of Ceramic Injection Molding Feedstocks. *Polymer Engineering and Science*, 57 (2017) 739-745.
5. **HNATKOVA, E.**, DVORAK, Z. Effect of the skin-core morphology on the mechanical properties of injection-moulded parts. *Materials and technology*, 50 (2016) 195-198.
6. KUCHARCZYK, P., **HNATKOVA, E.**, DVORAK, Z., SEDLARIK, V. Novel aspects of the degradation process of PLA based bulky samples under conditions of high partial pressure of water vapour, *Polymer Degradation and Stability*, 98 (2013) 150-157.

Scopus

1. MALOCH, J., **HNATKOVA, E.**, ŽALUDEK, M., KRATKY, P. Effect of Processing Parameters on Mechanical Properties of 3D Printed Samples, *Materials Science Forum*, 919 (2018) 230-235.
2. **HNATKOVA, E.**, SANETRNIK, D., PATA, V., HAUSNEROVA, B., DVORAK Z. Mold Surface Analysis after Injection Molding of Highly Filled Polymeric Compounds, *Manufacturing Technology*, 16 (2016) 1213-2489.
3. HUBA, J., SANETRNIK, D., **HNATKOVA, E.**, HAUSNEROVA, B., DVORAK, Z. New Application of Powder Injection Molded Product in Medical Field. *Manufacturing Technology*, 16 (2016) 94-98.

4. DVORAK, Z., **HNATKOVA, E.**, SEDLACIK, M. Mold Surface Contamination during Polymer Processing, *Manufacturing Technology*, 16 (2016) 63-69.
5. HUBA, J., SANETRNIK, D., **HNATKOVA, E.**, HAUSNEROVA, B. Mechanical Properties of New and Recycled PIM Feedstock. *Applied Mechanics and Materials*, 732 (2015) 103-106.
6. **HNATKOVA, E.**, KRATKY, P., DVORAK, Z. Production of anatomical models via rapid Prototyping. *International Journal of circuits, systems and signal processing*, 8 (2014) 479-486.
7. **HNATKOVA, E.**, DVORAK, Z., ZLINSKY, V. Design of the tool for production of ear ventilation tubes, *Applied Mechanics and Materials*, 693 (2014) 406-411.

Conference proceedings

1. HAUSNEROVA, B., KASPARKOVA, V., **HNATKOVA, E.** Rheological and thermal performance of newly developed binder systems for ceramic injection molding, *AIP Conference Proceedings*, 1736 (2016) 020120.
2. **HNATKOVA, E.**, JELINKOVA, L., MRACEK, A., FRYZA, L. Sušení polymerních materiálů s ohledem na kvalitu pohledových vstříkovaných dílů. *Conference Plastko 2016*, April 20 – 21, 2016, Zlín, Czech Republic.
3. DVORAK, Z., **HNATKOVA, E.** Sezónnost jakosti kaučukových směsí. *Conference Plastko 2016*, April 20 – 21, 2016, Zlín, Czech Republic.
4. **HNATKOVA, E.**, SANETRNIK, D., PATA, V., HAUSNEROVA, B., DVORAK, Z. Mold Surface Analysis after Injection Molding of Highly Filled Polymeric Compounds, *Conference ICTKI 2016*, February 3 – 4, 2016, Litoměřice, Czech Republic.
5. DVORAK, Z., **HNATKOVA, E.**, SEDLACIK, M. Mold Surface Contamination during Polymer Processing, *Conference ICTKI 2016*, Litoměřice, Czech Republic, February 3 - 4, 2016.
6. HUBA, J., SANETRNIK, D., **HNATKOVA, E.**, HAUSNEROVA, B., DVORAK, Z. New Application of Powder Injection Molded Product in Medical Field, *Conference ICTKI 2016*, February 3 - 4, 2016, Litoměřice, Czech Republic.
7. HAUSNEROVA, B., SANETRNIK, D., **HNATKOVA, E.** Wall-slip as a phenomenon attending processing of highly powder particle filled polymer melts. In *M2D2015: 6th International Conference on Mechanics and Materials in Design*, July26-30, 2015, Ponta Delgada, Azores.

8. **HNATKOVA, E., UREDNICEK, A., DVORAK, Z.** Optimization of segmented tire mould. *53rd Conference on Experimental Stress Analysis*, June 1-4, 2015, Český Krumlov, Czech Republic.
9. **HNATKOVA, E., SANETRNIK, D., HAUSNEROVA, B.** Effect of Molecular Weight on Entrance Pressure Drop in Highly Filled Systems. *2nd International Conference on Rheology and Modeling of Materials*, October 5-9, 2015, Miskolc-Lillafüred, Hungary.
10. **HNATKOVA, E., SANETRNIK, D., HAUSNEROVA, B.** Effects of stearic acid surfactant on critical solid loading and flow properties of powder injection molding feedstock. *2nd International Conference on Rheology and Modeling of Materials*, October 5-9, 2015, Miskolc-Lillafüred, Hungary.
11. **HNATKOVA, E., HAUSNEROVA, B., HALES, A., JIRANEK, L., ALCON, J. M.** Rheological Investigation of Highly Filled Polymers: Effect of Molecular Weight. *AIP 2015 conference proceedings*, 1662 (2015) 040003.
12. **HUBA, J., SANETRNIK, D., HAUSNEROVA, B., HNATKOVA, E., DVORAK, Z., ZLINSKY, V.** New Design of Adenoid Curette Produced via Powder Injection Molding Technology. *8th International Conference on Material Science*, November 7-9, 2015, Rome, Italy.
13. **HNATKOVA, E., PAVELOVA, P., DVORAK, Z.** Effect of skin-core morphology on mechanical properties in injection-molded parts. *22nd International Conference on Materials and Technology*, October 20–22, 2014, Portorož, Slovenia.
14. **HNATKOVA, E., BLEYAN, D., HALES, A., JIRANEK, L., DERGUTI, F., HAUSNEROVA, B., TODD I.** Comparative study of partially water-soluble metal injection moulding feedstock based on Inconel 718: the effect of polyethylene glycol molecular weight on rheology and debinding. *Euro PM2014 Congress & Exhibition*, September 21-24, 2014, Salzburg, Austria.
15. **HNATKOVA, E., KRATKY, P., DVORAK, Z.** Conversion of 2D medical scan data into 3D printed models. *18th International Conference on Circuits, Systems, Communications and Computers*, July 17-21, 2014, Santorini, Greece.
16. **DVORAK, Z., MALOCH, J., HNATKOVA, E.** Vady vznikající při výrobě výrobků vyráběných technologií vstřikování. *Conference Plastko 2014*, April 8 - 9, 2014, Zlín, Czech Republic.
17. **HNATKOVA, E., BLEYAN, D., HALES, A., JIRANEK, L., DERGUTI, F., HAUSNEROVA, B.** Vliv molekulové hmotnosti vysoce plněných polymerů na tokové vlastnosti. *Conference Plastko 2014*, April 8 - 9, 2014, Zlín, Czech Republic.

18. KRATKY, P., **HNATKOVA, E.**, DVORAK, Z. Možnost převodu 2D obrazových dat do reálných 3D medicinských modelů. *Conference Plastko 2014*, April 8-9, 2014, Zlín, Czech Republic.
19. PAVELOVA, P., **HNATKOVA, E.** Studium skin-core morfologických struktur u vstříkovaného polypropylenu. *Conference Plastko 2014*, April 8 - 9, 2014, Zlín, Czech Republic.
20. HUBA, J., SANETRNIK, D., **HNATKOVA, E.** HAUSNEROVA, B. Mechanické vlastnosti sintrovaných PIM tělísek. *Conference Plastko 2014*, April 8 - 9, 2014, Zlín, Czech Republic.
21. HUBA, J., SANETRNIK, D., **HNATKOVA, E.**, HAUSNEROVA B. Mechanical properties of sintered PIM test specimens. *52nd International Conference on Experimental Stress Analysis*, 2-5 June 2014, Mariánské Lázně, Czech Republic.
22. **HNATKOVA, E.**, KUCHARCZYK, P., SEDLARIK, V., DVORAK, Z. Investigation of Poly(L-lactic acid) Degradation Process under Various Abiotic Conditions. *Conference Plastko 2012*, April 11-12, 2012, Zlín, Czech Republic.
23. **HNATKOVA, E.**, DVORAK, Z. Development of the tool for a production of ear ventilation tubes. *Student Scientific Conference 2012*, Tomas Bata University in Zlín, May 10, 2012, Zlín, Czech Republic.
24. **HNATKOVA, E.**, SEDLARIK, V. The effect of crystallinity on mechanical and thermal properties of biodegradable polylactide. *Conference Plastko 2010*, April 13-14, 2010, Zlín, Czech Republic.

Others

1. **HNATKOVA, E.**, DVORAK, Z. Demoulding of Tires from Segmented Mould. *Applied Mechanics and Materials*, 827 (2016) 133-136.

Utility models and functional samples

1. DVORAK, Z., **HNATKOVA, E.**, SEDLARIK, V., ZLINSKY, V., STANEK, M. Optimalizovaná soustava zařízení k výrobě dutin forem tvarově specifických dílců, Utility model Nr. 25349, 2013, Tomas Bata University in Zlín, Czech Republic.
2. HAUSNEROVA, B., HUBA, J., SANETRNIK, D., **HNATKOVA, E.**, DVORAK, Z., ZLINSKY, V. Cutting tool for application in the nasopharynx, Functional sample, 2015 Zlín. Tomas Bata University in Zlín, Czech Republic.

CURRICULUM VITAE

Name Eva Hnátková

Date of birth: 9th June 1982

Address: Nad Stráněmi 4531, 760 05 Zlín

Nationality: Czech

Contact: ehnatkova@utb.cz

Telephone: +420 604 328 809



Education

2012 – present **Doctoral degree**
Process Engineering/Tools and Processes
Faculty of Technology, TBU in Zlín

2010 – 2012 **Master's degree**
Process Engineering/Technological Equipment Construction
Faculty of Technology, TBU in Zlín

2007 – 2010 **Bachelor's degree**
Process Engineering/Technological Equipment
Faculty of Technology, TBU in Zlín

Work experience

2016 – present **TBU in Zlín, Technology Transfer Centre, Czech Republic**
- Accreditation of footwear testing laboratory
- TAČR Gama - Development of a cereal mixture with an increased biological value
- TAČR Gama - Natural drinks with healthy effects

2014 – present **TBU in Zlín, Centre of polymer systems, Czech Republic (junior researcher)**
- TE01020216 - Project Competence Centres “Centrum of advanced polymer and composite materials” in consortium of TBU and 5 companies (Fatra a.s., Spur a.s., Quinn Plastics s.r.o., Zlín Precision s.r.o. a 5M s.r.o.) (2015-2016)
- Member of Research group: Rubber processes and materials

Membership in the bodies concerning HE policy

- 2017 - present **National Accreditation Bureau for HE, Czech Republic**
Evaluator in the field of Mechanical Engineering, Technology and Materials for doctoral study programmes
- 2015 - present **European Council for Doctoral Candidates and Junior Researchers (EURODOC)**
President (from 2019)
Vice-President (2018/2019)
General Board Member (2017-2018)
Coordinator of “Doctoral training WG” (2016 - 2018)
Representative delegate from the Czech Republic (from 2015)
- 2015 - present **Student Chamber of the Council of the HEIs, Czech Republic**
Ext. member of Committee for doctoral studies (from 2018)
Representative delegate from TBU (2015- 2017)
Member of Committee for doctoral studies (2015-2017)
EURODOC Coordinator for the Czech Republic (from 2015)
- 2012 - 2017 **Faculty of Technology Academic Senate at TBU**
Member of Legislative Committee (until 2016)
Member of Economical Committee (from 2016)
- 2013 - 2016 **Academic senate of TBU**
Chairperson of the Student Chamber
Member of Legislative Committee
Member of Rector's Advisory Council

Training and Certificates

- 2017 **Shoe maker training**
Custom manufacturing
- 2016 **BeEager Camp**
A self-developmental course in talent management
- 2015 - 2016 **Academic Centre for Student Activities - certifications**
Communication and argumentation I, II
Higher Education Legislation
Academic Senates
Time management
Motivation and work with members of student organizations

Training Abroad

2018 (4 days)	9 th UNICA PhD Master Class – The role of doctoral schools to enhance quality in doctoral education, Dubrovnik, Croatia
2018 (2 days)	PRIDE Network – Fundamentals for Professionals in Doctoral Education, Vienna, Austria
2017 (9 days)	SATRA – Accredited Footwear technologist, Kettering, UK
2016 (3 days)	KTU International PhD Summer School, Lithuania
2014 (3 months)	Karlsruhe Institute of Technology (KIT), Germany
2013 (2 months)	Mercury Centre, The University of Sheffield, United Kingdom
2013 (1 week)	EPMA Summer School, Trento, Italy
2013 (2 weeks)	Polymer processing and functionalization Summer school, Clermont-Ferrand, France

Projects

2018 - present	TAČR - ZETA (member of research team) Individual healthy footwear.
2018 - present	H2020-MSCA-ITN - Edulia (member of Advisory Board) Bringing down barriers to children's healthy
2016 - 2018	H2020-MSCA-ITN – SAF21 (member of Advisory Board) Social Science Aspects of Fisheries for the 21st Century
2016 – 2017	Strategic Development fund of TBU (project coordinator) Innovation of the production process of individual soles with anti-slipping properties
2012 - 2016	Internal Grant Agency of TBU (member of research team) IGA/FT/2016/002 - Processing properties characterization of highly filled compounds intended for PIM technology with the subsequent optimization of the mixture composition. IGA/FT/2015/001 - Development and testing of experimental compounds for PIM technology. IGA/FT/2014/003 - Study and characterization of highly filled PIM feedstocks based on stainless steels, reactive powder and ceramics. IGA/FT/2013/022 - Injection moulding of highly filled compounds based on metal or ceramic powder in combination with subsequent sintering. IGA/FT/2012/005 - Development and application of methodologies for the study of microsphere properties based on newly synthesized biodegradable block copolymers.

Language	Czech (mother), English (excellent), Italian (excellent), German (basic)
-----------------	--

Eva Hnátková

**Influence of binder composition on powder injection moulding
process**

Vliv kompozice polymerního pojiva na proces vstřikování práškových materiálů

Doctoral Thesis

Publication year: 2019